Ricardo Portas Marchão

Licenciado em Ciências de Engenharia Mecânica

Random vibration analysis design methodology applied on aircraft components - case study on a Lockheed Martin C-130H instrument panel retrofit

Dissertação para obtenção do Grau de Mestre em
Engenharia Mecânica

Orientador: Prof. Doutor João Cardoso, Professor
Auxiliar, FCT-UNL

Co-orientador: Eng. João Rui Duarte, Engenheiro
de Projeto, OGMA S.A

Júri:

Presidente: Tiago Alexandre Narciso da Silva, Professor
Auxiliar Convidado, FCT/UNL

Vogais: Carlos Manuel de Andrade Rodrigues, Engenheiro de
Projecto, OGMA

João Mário Burguete Botelho Cardoso, Professor Auxiliar,
FCT/UNL

FACULDADE DE
CIÊNCIAS E TECNOLOGIA
UNIVERSIDADE NOVA DE LISBOA

Setembro 2016

Random vibration analysis design methodology applied on aircraft components - case study on a Lockheed Martin C-130H instrument panel retrofit

Copyright @ Ricardo Portas Marchão, Faculdade de Ciências e Tecnologia, Universidade Nova de Lisboa

A Faculdade de Ciências e Tecnologia e a Universidade Nova de Lisboa têm o direito, perpétuo e sem limites geográficos, de arquivar e publicar esta dissertação através de exemplares impressos reproduzidos em papel ou de forma digital, ou por qualquer outro meio conhecido ou que venha a ser inventado, e de a divulgar através de repositórios científicos e de admitir a sua cópia e distribuição com objetivos educacionais ou de investigação, não comerciais, desde que seja dado crédito ao autor e editor.

Ricardo Portas Marchão

Licenciado em Ciências de Engenharia Mecânica

Random vibration analysis design methodology applied on aircraft components - case study on a Lockheed Martin C-130H instrument panel retrofit

Dissertação apresentada à Faculdade de Ciências e Tecnologia da Universidade Nova de Lisboa
para a obtenção do grau de Mestre em Engenharia Mecânica

Setembro 2016

À minha mãe e ao meu pai

Acknowledgements

I would like to express my gratitude to all of whom were involved throughout the development of this dissertation because it would not have been possible without them. My effort and commitment would not have been enough to achieve my dissertation objectives without their contribution:

To Dr. João Cardoso for his guidance and support throughout the whole process, and for making this project possible.

To Eng. João Rui Duarte for his support, commitment and availability during the whole process which was essential to carrying out this dissertation.

To OGMA-Indústria Aeronáutica de Portugal, S.A. and its collaborators which integrated me in their workplace and helped me when it was necessary.

To all Professors that I was able to learn from and contributed to the success of my academic career. I am very grateful to them for transmitting me knowledge and for clarifying my doubts and questions whenever I needed.

Finally, I would like to thank my parents for the unconditional support and for being always on my side. To them I dedicate this work.

Abstract

In the aeronautical industry, qualification and certification processes are very complex not only because safety has to be ensured, but also because there is regulation that must be fulfilled.

This dissertation has its origin on the necessity of assisting a design certified company credited as DOA (Design Organization Approval) in a preliminary phase of a modification project, and fulfill the need of developing an analysis methodology at a preliminary design phase that allows to produce confident results in a short time.

The modification in study consists in a flight instruments retrofit (upgrade) for Lockheed Martin C-130 H aircraft series. One of the main concerns on the modified instrument panel is its level of vibration.

Random vibration is recognized as the most realistic method of simulating the dynamic environment of military applications. PSD (Power Spectral Density) is a statistical measure defined as the limiting mean-square value of a random variable and it is used in random vibration analyses in which the instantaneous magnitudes of the response can be specified only by probability distribution functions that show the probability of the magnitude taking a certain value.

The purpose of this work is a creation of an efficient methodology which is intended to provide guidance for future possible projects of modification and fulfills the requirements of MIL-STD-810G.

The design methodology was implemented in a case study: the Lockheed Martin C-130H instrument panel retrofit (upgrade). Case study simulations were carried out through FEM (Finite Element Method).

Keywords: Power Spectral Density (PSD), Random Vibration, Design Methodology, Finite Element Analysis (FEA), Lockheed Martin C-130H, Instrument Panel Retrofit

Resumo

Na indústria aeronáutica, os processos de qualificação e certificação podem ser muito complexos não só porque a segurança tem de ser assegurada, mas também porque há regulamentação que tem de ser cumprida.

Esta dissertação surge com o intuito de apoiar uma empresa certificada para realizar projetos creditada como DOA (Design Organization Approval), numa fase preliminar do projeto de modificação, cumprindo a necessidade desenvolvendo uma metodologia de análise na fase preliminar de projeto que permita produzir resultados fidedignos num curto período de tempo.

A modificação em estudo consiste na modernização dos instrumentos de voo para a gama de aeronaves Lockheed Martin C-130 H. Uma das principais preocupações em relação ao novo painel de instrumentos é o seu nível de vibração.

O método mais consistente de simular o ambiente dinâmico de aplicações militares é através de vibrações aleatórias. O PSD (Power Spectral Density) é uma medida estatística que se define limitando o valor médio quadrático de uma variável aleatória e é usado em análises de vibrações aleatórias em que as magnitudes instantâneas da resposta são especificadas por funções de distribuição de probabilidade que mostram a probabilidade dessa resposta atingir um determinado valor.

O objetivo deste trabalho é a criação de uma metodologia eficiente que se destina a fornecer orientação para futuros possíveis projetos de modificação que cumpram os requisitos da norma MIL-STD-810G.

A metodologia de projeto foi implementada num estudo de caso: o painel de instrumentos da aeronave Lockheed Martin C-130H. As simulações do estudo de caso foram realizadas através de uma análise de elementos finitos.

Palavras-Chave: Densidade Espectral, Vibrações Aleatórias, Metodologia de Projeto, Análise de Elementos Finitos, Lockheed Martin C-130H, Painel de Instrumentos

List of Contents

1 Introduction ... 1

1.1 Motivation ... 1

1.2 Objectives ... 3

1.3 Thesis Structure ... 4

2 Confidence Assurance in Engineering Simulation ... 5

2.1 Quality Management in Engineering Simulation ... 5

2.2 Verification and Validation Processes ... 6

3 Theoretical Framework ... 9

3.1 Non-random Vibration Analysis Background ... 9

3.1.1 Harmonic Motion ... 9

3.1.2 Undamped free vibration ... 10

3.1.3 Damped Free Vibration ... 12

3.1.4 Forced Vibration ... 14

3.2 Random Vibration Analysis Background ... 19

3.2.1 Types of signal ... 19

3.2.2 Random vibration ... 21

3.2.3 Gaussian distribution ... 24

3.2.4 Statistical Properties of Random Vibration ... 26

3.2.5 How to calculate PSD ... 28

3.2.6 The meaning of gRMS in sine and random vibration ... 31

3.2.7 Dynamic analysis ... 32

4 Aeronautic Regulation ... 35

4.1 Scope of change ... 35

4.2 Regulations ... 36

4.2.1 MIL-STD-810G ... 36

5 Case Study 43

5.1 Introduction 43

5.2 Finite Element Method 43

5.3 Material Properties 44

5.4 Strategic simplifications 45

5.5 Elements 46

5.6 Connections 48

5.7 Mesh 49

5.8 Boundary Conditions 51

5.9 Natural Frequencies 51

5.10 Geometries 54

5.10.1 Structure I 54

5.10.2 Structure II 55

5.10.3 Structure III 56

6 Results 59

6.1 Structure I 59

6.1.1 X-axis input simulation 60

6.1.2 Y-axis input simulation 62

6.1.3 Z-axis input simulation 64

6.1.4 Data Evaluation 65

6.2 Structure II 67

6.2.1 X-axis input simulation 67

6.2.2 Y-axis input simulation 69

6.2.3 Z-axis input simulation 71

6.2.4 Data evaluation 73

6.3 Structure III 74

6.3.1 X-axis input simulation 75

6.3.2 Y-axis input simulation 77

6.3.3 Z-axis input simulation 79

6.3.4 Data evaluation 81

6.4 Concluding Remarks 82

7 Vibration Isolation 85

8 Methodology 91

9 Conclusions 95

9.1 Concluding remarks 95

9.2 Future considerations 96

10 Bibliography 99

11 Appendix A 103

11.1 The Fourier Transform 103

11.1.1 Discrete Fourier Transform 106

11.1.2 Fast Fourier Transform 107

12 Appendix B 111

List of Figures

Figure 1.1 - Information versus cost changes during product development (adapted from [3]) ... 2

Figure 1.2-The Iron Triangle[8] ... 2

Figure 1.3 - Thesis work flowchart ... 3

Figure 2.1 - ISO 9001:2008 Quality Management System model [10] ... 5

Figure 2.2 - Three pillars of engineering design on the foundations of Verification and Validation ... 6

Figure 2.3 - Simulation and V&V process flow diagram [12] ... 7

Figure 2.4 - Application of the simulation process [12] ... 7

Figure 3.1 - Harmonic Motion ... 9

Figure 3.2 - Undamped single-degree-of-freedom system ... 11

Figure 3.3 – Mass-spring system [14] ... 12

Figure 3.4- System responses[15] ... 14

Figure 3.5 - Excited system with harmonic force ... 14

Figure 3.6 - Total Response of the System[16] ... 15

Figure 3.7 - Gain function for force-excited system[17] ... 16

Figure 3.8 - Base-excited system ... 17

Figure 3.9 - Gain function for base-excited system (absolute displacement)[17] ... 18

Figure 3.10 - Gain function for base-excited system (relative displacement)[17] ... 19

Figure 3.11 - Mono-frequent time signal ... 20

Figure 3.12 - Multi-frequent time signal ... 20

Figure 3.13 - Pseudo-stochastic[19] ... 20

Figure 3.14 - Pulse type time signal ... 20

Figure 3.15 - Step type time signal ... 20

Figure 3.16 - Sine sweep time signal[20] ... 20

Figure 3.17 - White noise (frequency domain) ... 21

Figure 3.18 - Broad-band (frequency domain) ... 21

Figure 3.19 -Narrow-band (frequency domain) 21

Figure 3.20 - Deterministic and Random Excitation [22] 22

Figure 3.21- Random and Sine Waves[24] 23

Figure 3.22- White Light Passed Through a Prism 23

Figure 3.23 - Random vibration signal analogy with white light 24

Figure 3.24 - Gaussian distribution [27] 25

Figure 3.25 - Transformation of a time signal in a histogram 27

Figure 3.26 - Equivalence between g_{rms} and σ 27

Figure 3.27 - Statistical Properties of a Random Vibration Signal 28

Figure 3.28 - Spectral analysis procedure using analog filters 29

Figure 3.29 - Calculation of a Power Spectral Density in a standardized unit of measure 30

Figure 3.30 - PSD calculation technique... 31

Figure 3.31 – g_{rms} on a sine test 32

Figure 3.32 – g_{rms} on random test 32

Figure 3.33 - Dynamic Analysis Methodology 32

Figure 3.34 - Eigenvalues solution... 33

Figure 3.35 - Transfer Function Hf. 33

Figure 3.36 - PSD input and PSD response 34

Figure 4.1- Lockheed Martin C-130H... 35

Figure 4.2 - Analog Instrument Panel 35

Figure 4.3 - Digital Instrument Panel 35

Figure 4.4 - Vibration environment categories 37

Figure 4.5- Preparation for test - preliminary steps... 37

Figure 4.6 - Propeller aircraft vibration exposure (1)[31] 39

Figure 4.7 - Propeller aircraft vibration exposure (2)[31] 39

Figure 4.8 - Propeller vibration exposure that will be applied as input in all simulation analysis 40

Figure 5.1 - Lockheed Martin Hercules C-130 instruments panel 43

Figure 5.2 - Simulation Methodology 44

Figure 5.3 – Chamfers and notches simplification 45

Figure 5.4 - Geometry simplification 45

Figure 5.5 - Bolts simplification 46

Figure 5.6- Solid187 in comparison to a 4-node tetrahedral element 46

Figure 5.7 - Solid186 in comparison to an 8-node cube element 47

Figure 5.8 - Target170-Conta174 and Targe170-Conta175 Contact Pairs 47

Figure 5.9 - Beam188 Element 47

Figure 5.10 - Shell181 Element 48

Figure 5.11 - Bolt-sheet plate, beam-sheet plate, body-ground interactions 48

Figure 5.13 - Part meshed with solid elements 50

Figure 5.12 - Part meshed with shell elements 50

Figure 5.14 - Boundary Conditions 51

Figure 5.15 - Boundary Conditions Localization 51

Figure 5.16 - Fixation on areas A, B, C, D 52

Figure 5.17 - Fixation on areas E, F, G, H 52

Figure 5.18 - Fixation on areas A, B, C, D for simulation 6 52

Figure 5.19 - Structure I 54

Figure 5.20 - Structure II 55

Figure 5.21 - Structure III 56

Figure 6.1 - Color scale 59

Figure 6.2 - Coordinate system 59

Figure 6.3 - Identification of points that will provide information about PSD response (1)....... 61

Figure 6.4 - PSD response of point 1 and clarification of the concepts peak value and most critical frequency 61

Figure 6.5 - Identification of points that will provide information about PSD response (2)....... 63

Figure 6.6 - Identification of points that will provide information about PSD response (3)....... 65

Figure 6.7 - Identification of points that will provide information about PSD response (4)....... 68

Figure 6.8 - Identification of points that will provide information about PSD response (5)....... 70

Figure 6.9 - Identification of points that will provide information about PSD response (6)....... 72

Figure 6.10 - Identification of points that will provide information about PSD response (7)..... 76

Figure 6.11 - Identification of points that will provide information about PSD response (8)..... 78

Figure 6.12 - Identification of points that will provide information about PSD response (9)..... 80

Figure 6.13 - Identification of most critical areas 83

Figure 6.14 - Glare-shield 83

Figure 6.15 - Center panel engine indicator 83

Figure 7.1 - Localization of damping isolators 85

Figure 7.2 - Isolator using friction damped spring 86

Figure 7.3 - Amplification and isolation regions 87

Figure 7.4 - L44 Dimensional Drawing 88

Figure 8.1 - Transformation of inputs and outputs 91

Figure 8.2 – FEM Modelling sub-process 92

Figure 8.3 - Shock mounts installation sub-process 92

Figure 8.4 - Random vibration sub-process 93

Figure 9.1 - Equivalent sinusoidal history 97

Figure 11.1-Relationship between time domain and frequency domain[46] 103

Figure 11.2- Arbitrary periodic function of time[47] 103

Figure 11.3 - Real and imaginary Fourier coefficients 105

Figure 11.4 - The Fourier density spectrum 105

Figure 11.5 - Analog to Digital Conversion [50] 106

Figure 11.6 - Buffer example 108

Figure 11.7 - Discontinuity between repeating buffers results in spectral leakage 108

Figure 11.8 - Hanning window function 108

Figure 11.9 - Reduction of spectral leakage by multiplying the signal with a window functio 109

Figure 11.10 - 50% Overlapping 109

Figure 11.11 - Fourier Transform and its inverse 110

List of Tables

Table 3.1 - Types of stationary signals 20

Table 3.2- Differences between sinusoidal and random vibration 22

Table 3.3 - Probability of random amplitudes (1) 25

Table 3.4 - Probability of random amplitudes (2) 25

Table 3.5 - Influence of the bandwidth filter on measurements 29

Table 4.1 - ASD level of vibration calculation 40

Table 5.1 - Mechanical Properties of Aluminum 2024-T3 44

Table 5.2 - Mesh characteristics on Workbench 17.0 49

Table 5.3- Comparison of generated elements according to solid and shell formulation 50

Table 5.4 - Comparison of number of elements between a 3D mesh without simplifications and 2D mesh with simplifications 50

Table 5.5 - Fixation types applied for all simulations 52

Table 5.6 – Natural Frequencies Results 53

Table 5.7 - Structure I element types 54

Table 5.8 - Structure I model properties 55

Table 5.9 - Structure II element types 55

Table 5.10 - Structure II model properties 56

Table 5.11 - Structure III element types 56

Table 5.12 - Structure III model properties 57

Table 5.13 - Representation of instruments as lumped point masses 57

Table 6.1 - Structure I Natural Frequencies 59

Table 6.2 - Structure I most critical areas after X-Axis Input 60

Table 6.3 - Most critical results after X-Axis Input 60

Table 6.4 - Range of excitation frequencies generated by the propeller 61

Table 6.5 - PSD response for X-axis excitation 62

Table 6.6 - Structure I most critical areas after Y-Axis Input 62

Table 6.7 - Most critical results after Y-Axis Input 63

Table 6.8 - PSD response for Y-axis excitation 63

Table 6.9 - Structure I most critical areas after Z-Axis Input 64

Table 6.10 - Most critical results after Z-Axis Input 64

Table 6.11 - PSD response for Z-axis excitation 65

Table 6.12 - Structure I data collection 66

Table 6.13 - Number of points whose critical frequency is within the range of propellers 66

Table 6.14 – Structure II Natural Frequencies 67

Table 6.15 -Structure II most critical areas after X-Axis Input 67

Table 6.16 - Most critical results after X-Axis Input 68

Table 6.17 - PSD response for X-axis excitation 68

Table 6.18 – Structure II most critical areas after Y-Axis Input 69

Table 6.19 - Most critical results after Y-Axis Input 70

Table 6.20 - PSD response for Y-axis excitation 70

Table 6.21 – Structure II most critical areas after Z-Axis Input 71

Table 6.22 - Most critical results after Z-Axis Input 72

Table 6.23 - PSD response for Z-axis excitation 72

Table 6.24 - Structure II data collection 73

Table 6.25 - Number of points whose critical frequency is within the range of propellers 74

Table 6.26 - Structure III Natural Frequencies 74

Table 6.27 - Structure III most critical areas after X-Axis Input 75

Table 6.28 - Most critical results after X-Axis Input 75

Table 6.29 - PSD response for X-axis excitation 76

Table 6.30 - Structure III most critical areas after Y-Axis Input 77

Table 6.31 - Most critical results after Y-Axis Input 77

Table 6.32 - PSD response for Y-axis excitation 78

Table 6.33 - Structure III most critical areas after Z-Axis Input 79

Table 6.34 - Most critical results after Z-Axis Input 79

Table 6.35 - PSD response for Z-axis excitation.. 80

Table 6.36 - Structure III data collection 81

Table 6.37 - Number of points whose critical frequency is within the range of propellers 81

Table 6.38 - Overall data collection 82

Table 6.39 - Number of points whose critical frequency is within the range of propellers 82

Table 7.1 - L-Mount Specifications 85

Table 7.2 - L44 Height of aluminum core 89

Table 8.1 - Meaning of flowchart symbols 91

Table 11.1 - FFT and DFT Computational Effort 107

Acronyms and Nomenclature

AFM – Aircraft Flight Manual

ANAC – Autoridade Nacional da Aviação Civil

ASD – Acceleration Spectral Density

c – Damping Coefficient

c_c – Critical Damping Coefficient

CPM – Cycles per Minute

DFT – Discrete Fourier Transform

DOA – Design Organization Approval

EASA – European Aviation Safety Agency

f – Frequency

F_o – External Force

Fc – Center Frequency

Fd – Disturbing Frequency

FEA – Finite Element Analysis

FEM – Finite Element Method

FFT – Fast Fourier Transform

F_n – Natural Frequency

$F_{n,min}$ – Minimum Isolator Natural Frequency

g_{rms} – Root Mean Square Acceleration

Hf – Transfer Function

ICAO – International Civil Aviation Organization

ISO – International Organization for Standardization

k – Spring Constant

m – Mass

MS – Margin of Safety

OEM – Original Equipment Manufacturer

PSD – Power Spectral Density

PSD_{in} – Input Power Spectral Density

PSD_{out} – Output Power Spectral Density

QMS – Quality Management System

r – Frequency Ratio

RMS – Root Mean Square

RPM – Revolutions per Minute

T – Transmissibility

T_r – Resonant Transmissibility

V – Level of Isolation

V&V – Verification and Validation

ω_n – Natural Frequency

$\bar{X}$ – Mean

$\overline{X^2}$ – Mean Square

δ_{est} – Static Equilibrium Position

ξ – Damping Factor

σ – Standard Deviation

τ – Period

ω – Angular Velocity

1 Introduction

1.1 Motivation

In the aeronautical industry, modification and design processes always carry an associated risk. These processes are very complex not only because safety has to be ensured, but also because there is regulation that must be fulfilled [1].

The design process is a very important stage in the development of a product. The committed costs with this stage are about 80% of the overall cost of a project, the majority of decisions are made by the end of this stage. On the other hand, the committed costs with manufacturing are only about 5% [2]. This concept clarifies the importance of making a decision in the design phase.

Figure 1.1 represents the variation of the cost when modifications are implemented, information about the product and the possibility to modification process over time [3]. This fact justifies the need to carefully proceed with the modification project, from the early stages of the design process in order to obtain the most efficient design with lesser costs and better quality in a perfect balance with time.

The focus of this work is to create a methodology for modification of aircraft design which meets all the standard requirements in the aeronautical industry. This dissertation has its origin on the necessity of assisting a design certified company credited as DOA (Design Organizational Approval) in a preliminary phase of project modification.

An organization credited as DOA has some privileges as to classify modifications and repairs as major or minor, approve modifications and minor repairs, approve major repairs and approve minor revisions to the AFM (Aircraft Flight manual), among others.

Currently, aeronautical standards and certifications are managed by international organizations [4]. ICAO (International Civil Aviation Organization) is a specialized United Nations agency that regulates international civil aviation since the Chicago Convention on the International Civil Aviation, held in Chicago in 1944 [5]. EASA (European Aviation Safety Agency) is the organization which assists member states of the European Union to meet its obligations to the ICAO. EASA aims to promote the highest standards of safety and environmental protection in civil aviation of the European Union. This organism has the right to approve organizations involved in the design, production and maintenance of aircraft components [6]. In Portugal, the regulatory authority is ANAC (Autoridade Nacional de Aviação Civil) [7].

Another motivation for this dissertation is the case study that was chosen to validate the methodology: the instrument panel modification of a Lockheed Martin C-130 H. This case allowed me to learn about the processes of certification and qualification in aeronautical industry.

A dynamic study on the modified structural components is very important in order to prevent that their natural frequencies and vibration modes approach the excitation frequencies. Without this study, it may run up risks of undesired vibrations that can cause, for example, wear by fatigue in aircraft components. Another risk which is vital to be avoided is the vibration of the instrument panel, which in turn can disturb its readability by the pilot.

The present work can be very useful and its purpose is to serve as a reference when the company will be starting the future modification projects.

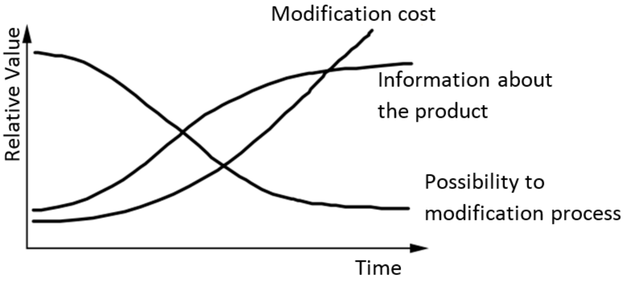

Figure 1.1 - Information versus cost changes during product development (adapted from [3])

The success of a project management depends on the perfect balance between Quality, Time and Cost. These are the main concerns when developing a methodology for a project design. The methodology carried out in this dissertation aims to increase the quality of the design phase of the modification project while reducing cost and time. On Figure 1.2, it is represented the model of the Iron Triangle presented by Roger Atkinson[8].

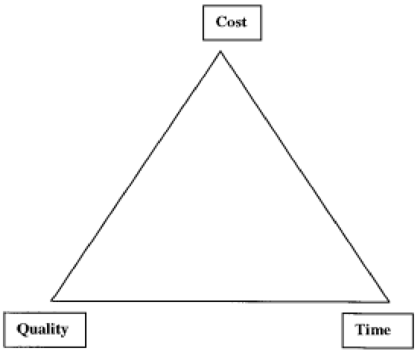

Figure 1.2-The Iron Triangle[8]

The development of this dissertation resulted in a cooperation between Faculdade Ciências e Tecnologia – Universidade Nova de Lisboa and the company OGMA - Indústria Aeronáutica de Portugal, SA.

1.2 Objectives

This dissertation aims to develop a methodology for aircraft components modification. It is intended to develop a useful tool for a project team which allows a DOA to obtain, efficiently, a final solution that complies with existing certification requirements in the aviation industry.

The study was carried out through the flowchart described on Figure 1.3 - Thesis work flowchart. The outputs described in the flowchart represent the thesis milestones in order to achieve the major objective of this dissertation, which was the implementation of recommended procedure guidelines for a vibration analysis on a modified structure.

The methodology was applied through a case study: the instrument panel vibration analysis after a flight instruments retrofit (upgrade) for Lockheed Martin C-130 H aircraft series.

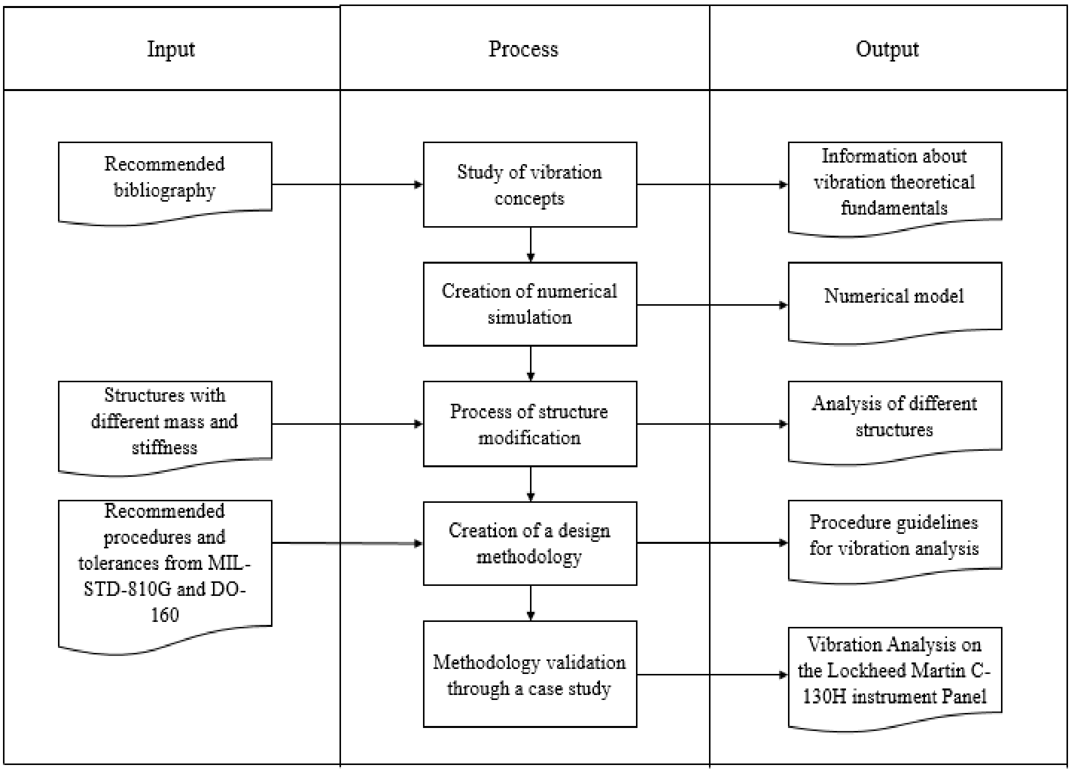
Input
Process
Output
Recommended bibliography
Study of vibration concepts
Information about vibration theoretical fundamentals
Creation of numerical simulation
Numerical model
Structures with different mass and stiffness
Process of structure modification
Analysis of different structures
Recommended procedures and tolerances from MIL-STD-810G and DO-160
Creation of a design methodology
Procedure guidelines for vibration analysis
Methodology validation through a case study
Vibration Analysis on the Lockheed Martin C-130H instrument Panel

Figure 1.3 - Thesis work flowchart

1.3 Thesis Structure

The inherent information provided by this dissertation is distributed along nine chapters regarding its main purpose which is the vibration analysis methodology on modified aircraft components.

- The first chapter refers to the motivation and a brief description of the entities that regulate the international aeronautical standards. The thesis main objectives and milestones are also included and they are expressed in the flowchart of the dissertation outputs.
- The second chapter is an introductory approach to quality management system in engineering simulation and the processes of verification and validation in engineering design.
- The third chapter is a comprehensive explanation of vibration analysis fundamentals. On this chapter, it is reviewed the concepts of one degree of freedom including the notion of resonance. The concept of Power Spectral Density (PSD) and its importance of measuring vibration is clarified. This chapter also includes an overview of several types of signals. It also clarifies the difference between harmonic and random vibration analyses.
- The fourth chapter is related to certification process according with international standards. The procedures and tolerances which were taken into consideration on the simulations are presented in this chapter.
- The fifth chapter presents the case study as well as considerations about the Finite Element Method. Modeling decisions about material properties, implemented simplifications, meshing and connections are referred. Details about structure geometries which will be simulated in a Finite Element Analysis are discussed.
- The sixth chapter shows the obtained PSD results after performing the recommended vibration simulations. A detailed discussion of the results is also included.
- On the seventh chapter, the methodology of a shock mount selection is addressed. The theory related to vibration isolation is clarified by choosing the most appropriate mount, the verification procedure is also presented. This chapter is related to the shock mount selection procedure according to the suggested methodology by the OEM (Original Equipment Manufacturer)
- The eighth chapter aims to clarify the definition of the procedures to be followed during the proposed modification methodology.
- The ninth chapter includes final remarks and conclusions of this dissertation and also future developments that can be implemented on the subject.

2 Confidence Assurance in Engineering Simulation

2.1 Quality Management in Engineering Simulation

The ISO 9000 family of standards provides guidance and tools for companies and organizations that want to ensure that their product and services consistently meet customers´ requirements and that quality is continually improved. There are three standards: ISO 9000 covers the basic concepts of quality management and associated language, ISO 9001 sets out the requirements of a Quality Management System (QMS). The ISO 9002 and ISO 9003 standards were incorporated into ISO 9001 standard. ISO 9004 focuses on how to make a QMS more efficient [9].

The primary purpose of the QMS is to provide the framework for an organization´s management process. Instituting a quality management system will ensure that quality principles are built into the simulation production process at a fundamental level, thereby facilitating quality control in all aspects of the work. The quality system will provide a framework within which simulation work can be properly planned and executed under controlled conditions to achieve consistent simulation product quality. The usual purpose of an engineering simulation is to predict the behavior of an engineered object or system in order to assess its ability to support design loadings. The success of the simulation will be strongly influenced by the quality of its planning, process, verification and validation activities. On Figure 2.1, it is presented the QMS model for engineering simulation.

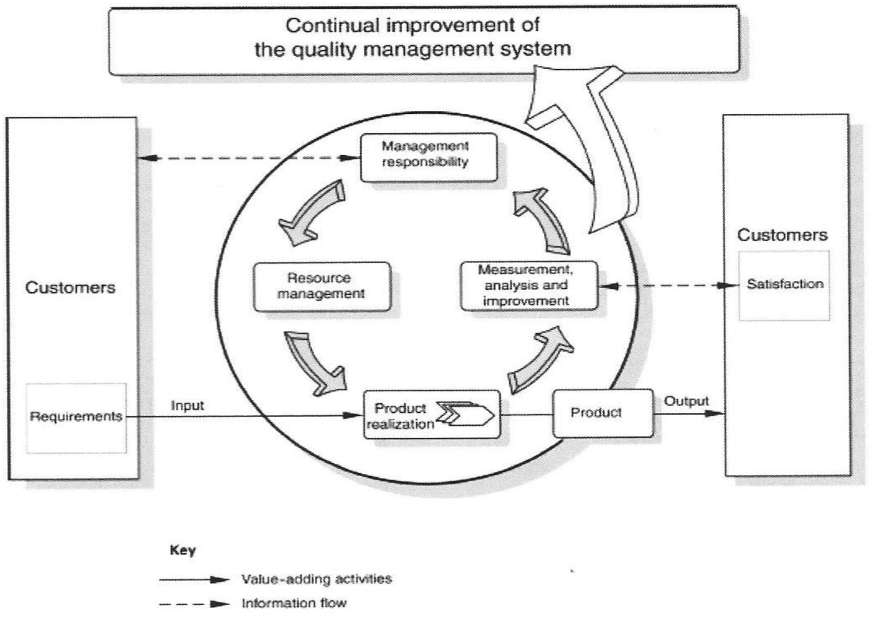
Continual improvement of the quality management system
Customers
Requirements
Input
Management responsibility
Resource management
Measurement, analysis and improvement
Product realization
Product
Output
Customers
Satisfaction
Key
Value-adding activities
Information flow

Figure 2.1 - ISO 9001:2008 Quality Management System model [10]

The QMS requires a tool to access the design process, of which the simulation process is a core component; this tool is largely the process of Verification & Validation (V&V) which is a requirement of ISO 9001.

2.2 Verification and Validation Processes

A sound engineering design is supported on the three pillars of numerical simulation, mathematical models and physical experiments as presented on Figure 2.2. The goal of good simulation governance is to match numerical simulation with physical experiments. This cannot be done in any rational manner without consideration of the mathematical models that govern the physics of the problem. Whilst the two terms, at first sight, may appear to be almost synonyms, the processes of verification and validation are different. They provide the foundations for engineering design by tying together the three pillars of engineering design, these cannot exist without the mathematical models [11].

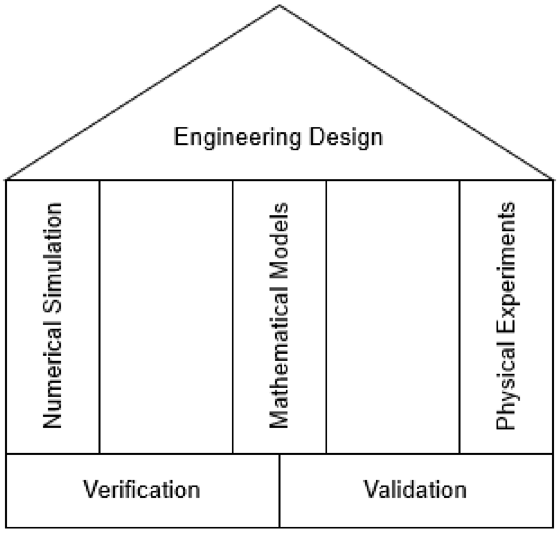

Figure 2.2 - Three pillars of engineering design on the foundations of Verification and Validation

The process of verification and validation is the mechanism used to demonstrate that a simulation is robust and that it has been performed using best practices. The major concern in engineering simulation is the degree to which a simulation model can accurately represent the real word behavior. Any model of an engineered system will necessarily be approximate and simulation error will inevitably be introduced. Therefore, before any real confidence can be placed in predictions of the model, it needs to be demonstrated that the model is capable of accurately predicte the real world engineering behavior and generate results that are valid for the purpose of engineering design substantiation. This can be achieved through the application of appropriate simulation verification and validation activities.

The simulation process is presented on Figure 2.3 and an application of this process is presented on Figure 2.4.

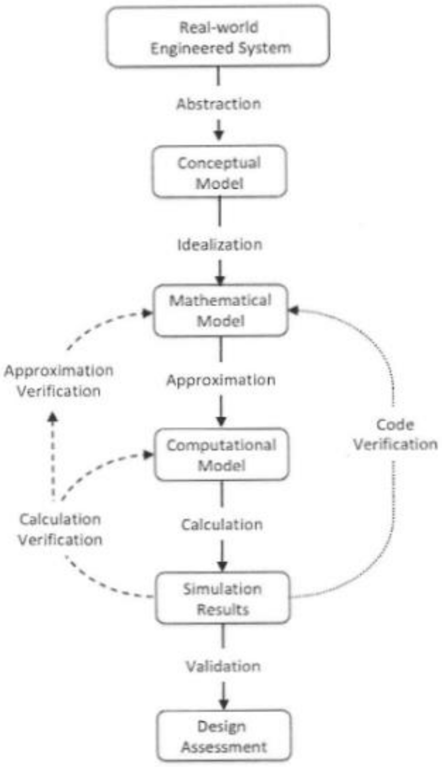
Real-world Engineered System
Abstraction
Conceptual Model
Idealization
Mathematical Model
Approximation Verification
Approximation
Code Verification
Computational Model
Calculation Verification
Calculation
Simulation Results
Validation
Design Assessment

Figure 2.3 - Simulation and V&V process flow diagram [12]

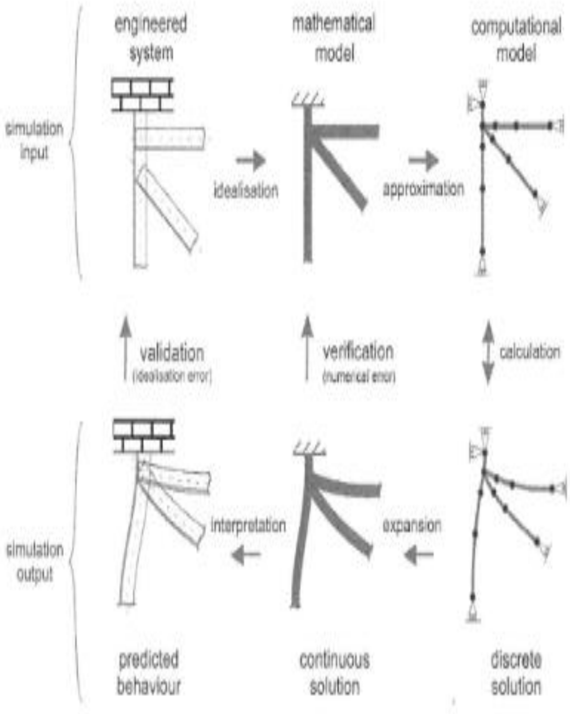
engineered system
mathematical model
computational model
simulation input
idealisation
approximation
validation
(idealisation error)
verification
(numerical error)
calculation
simulation output
interpretation
expansion
predicted behaviour
continuous solution
discrete solution

Figure 2.4 - Application of the simulation process [12]

Verification is the process of determining that a computational model accurately represents the underlying mathematical model and its solution. Validation is the process of determining the degree to which a model is an accurate representation of the real world. Both processes are related to one another and are taken into account in the Quality Management System model applied for engineering simulation.

Good simulation governance, which enables the practicing engineer to have confidence in his results, is all about matching the results from numerical simulation with whenever possible, those of physical experiments, and must take place regarding mathematical models. Verification is the process which ensures the quality of the match between the numerical simulation results and the mathematical model. Simulation process has been updated based on supporting physical experiments along years providing more confidence assurance in engineering simulation.

Finite Element Analysis (FEA) has become widely used and globally accepted in many industry sectors. FEA is a powerful technique which can produce solutions to challenging structural analysis problems. The technology and computational efficiency of the method, together with the rapid increases in computer processing power means that nowadays the scope and size of simulations far exceeds the capabilities of even a few years ago.

3 Theoretical Framework

This chapter contains a description of vibration analysis fundamentals. On this chapter, it will be reviewed the concepts of one degree of freedom including the notion of resonance. The concept of Power Spectral Density (PSD) and its importance for measuring vibration is clarified. This chapter also includes an overview of several types of signals. Differences between sine and random vibration analysis are explained.

3.1 Non-random Vibration Analysis Background

3.1.1 Harmonic Motion

It is important to understand the fundamentals of vibration theory. On the following paragraphs, the concepts and definitions associated with linear and elastic vibrations of systems with a single degree of freedom will be reviewed. These systems only require one coordinate to describe their position at any instant of time.

On Figure 3.1 it is shown a vector OP with a length A that rotates counterclockwise with constant angular velocity ω. The angle that OP makes with the horizontal axis at any time t is represented by $\theta = \omega t$. The projection of OP on the vertical axis is represented by x in (3.1):

$$x = A \sin \omega t \tag{3.1}$$

As seen before, x is a function of time. This function which is represented on Figure 3.1 is called the harmonic motion.

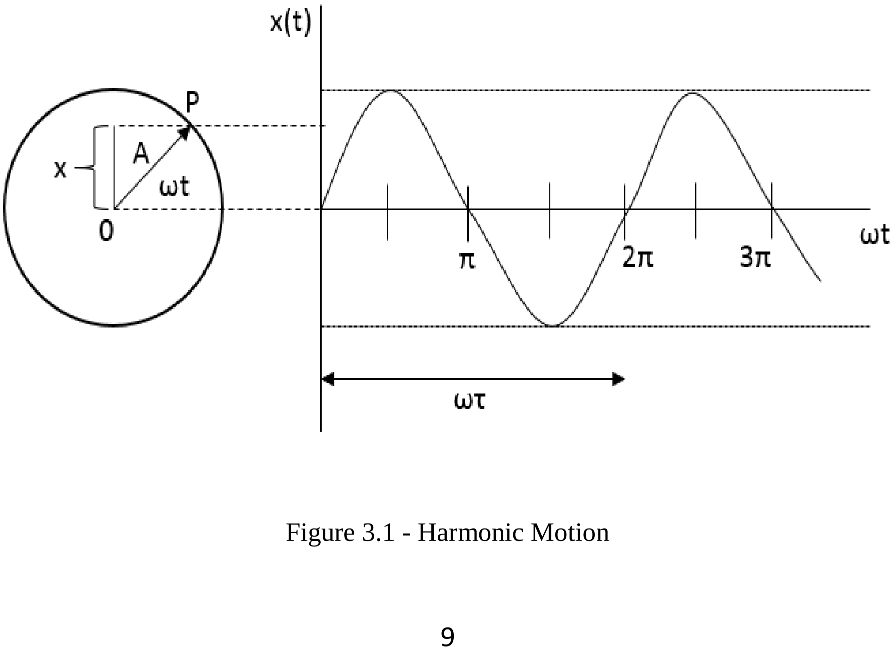

Figure 3.1 - Harmonic Motion

These are some basic definitions of harmonic motion [13]:

- A represents the amplitude. The range of $2A$ represents the peak-to-peak displacement.
- The period is the time for the motion to repeat and it is represented by τ in (3.2):

$$\omega\tau = 2\pi \tag{3.2}$$

- A cycle is the motion in one period.
- Frequency is the number of cycles per time unit, usually it is expressed in Hz. In terms of the period, the frequency is represented as (3.3):

$$f = \frac{1}{\tau} \tag{3.3}$$

From (3.3) the frequency is related to ω as (3.4):

$$f = \frac{\omega}{2\pi} \tag{3.4}$$

- The velocity of a particle is (3.5):

$$v = \frac{dx}{dt} = \dot{x} \tag{3.5}$$

- The acceleration of a particle is (3.6):

$$a = \frac{dv}{dt} = \frac{d^2x}{dt^2} = \ddot{x} \tag{3.6}$$

Thus, in harmonic motion displacement, velocity and acceleration are related by (3.7), (3.8) and (3.9):

$$x = A\sin\omega t \tag{3.7}$$

$$v = \dot{x} = A\omega\cos\omega t \tag{3.8}$$

$$a = \ddot{x} = -A\omega^2\sin\omega t \tag{3.9}$$

3.1.2 Undamped free vibration

Figure 3.2 shows a spring-mass system with a single degree of freedom. The spring is originally in the unstretched position. It is assumed that the spring obeys Hook´s law. In (3.10), F represents the force in the spring and k represents the spring constant.

$$F = kx \tag{3.10}$$

When the mass m is added in, the spring deflects to a static equilibrium position represented as δ_{est}. If the mass is perturbed and allowed to move dynamically, the displacement measured from the equilibrium position represented as x is a function of time. $x\ (t)$ represents the absolute motion of the mass. The equations of motion are employed to determine the position as a function of time. The free-body diagrams are shown on Figure 3.2. Applying Newton's second Law, it is obtained (3.11)

$$W - k(x + \delta_{est}) = m\ddot{x} \tag{3.11}$$

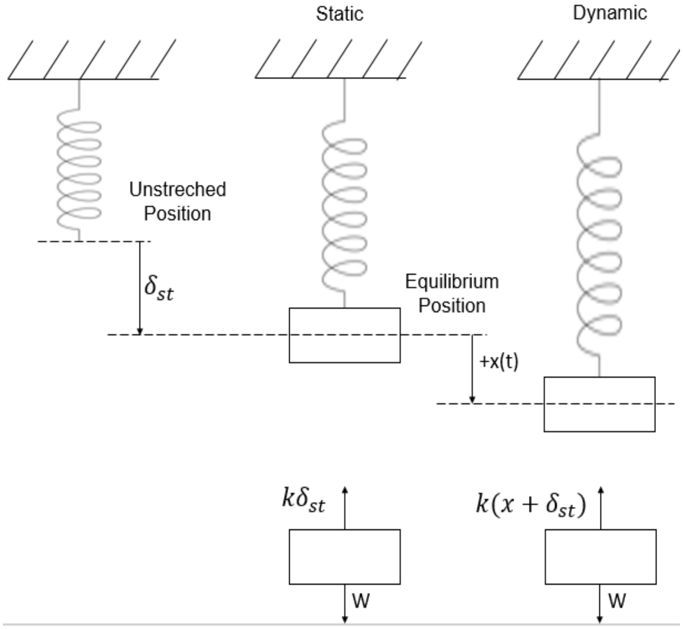

Figure 3.2 - Undamped single-degree-of-freedom system

As seen from the static condition, $W = k\delta_{est}$. Therefore the equation of motion results in (3.12):

$$m\ddot{x} + kx = 0 \tag{3.12}$$

Equation (3.12) is considered as a linear differential equation of second order with the solution of the type:

$$x(t) = Ce^{st} \tag{3.13}$$

Performing the Laplace Transform:

$$\zeta\{m[\ddot{x}(t)]\} + \zeta\{k[x(t)]\} = \zeta\{0\} \tag{3.14}$$

$$\Leftrightarrow s^2m + k = 0 \tag{3.15}$$

Equation (3.15) is called the characteristic equation. Its roots represented in (3.16):

$$\Rightarrow s = \pm i\sqrt{\frac{k}{m}} \tag{3.16}$$

The natural frequency of the system is shown in (3.17):

$$w_n = \sqrt{\frac{k}{m}} \tag{3.17}$$

Replacing s on the equation $x(t) = Ce^{st}$, the response of the system results in (3.19):

$$x(t) = C_1 e^{iw_n t} + C_2 e^{-iw_n t} \tag{3.18}$$

$$\Leftrightarrow x(t) = A_1 \cos(w_n t) + A_2 \sin(w_n t) \tag{3.19}$$

The constants A_1 and A_2 are calculated from the initial conditions:

$$\begin{aligned} &\text{For x(t), t=0} \Rightarrow A_1 = x_0 \\ &\text{For } \dot{x}(t)\text{, t=0} \Rightarrow A_2 = \frac{\dot{x_0}}{w_n} \end{aligned} \tag{3.20}$$

3.1.3 Damped Free Vibration

On Figure 3.3 it is shown the spring-mass system with an energy-dissipating mechanism described by the damping force. This force is proportional to the velocity of the mass. The damping coefficient is represented by c. Applying Newton's second law, this model leads to the following linear differential equation of second order (3.21):

$$m\ddot{x} + c\dot{x} + kx = 0 \tag{3.21}$$

Assuming the solution $x(t) = Ce^{st}$, the characteristic equation is represented in (3.22):

$$s^2 m + cs + k = 0 \tag{3.22}$$

Its roots are represented in (3.23):

$$s_{1,2} = \frac{-c}{2m} \pm \sqrt{\left(\frac{c}{2m}\right)^2 - \frac{k}{m}} \tag{3.23}$$

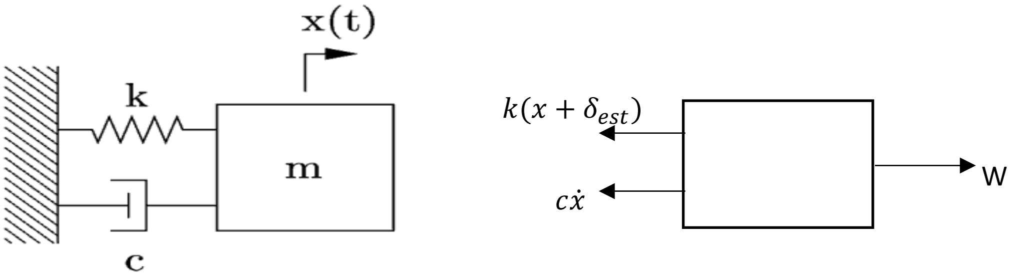

Figure 3.3 – Mass-spring system [14]

The critical damping coefficient c_c is defined when that value c makes the radical equal to zero and it is represented in (3.24):

$$\Rightarrow c_c = 2mw_n \tag{3.24}$$

The damping factor is defined in (3.25):

$$\xi = \frac{c}{c_c} \tag{3.25}$$

There are three different cases which generates three different responses of the system: over damping, critical damping and under damping.

Over damping occurs when $c > c_c$. Both roots are real and the solution to the differential equation (3.21) is represented in (3.26).

$$x(t) = Ae^{s1t} + Be^{s2t} \tag{3.26}$$

The constants of integration are represented as A and B. s_1 and s_2 will be both negative. Therefore, given an initial displacement, the mass will decay to its equilibrium position without oscillating motion.

Critical Damping occurs when $c = c_c$. Both roots are equal and the general solution of the differential equation is represented in (3.27).

$$x(t) = e^{-w_n t}(A + Bt) \tag{3.27}$$

The motion decays to the equilibrium position again, so the response is not oscillatory.

Under Damping occurs when $0 < c < c_c$. In this case the roots of the characteristic equation are complex. Using the Euler's formula, the general solution of the differential equation is shown in (3.28) wherein A and ϕ are the constants of integration:

$$x(t) = [A\cos(\omega_d t + \phi)]e^{-\xi w_n t} \tag{3.28}$$

The damped natural frequency ω_d is defined in (3.29).

$$\omega_d = \omega_n\sqrt{1 - \xi^2} \tag{3.29}$$

On Figure 3.4, it is shown the undamped and damped responses of the system.

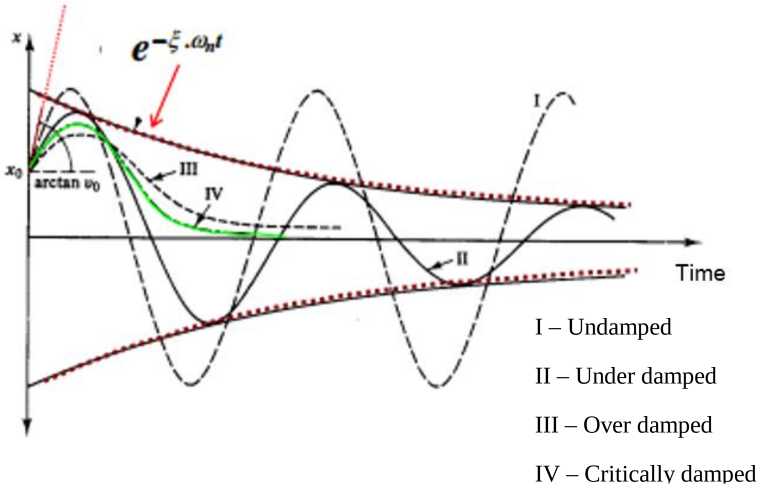

Figure 3.4- System responses[15]

3.1.4 Forced Vibration

3.1.4.1 Harmonic excitation

A diagram of a single degree of freedom with an external force $F\ (t)$ is shown on Figure 3.5. The coordinate $x\ (t)$ represents the absolute motion of the mass. It is considered that the external force is harmonic. Applying Newton's second law, the equation of motion results in (3.30):

$$m\ddot{x} + c\dot{x} + kx = F_0 \sin \omega t \tag{3.30}$$

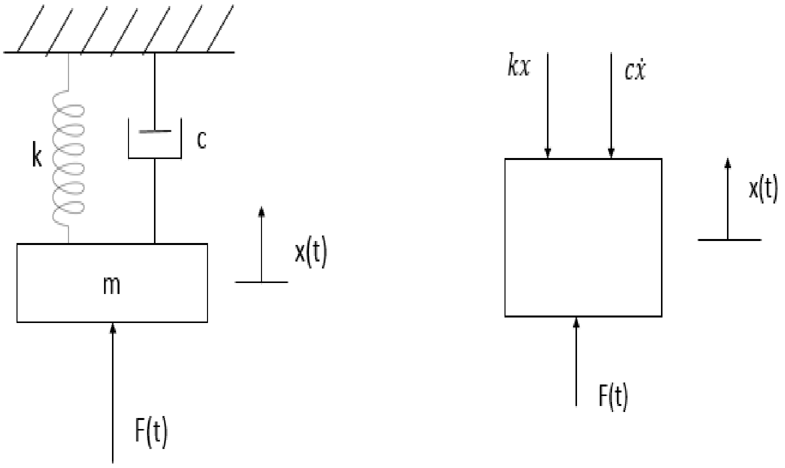

Figure 3.5 - Excited system with harmonic force

This is a nonhomogeneous linear differencial equation. The general solution is given in (3.31).

$$\mathrm{x(t)} = \mathrm{x_h(t)} + \mathrm{x_p(t)} \tag{3.31}$$

The homogeneous solution is represented as $\mathrm{x_h(t)}$ wherein are included the free vibrations of the system and the particular solution is represented as $\mathrm{x_p(t)}$ which is also called the steady-state solution. The concepts are exposed on Figure 3.6.

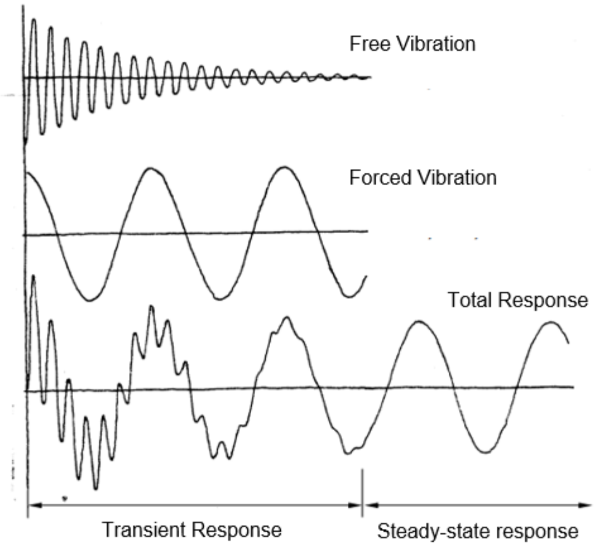

Figure 3.6 - Total Response of the System[16]

Using complex algebra and assuming that the response has the same frequency as the force, $F(t)$ and $x(t)$ are shown in (3.32).

$$\begin{gathered} F(t) = F_0 e^{i\omega t} \\ x(t) = X e^{i\omega t} \end{gathered} \tag{3.32}$$

Replacing x and F on the differential equation of motion results in (3.33):

$$(-m\omega^2 + ic\omega + k)Xe^{i\omega t} = F_0 e^{i\omega t} \tag{3.33}$$

The frequency response function or transfer function, $H(\omega)$, is defined as the complex displacement due to a force of unit magnitude, $F_0 = 1$. Therefore, this function results in (3.34).

$$H(\omega) = \frac{1}{(k - m\omega^2) + ic\omega} \tag{3.34}$$

The gain function is defined as the modulus of the transfer function in (3.35):

$$|H(\omega)| = \sqrt{H(\omega)H^*(\omega)} = \sqrt{(Re\ H)^2 + (Im\ H)^2} \tag{3.35}$$

The gain function is the amplitude of the displacement for $F_0 = 1$ represented in (3.36).

$$\frac{X_0}{F_0} = |H(\omega)| \tag{3.36}$$

The frequency ratio is defined in (3.37):

$$r = \frac{\omega}{\omega_n} \tag{3.37}$$

After calculating the modulus of the transfer function, multiplying by k and employing the definitions for ξ, ω_n and c_c it is possible to obtain the nondimensional gain function in (3.38).

$$\frac{X_0}{F_0/k} = \frac{1}{\sqrt{(1-r^2)^2 + (2\xi r)^2}} \tag{3.38}$$

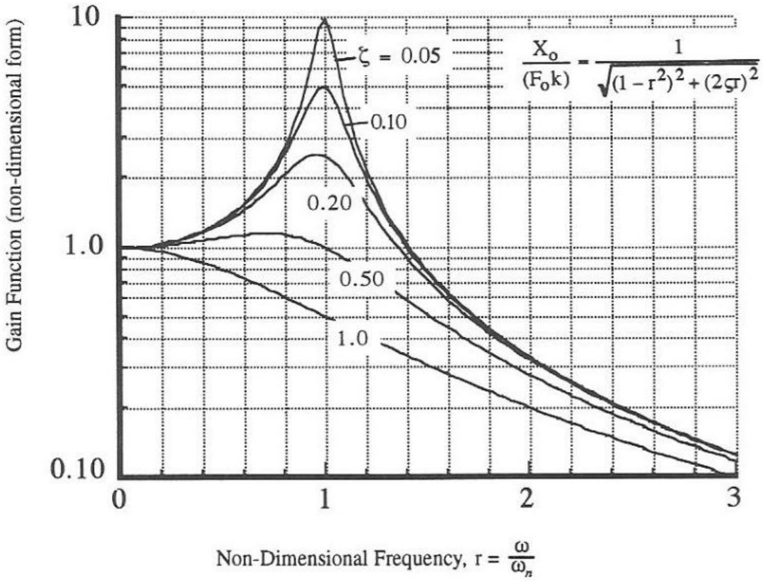

Figure 3.7 - Gain function for force-excited system[17]

When r is close to 1 or when ω is close to ω_n, the gain function tends to be higher as the damping coefficient is lower. In fact, the response tends to infinite without damping and this phenomenon is called resonance.

3.1.4.2 Base Excitation

Absolute Motion

A diagram of a base-excited system is shown on Figure 3.8. The coordinate $x(t)$ represents the absolute motion of the mass given the base motion $y(t)$. From the free-body diagram of Figure 3.8 and applying the Newton's second law, the equation of motion is represented as (3.39).

$$m\ddot{x} + c\dot{x} + kx = ky + c\dot{y} \tag{3.39}$$

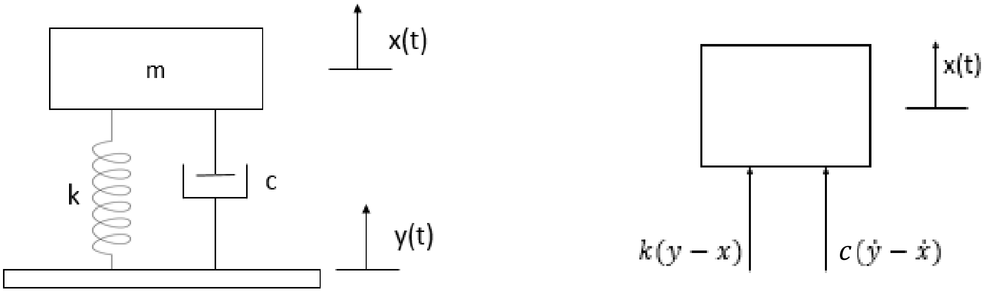

Figure 3.8 - Base-excited system

Assuming that both base motion and response are harmonic in (3.40).

$$\begin{aligned} y(t) &= Y_0 e^{iwt} \\ x(t) &= X e^{iwt} \end{aligned} \tag{3.40}$$

The transfer function and the gain function are derived in the same manner as for the force-excited system. The transfer function is expressed in (3.41).

$$H(\omega) = \frac{k + ic\omega}{(k - m\omega^2) + icw} \tag{3.41}$$

After calculating the modulus of the transfer function and employing the definitions for ξ, ω_n and c_c it is possible to obtain the nondimensional gain function in (3.42)

$$\frac{X_0}{Y_0} = \sqrt{\frac{1 + (2\xi r)^2}{(1 - r^2)^2 + (2\xi r)^2}} \tag{3.42}$$

The equation above can be also being interpreted as the gain function for acceleration output given acceleration input. It is actually more common to use it in this form. On Figure 3.9, it is shown the gain function for absolute displacement or acceleration for the base-excited system.

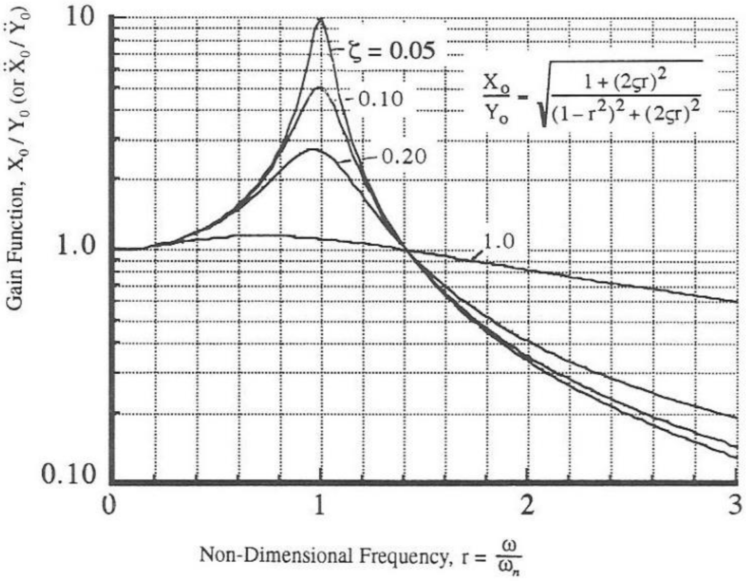

Figure 3.9 - Gain function for base-excited system (absolute displacement)[17]

Relative Motion

Considering the same diagram of a base-excited system shown on Figure 3.8. The coordinate $x(t)$ represents the absolute motion of the mass given the base motion $y(t)$. Now the response variable under consideration is the relative displacement in (3.43).

$$z(t) = x(t) - y(t) \tag{3.43}$$

Thus the new equation of motion is represented in (3.44):

$$m\ddot{z} + \dot{z} + kz = -m\ddot{y} \tag{3.44}$$

Assuming that both base motion and response are harmonic, and following the procedures described above, the new transfer function is represented in (3.45).

$$H(\omega) = \frac{m\omega^2}{(k - m\omega^2) + icw} \tag{3.45}$$

The gain function in a nondimensional form is obtained following the procedures described above and it is represented in (3.46).

$$\frac{Z_0}{Y_0} = \frac{r^2}{\sqrt{(1-r^2)^2 + (2\xi r)^2}} \tag{3.46}$$

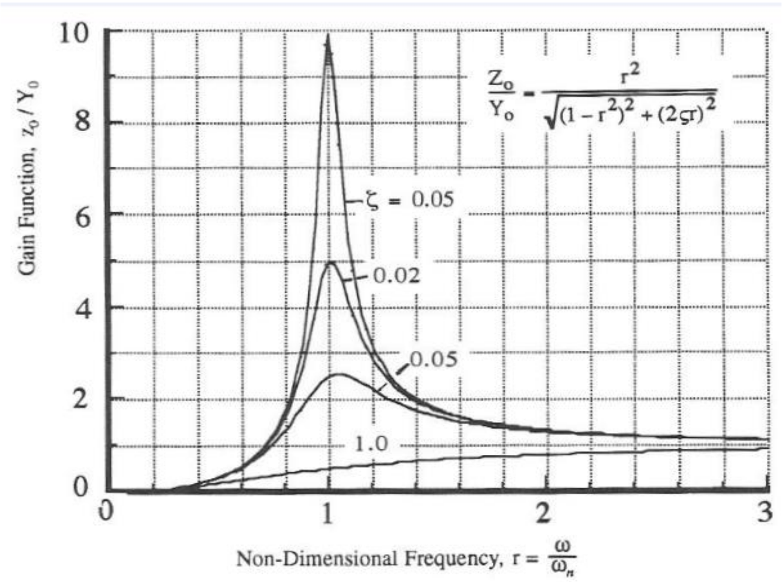

Figure 3.10 - Gain function for base-excited system (relative displacement)[17]

3.2 Random Vibration Analysis Background

3.2.1 Types of signal

Signals can be classified as stationary or nonstationary. If statistical properties remain constant with time, the signal is considered to be stationary. Stationary vibration is an idealized concept. Nevertheless, certain types of random vibration may be regarded as reasonably stationary [18].

On the following flowchart it is presented different stationary types of signal in which is included stochastic ones, or often called random.

$$Test\ Signal\ (Stationary)\begin{cases} Deterministic\begin{cases} Periodic\begin{cases} Monofrequent \\ Multifrequent \\ Pseudo-stochastic \end{cases} \\ Transient\begin{cases} Pulse\ type \\ Step\ type \\ Sine\ sweep \end{cases} \end{cases} \\ Stochastic\ (Random)\begin{cases} White\ Noise \\ Broadband \\ Narrowband \end{cases} \end{cases}$$

Table 3.1 gives a practical example of each stationary type signal:

Table 3.1 - Types of stationary signals

Types of Signal	Illustration
Mono-frequent time signal	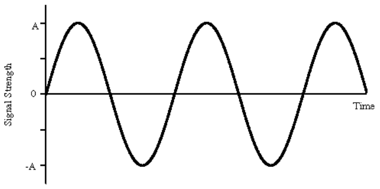 Figure 3.11 - Mono-frequent time signal
Multi-frequent time signal (Time vs. Amplitude)	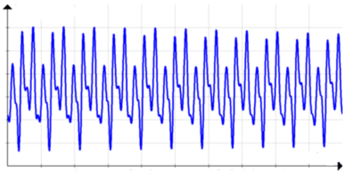 Figure 3.12 - Multi-frequent time signal
Pseudo-stochastic	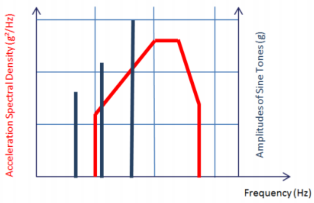 Figure 3.13 - Pseudo-stochastic[19]
Pulse type time signal	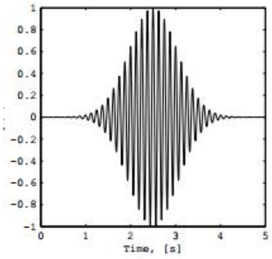 Figure 3.14 - Pulse type time signal
Step type time signal	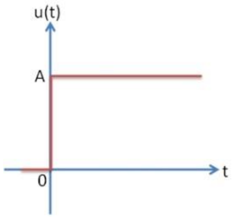 Figure 3.15 - Step type time signal
Sine sweep time signal	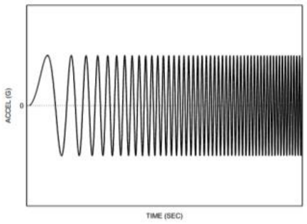 Figure 3.16 - Sine sweep time signal[20]

Types of Signal	Illustration
White noise (frequency domain)	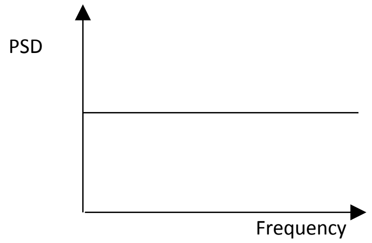 Figure 3.17 - White noise (frequency domain)
Broad-band (frequency domain)	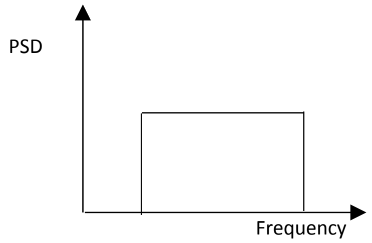 Figure 3.18 - Broad-band (frequency domain)
Narrow-band (frequency domain)	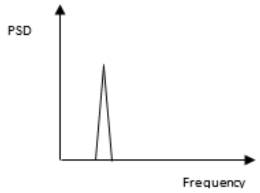 Figure 3.19 -Narrow-band (frequency domain)

3.2.2 Random vibration

Random vibration analysis is probabilistic in nature because both input and output quantities represent only the probability that they take on certain values. Thus, it is not possible to express its amplitude in terms of a deterministic mathematical function.

Random vibration can be broadband or narrowband. The difference between them is the range of frequencies contained in the signal. Narrow-banded signals contain only a narrow range of frequencies, whereas broad-banded signals contain a wide range of frequencies. A white-noise signal is a special case which implies that the time signal comprises a whole series of harmonics with exactly the same amplitude, but with purely random phase angles.

The most obvious characteristic of random vibration is that it is no periodic. A knowledge of the past history of random motion is adequate to predict the probability of occurrence of various acceleration and displacement magnitudes, but it is not sufficient to predict the precise magnitude at a specific instant [21].

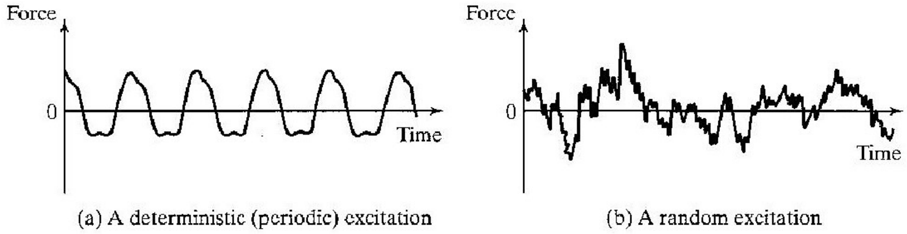

Figure 3.20 - Deterministic and Random Excitation [22]

Random vibration is a varying waveform whereas sinusoidal or harmonic vibration occurs at distinct frequencies, in other words random vibration contains all frequencies simultaneously. However random and sine vibration testing cannot be directly compared.

In the past, most vibration was characterized in terms of sinusoids. Nowadays, most vibration is correctly understood to be random in nature and because of that it is the best way to characterize them.

Table 3.2- Differences between sinusoidal and random vibration

Harmonical Vibration	Random Vibration
- Oscillation	- Oscillation
- Predictable	- Unpredictable Instantaneous Magnitudes
- Single Frequency	- All Frequencies at Once
- Pure Tone/Motion	- Statistics
	- Spectral Density
	- Probability Distribution

One of the purposes of using random vibration tests in industry is to prevent failures. The desire is to find out how a particular equipment may fail because of multiple environmental vibrations it may encounter. Testing the equipment to failure provides important information about its design weaknesses and ways to improve it. Random vibration is more realistic than sinusoidal vibration testing because random simultaneously includes all the forcing frequencies and simultaneously excites all the equipment resonances. Under a sinusoidal test, a particular resonance frequency might be found for one part of the device under test and at a different frequency another one may resonate. Arriving at separate resonance frequencies at different times may not cause any kind of failure, but when both resonance frequencies are excited at the same time, a failure may occur. Random testing will cause both resonances to be excited at same time, because all frequency components in the testing range will be present at the same time [23]. This is one of the big advantages of random vibration testing.

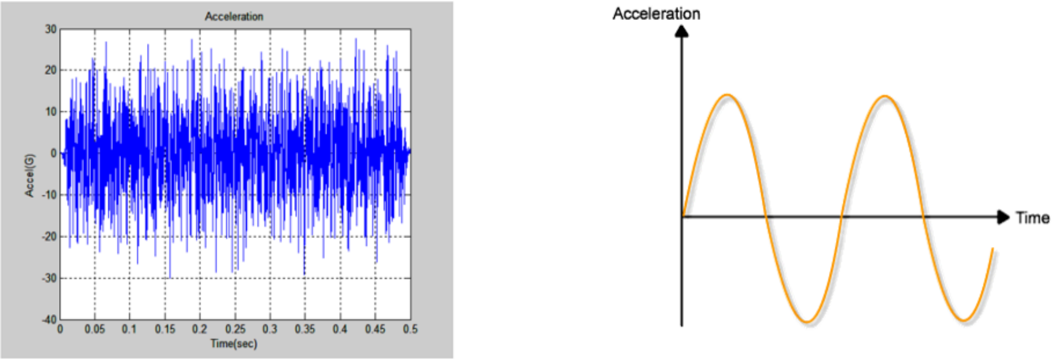

Figure 3.21- Random and Sine Waves[24]

In order to clarify the concept of spectrum, the idea can be explained by an experimental test. According to the experience shown on Figure 3.22 a white light passed through a prism produces a spectrum of colors. Analogously a random vibration test excites all the frequencies in a defined spectrum at any given time. So random vibration resembles to white light and sinusoidal vibration resembles to a one colored laser beam. Another analogy, this one applied in music, can be clarified in order to simplify the concept. Playing a single piano key produces sinusoidal vibration, on other hand playing all the piano keys simultaneously produces a signal which approximates random vibration.

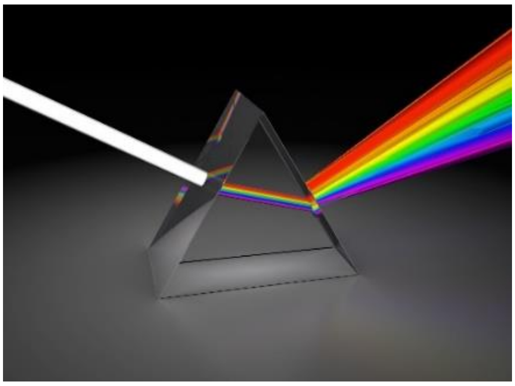

Figure 3.22- White Light Passed Through a Prism

Fig 2.23 has the purpose of clarifying the white light analogy by dividing the random signal represented as the white light in multiple constant frequency signals represented as different colors.

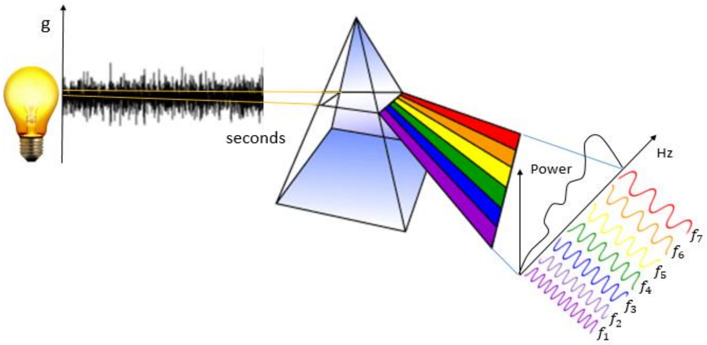

Figure 3.23 - Random vibration signal analogy with white light

Even though random time signals are not periodic their amplitude spectrum show that time signals are statistically stationary. This means the statistics of the signal does not change through time. Another assumption is that the random signal is assumed to be ergodic, this means we could take a sample across a large set of similar signals at a given time, and expect to get the same mean value and standard deviation. It was proven that measuring gusting wind loads on a wind turbine at equal periods of time, all time signals were different in time domain. However, Power Spectral Density (PSD) plots in frequency domain were identical [25].

3.2.3 Gaussian distribution

It is assumed that the random signal follows a Gaussian distribution. The probability density function of a Gaussian distribution is calculated from the following equation whereas x is a continuous random variable, $\bar{X}$ is the mean and σ is the standard deviation. The standard deviation and the mean vary with time for a nonstationary process but are constant for a stationary one. Even though random time signals are not periodic their amplitude spectrum show that time signals are statistically stationary. This means the statistics of the signal does not change through time. A study carried out by Hafpenny [26] shows that measuring gusting wind loads on a wind turbine at equal periods of time, all time signals were different in time domain and the plots in frequency domain were very similar. Thus, random vibration is assumed to be a stationary process that follows a Gaussian distribution in (3.47).

$$p(x) = \frac{1}{\sigma\sqrt{2\pi}} e^{-\frac{1}{2}\left(\frac{x-\bar{X}}{\sigma}\right)^2} \tag{3.47}$$

The curve of the Gaussian distribution has the bell-shaped shown on Figure 3.24:

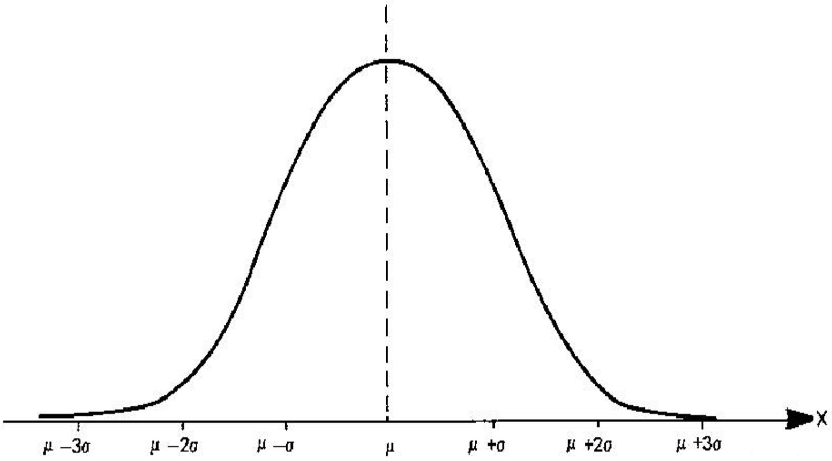

Figure 3.24 - Gaussian distribution [27]

Since random vibrations theory is based on the probability density function (PDF) of a Gaussian process, it is important to understand its statistical properties. Random vibration analysis is purely probabilistic, so both input and output quantities represent only the probability that they take on certain values. In the last chapter of this dissertation the results in terms of displacement, velocity and acceleration will be presented as σ-values. These values represent the amplitude of the signal, on the following Table 3.3 and Table 3.4 are shown the probabilities of those random amplitudes.

Table 3.3 - Probability of random amplitudes (1)

Statement	Probability Ratio	Percent Probability
$-\,\sigma < x < +\,\sigma$	0.6827	68.27%
$-2\,\sigma < x < +\,2\,\sigma$	0.9545	95.45%
$-3\,\sigma < x < +\,3\,\sigma$	0.9973	99.73%

Table 3.4 - Probability of random amplitudes (2)

Statement	Probability Ratio	Percent Probability
$\lvert x\rvert > 1\,\sigma$	0.3173	31.73%
$\lvert x\rvert > 2\,\sigma$	0.0455	4.55%
$\lvert x\rvert > 3\,\sigma$	0.0027	0.27%

3.2.4 Statistical Properties of Random Vibration

The following paragraphs are referred to statistical properties applied in random vibration analyses. It is important to understand how the root mean square value is related to the standard deviation of random signals [28].

The mean square value $\overline{X^2}$ can be determined from a time history signal $x(t)$. $x(t)$ is a generic signal and it can represent displacement, velocity or acceleration. The duration of the time history is represented as T. The mean square value can be computed for either continuous or discrete signals by the following equations (3.48) and (3.49), respectively.

$$\overline{X^2} = \lim_{T\to\infty} \frac{1}{T} \int_0^T [x(t)]^2\, dt \tag{3.48}$$

$$\overline{X^2} = \lim_{N\to\infty} \frac{1}{N} \sum_i^N {x_i}^2 \tag{3.49}$$

The Root Mean Square (RMS) value is simply the square root of the mean square value, as represented in (3.50).

$$RMS = \sqrt{\overline{X^2}} \tag{3.50}$$

The fluctuation about the mean value is described by the variance represented as σ^2. The standard deviation is represented as σ. The mean value is represented as $\bar{X}$. Variance can be calculated for either continuous or discrete signals by the equations (3.51) and (3.52), respectively.

$$\sigma^2 = \lim_{T\to\infty} \frac{1}{T} \int_0^T [x(t) - \bar{X}]^2\, dt \tag{3.51}$$

$$\sigma^2 = \lim_{N\to\infty} \frac{1}{N} \sum_i^N (x_i - \bar{X})^2 \tag{3.52}$$

From the equations (3.51) and (3.52) it is possible to deduce the following relationship in (3.53).

$$\overline{X^2} = \sigma^2 + \bar{X}^2 \tag{3.53}$$

Assuming that random signals have a mean value equal to zero, it is possible to obtain (3.54).

$$\Longrightarrow RMS = \sigma \tag{3.54}$$

In order to clarify the concepts, concluding remarks are explained in this paragraph. A random signal can be converted into a histogram by dividing the signal amplitude into n subdomains and counting the number of times the signal amplitude is inside each subdomain. The shape of the histogram of a random signal converges to a Gaussian distribution as n tends to infinitive. The histogram in Figure 3.25 - Transformation of a time signal in a histogram shows that the random vibration signal has a tendency to remain near its mean value, which in this case is zero. Random vibrations are expressed in terms of probability of occurrence. Figure 3.25 - Transformation of a time signal in a histogram shows a white noise random signal converted into a histogram. In this figure, x represents acceleration expressed in g unit. This unit is obtained by dividing a signal representing acceleration and expressed in m/s^2 by 9.81.

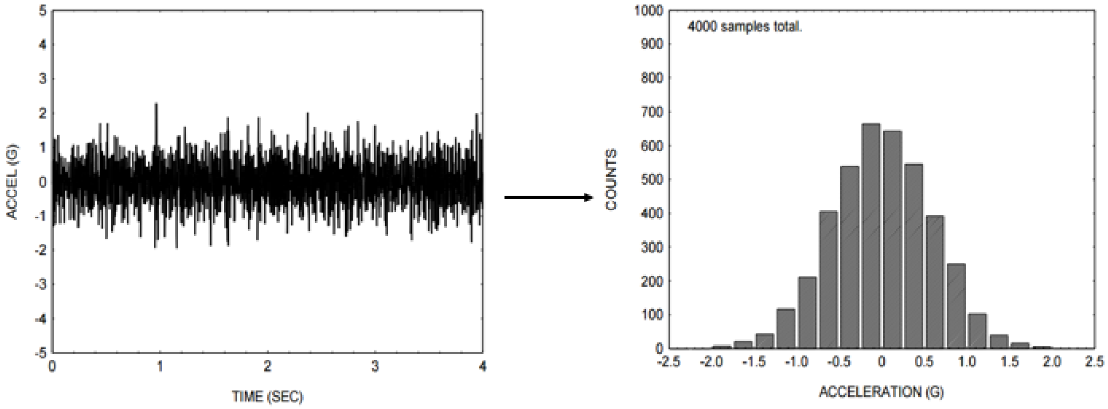

Figure 3.25 - Transformation of a time signal in a histogram

This histogram can be converted to a probability density function by dividing each bar by the total number of samples. The resulting probability density function is an approximated Gaussian density function. [18] Considering that random vibration theory is based on the assumption that the signal follows a Gaussian distribution, it is possible to determine the probability that an amplitude will occur inside or outside certain limits. Thus, considering these statistical properties and assumptions, the root-mean-square value is equal to the standard deviation as shown in Figure 3.26.

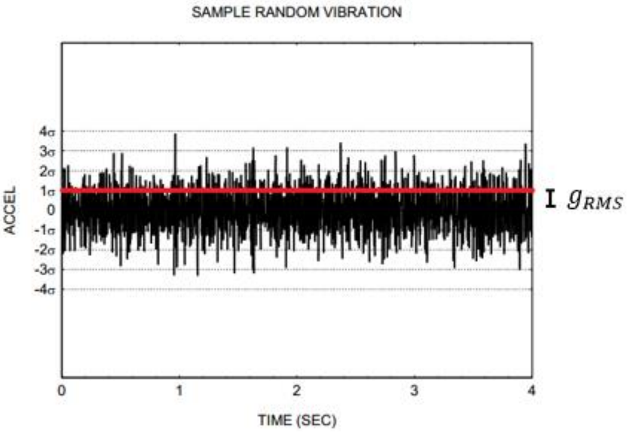

Figure 3.26 - Equivalence between g_{rms} and σ

As a concluding remark, Figure 3.27 simplifies the statistical properties of a random vibration signal in time domain assumed as stationary and ergodic.

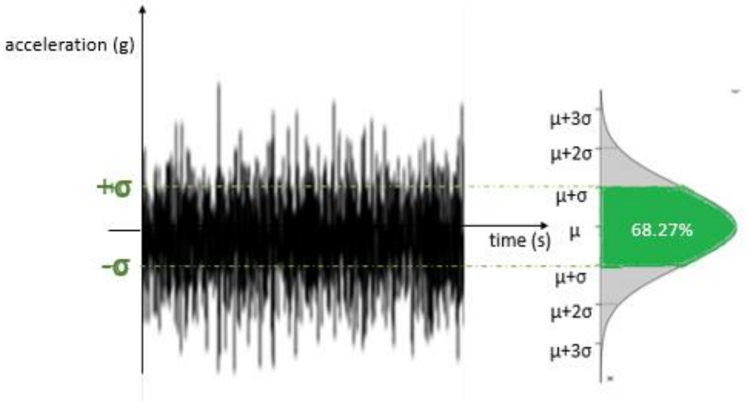

Figure 3.27 - Statistical Properties of a Random Vibration Signal

3.2.5 How to calculate PSD

Time histories can be represented in the frequency domain in different formats. Power Spectral Density (PSD) is the most effective format to analyze random vibration. A PSD analysis is a sophisticated and extremely useful form to measure vibration. PSD functions may be calculated via three distinct methods.

The first one is based on measuring the RMS value of the amplitude in successive frequency bands, where the signal in each band has been bandpass filtered. This technique used by electrical engineers near the year of 1940 actually generated what nowadays is known by PSD functions. They were interested to see the amplitude spectrum based on measured randomly varying signals [17]. Since digital acquisition system had not been invented yet, they had to invent a procedure using analog filters. The waveform was iteratively filtered to a signal with only a single frequency. The filtered signal's mean-square value was then measured and plotted. This was called the 'power' at that frequency. However, in practice, it is impossible to produce a physical filter that outputs only a single frequency; the output is actually a signal which is dominated within a narrow bandwidth Δf. The PSD gets his name from the fact that these electrical engineers who invented this technique were interested in electrical power, plotting a spectrum of frequencies and displaying the plot as a histogram or density function.

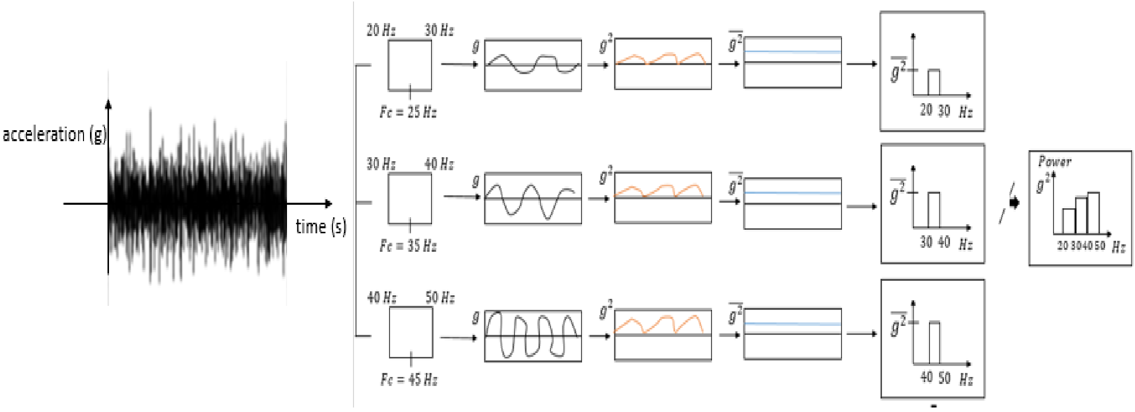
acceleration (g)
time (s)
20 Hz
30 Hz
Fc = 25 Hz
30 Hz
40 Hz
Fc = 35 Hz
40 Hz
50 Hz
Fc = 45 Hz
g
g^2
$\overline{g^2}$
20 30 Hz
30 40 Hz
40 50 Hz
Power
20 30 40 50 Hz

Figure 3.28 - Spectral analysis procedure using analog filters

However, this plot of Power is ambiguous. It was proven by Wayne Tustin [29] that the bandwidth influences the Power in g^2 units. The measured power was divided by the bandwidth Δf to cancel its influence on data producing the units of $units^2/Hz$.

It was extremely important to normalize data in order to quantify vibration levels with a unique and standard unit of measurement. The reason why vibration unit of measurement is g^2/Hz is explained with a practical example which was performed in a laboratory.

For this experimental test, it was needed an accelerometer attached to a small electrodynamic shaker and suitable signal conditioner, a band-pass filter and a true RMS readout voltmeter.

The results of a filtered signal measurement with a center frequency (fc) of 1000 Hz and several bandwidths are shown on Table 3.5:

Table 3.5 - Influence of the bandwidth filter on measurements

$fc = 1000\ Hz$	$fc = 1000\ Hz$	$fc = 1000\ Hz$
$Bandwidth = 160\ Hz$	$Bandwidth = 40\ Hz$	$Bandwidth = 10\ Hz$
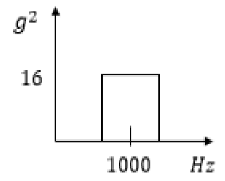	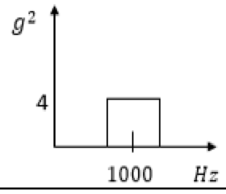	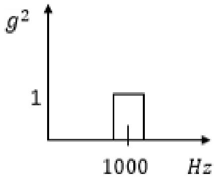
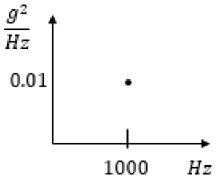	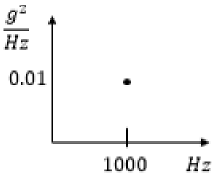	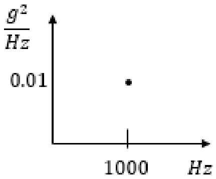

It was concluded that when measuring the exact same signal with g^2 units, the results were not uniform. It was desirable to normalize data to a common value to compensate the difference of the analyzer bandwidth, thus eliminating ambiguity. This unit of $\boldsymbol{g_{RMS}^2/Hz}$ is nowadays the standard unit to measure vibration and it also is the unit used for quantify Power Spectral Density, in this specific case for Acceleration Spectral Density. The standard unit to quantify Displacement Spectral Density is mm^2/Hz and to quantify Velocity Spectral Density is $\left(\frac{mm}{s}\right)^2/Hz$.

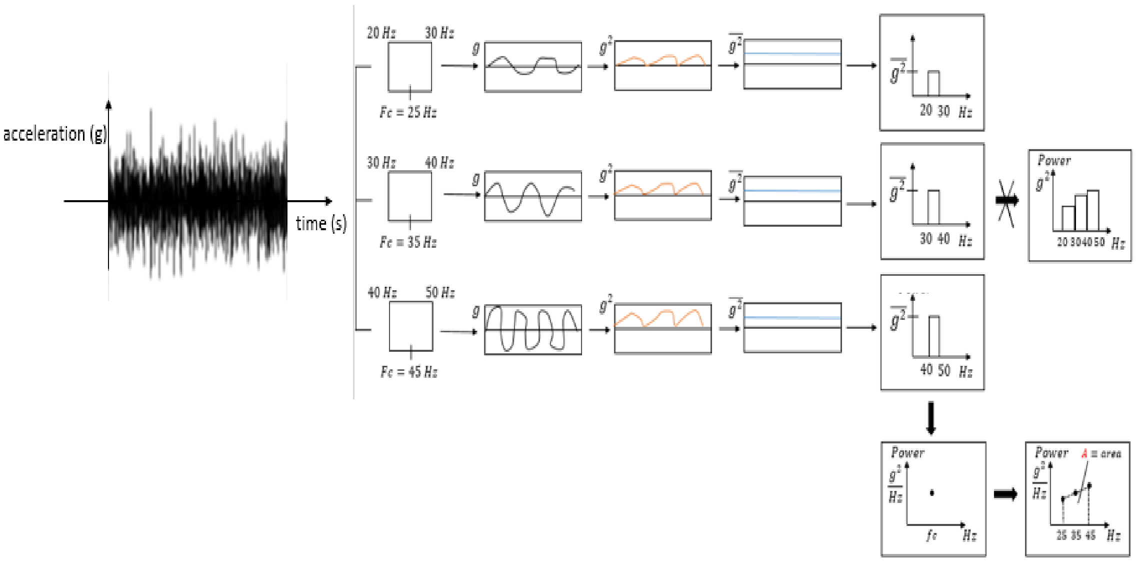

Figure 3.29 - Calculation of a Power Spectral Density in a standardized unit of measure

There are two advantages of measuring the signal in this way: the bandwidth of the filter does not influence the level of power spectral density and due to the statistical properties and assumptions of the random signal, the area under the spectral density function is equal to the root mean square of the waveform.

Therefore, it is possible to quantify and analyze random vibration. Using this method, various laboratories, firms, and agencies can communicate regarding random vibration intensity.

Nowadays this method of obtaining PSD is not used very often, it is more usual to take advantage of computers to calculate the PSD plot directly from digitized time signals. In this analysis, it is applied the Fast Fourier Transform algorithm. In the Appendix A, it is presented the Fourier Transform background. The PSD is calculated from the technique shown on the following flowchart:

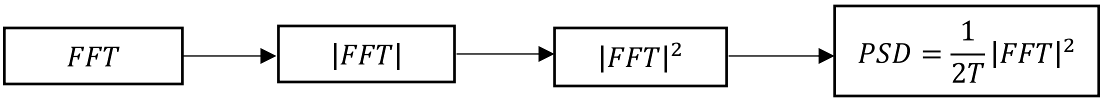

Figure 3.30 - PSD calculation technique

Firstly, it is performed the FFT to the time signal waveform decomposing it into its constituent harmonics described in terms of amplitude, frequency and phase. The Amplitude Spectrum which is a plot of amplitude vs. frequency is obtained after calculating the modulus of the complex numbers. The Power Spectrum is obtained by squaring the amplitude spectrum. Finally, dividing by 2 times the duration of the time signal in seconds it is obtained the PSD which, actually represents the density function of the mean of the amplitude-squared spectrum. In the Appendix A, the Fourier Transform background is comprehensively explained.

There is another method to obtain PSD which is based on taking the Fourier transform of the autocorrelation function. This technique is more theoretical and it is known as the Wierner-Khintchine Theorem [30].

3.2.6 The meaning of g_{RMS} in sine and random vibration

The need to use material that was developed to harmonic, also referred as sine by the Military Standard [31], requirements has generated a demand to understand and to determine equivalence between sine and random vibration. A general definition of equivalence is not feasible since both characterizations of vibration are based on distinctly different sets of mathematics. The details of material dynamic response have to be known in order to compare the effects of given random and sine vibration on material.

Despite dimensional units are quantified as typically acceleration in standard gravity (g) on both tests, these are not equivalent and cannot be directly compared. Peak acceleration of sine measured in g is not equivalent to the result measured in g of a random test, so both values of g_{RMS} are also not comparable. On one hand, g_{RMS} sine acceleration is the root mean square of a time signal at one specific frequency. On the other hand, random g_{RMS} is the square root of the area under the spectral density curve including all frequencies simultaneously.

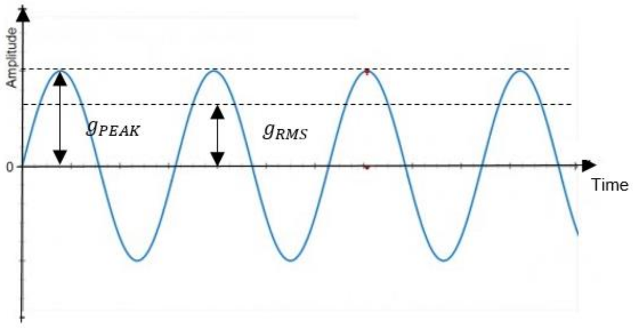

$$g_{PEAK} = \sqrt{2} \cdot g_{RMS}$$

Figure 3.31 – g_{rms} on a sine test

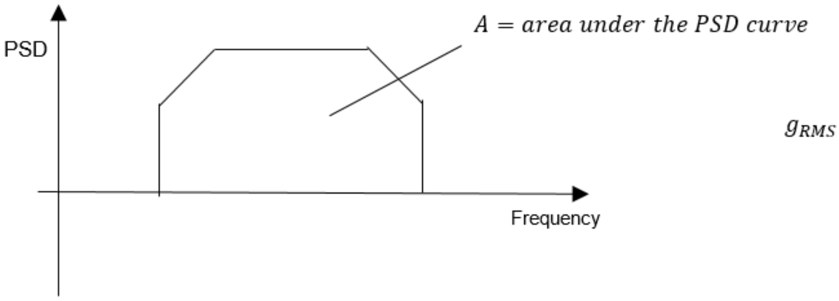

$$g_{RMS} = \sqrt{A}$$

Figure 3.32 – g_{rms} on random test

3.2.7 Dynamic analysis

The dynamic analysis methodology is based on three stages as shown on Figure 3.33:

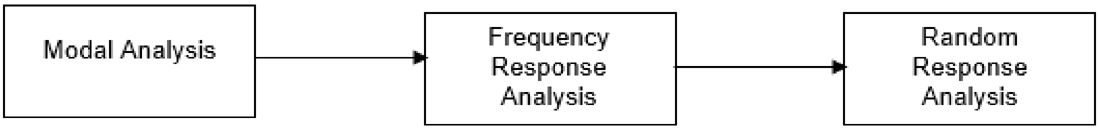
Modal Analysis
Frequency Response Analysis
Random Response Analysis

Figure 3.33 - Dynamic Analysis Methodology

The purpose of carrying out a modal analysis is to obtain the natural frequencies and normal modes of vibration of the structure. Considering the equation of motion in the absence of applied external forces and damping in (3.55).

$$[M]\{\ddot{x}\} + [K]\{x\} = 0 \tag{3.55}$$

And assuming a sinusoidal response wherein $\bar{x}$ represents the amplitude of the sinusoidal vibration in equations (3.56).

$$\begin{cases} x = \bar{x} \sin \omega t \\ v = \dot{x} = \bar{x}\omega \cos \omega t \\ a = \ddot{x} = -\bar{x}\omega^2 \sin \omega t \end{cases} \tag{3.56}$$

Replacing the sinusoidal response in the equation of motion (3.55):

$$\begin{gathered} (-\omega^2[M]\bar{x} + [K]\bar{x}) \sin(wt) = 0 \\ \Rightarrow (-\omega^2[M] + [K])\bar{x} = 0 \end{gathered} \tag{3.57}$$

Equation (3.57) represents the formulation of a generalized eigenproblem. The natural frequencies are represented by the eigenvalues and the normal modes of vibration are represented by the eigenvectors.

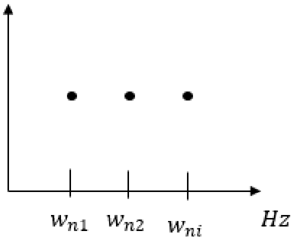

Figure 3.34 - Eigenvalues solution

The frequency response analysis is carried out by exciting the structure with a unit of acceleration over frequency range using the saved eigenvalues. This excitation is similar to a Dirac Impulse in time domain. This excitation generates the transfer function, H_f.

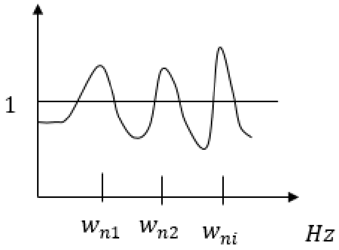

Figure 3.35 - Transfer Function H_f.

The random response analysis is essentially a post processing exercise on the frequency response analysis. The PSD response is obtained from the PSD input and the transfer function calculated from the previous stage trough equation (3.58).

$$PSD_{out} = |Hf|^2 . PSD_{in} \tag{3.58}$$

The formulation above is carried out for each selected point of the structure and for every requested degree of freedom. The purpose of the following figures is to clarify how it is obtain the PSD response for every degree of freedom.

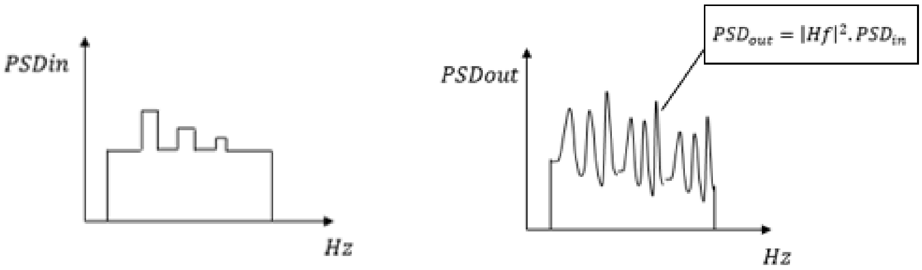
PSDin
Hz
$PSD_{out} = |Hf|^2.PSD_{in}$
PSDout
Hz

Figure 3.36 - PSD input and PSD response

4 Aeronautic Regulation

4.1 Scope of change

The purpose of vibration study lies in the integration of a new digital instrument panel. This structural change will be implemented on the Lockheed Martin C-130H aircraft. The aircraft in consideration is shown in Figure 4.1.

Figure 4.1- Lockheed Martin C-130H

Modification consists in replacing the cockpit on the aircraft. The outside of the aircraft remains identical whereas the inside is quite different after modification. The following pictures provide some clarity on the contrast between older and more recent versions of panel models. In Figure 4.2, it is shown an unmodified analog instrument panel. In Figure 4.3, it is shown a digital instrument panel version integrated with latest technology.

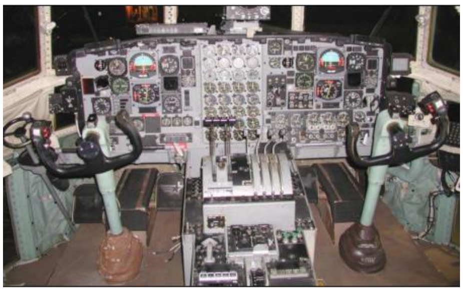

Figure 4.2 - Analog Instrument Panel

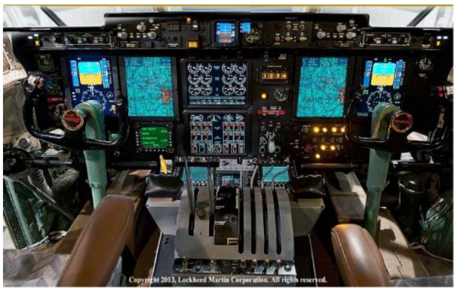
Copyright 2013, Lockheed Martin Corporation. All rights reserved.

Figure 4.3 - Digital Instrument Panel

Structural modifications imply testing the equipment. Tests should meet international standards and certifications. This procedure is essential in order to approve the modification. One of the main concerns on the modified panel is its level of vibration. The aim is to ensure that possible undesirable vibrations on the modified panel are avoided. It is important to guarantee that the pilot´s capability of reading the instruments is not affected.

Several studies about the perception of flight information from aircraft displays have been presented. The pilot´s perception of the information provided from the displays is crucial to secure a safe flight. The accuracy and the speed of the perception process in an interface of man and machine have been studied by Hosman and Muider [32]. Suzanne Smith studied the human perception of vibration aboard a military propeller aircraft [33]. Another study in the area of perspective aircraft displays has been presented by Anderson and Alm. The research focus was to explore the possibilities to understand symbol relations in the 3D environment [34]. A study about the readability of vertically vibrating aircraft displays has been presented by Andersson and Hofsten [35].

4.2 Regulations

In order to approve a process of aircraft components modifications, it is fundamental that these components are tested. Tests which meet international standards and certifications are essential for a part being considered acceptable. Currently these standards are managed by international organizations. For the purpose of getting a better understanding of vibration testing, MIL-STD-810G standard is reviewed to provide a basis for the testing process. The following paragraphs summarize this standard. Another standard RTCA-DO-160E [36] is usually also taken into account as a reference. However, RTCA-DO-160E recommends a sinusoidal vibration test and will not be applied in this dissertation.

4.2.1 MIL-STD-810G

MIL-STD-810 is a United States Military Standard which suggests tailoring an equipment's environmental design and test limits to the conditions that it will experience throughout its service life, and establishing test methods that replicate the effects of environments on the equipment rather than imitating the environments themselves. It has been revised several times over the years, the most recent was in 2008 resulting in the MIL-STD-810G version of the standard. The vibration chapter is on Method 514.6 and provides important information such as method selections, procedures and parameter levels based on tailoring processes. Information is divided into annexes depending on the life phase, platform and category. For each category there is a test which is more recommendable.

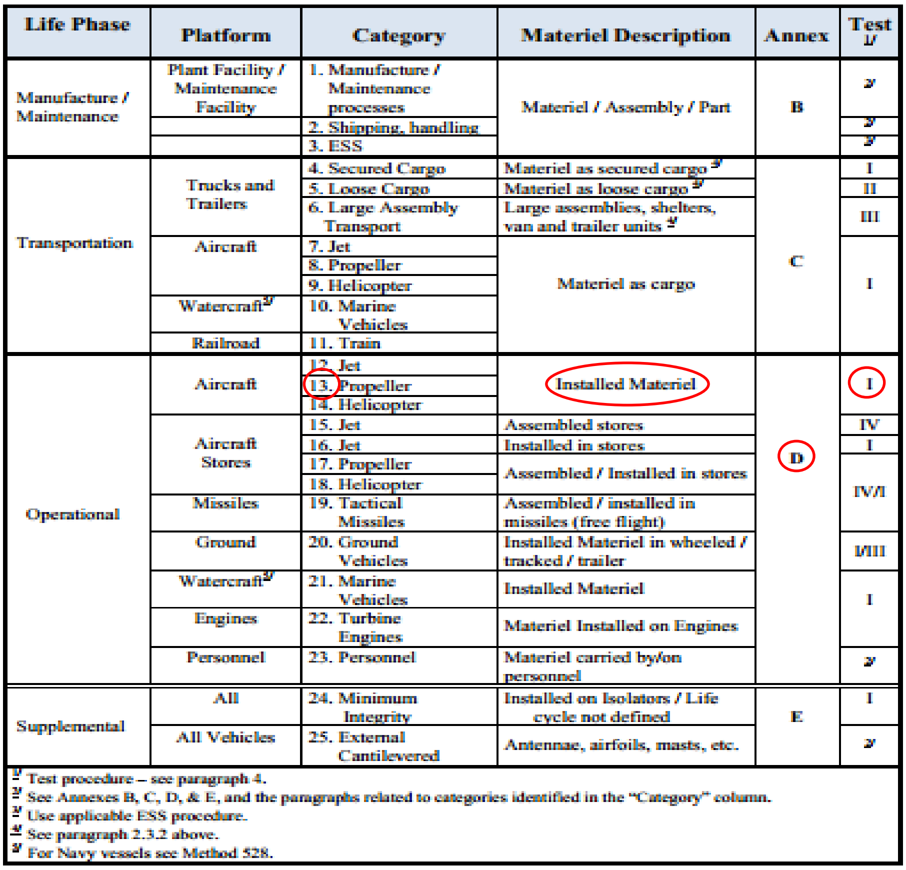

Life Phase	Platform	Category	Materiel Description	Annex	Test [1]
Manufacture / Maintenance	Plant Facility / Maintenance Facility	1. Manufacture / Maintenance processes	Materiel / Assembly / Part	B	[2]
		2. Shipping, handling			[2]
		3. ESS			[3]
Transportation	Trucks and Trailers	4. Secured Cargo	Materiel as secured cargo [4]	C	I
		5. Loose Cargo	Materiel as loose cargo [4]		II
		6. Large Assembly Transport	Large assemblies, shelters, van and trailer units [4]		III
	Aircraft	7. Jet	Materiel as cargo		I
		8. Propeller			
		9. Helicopter			
	Watercraft[5]	10. Marine Vehicles			
	Railroad	11. Train			
Operational	Aircraft	12. Jet	Installed Materiel	D	I
		13. Propeller			
		14. Helicopter			
	Aircraft Stores	15. Jet	Assembled stores		IV
		16. Jet	Installed in stores		I
		17. Propeller	Assembled / Installed in stores		IV/I
		18. Helicopter			
	Missiles	19. Tactical Missiles	Assembled / installed in missiles (free flight)		
	Ground	20. Ground Vehicles	Installed Materiel in wheeled / tracked / trailer		I/III
	Watercraft[5]	21. Marine Vehicles	Installed Materiel		I
	Engines	22. Turbine Engines	Materiel Installed on Engines		
	Personnel	23. Personnel	Materiel carried by/on personnel		[2]
Supplemental	All	24. Minimum Integrity	Installed on Isolators / Life cycle not defined	E	I
	All Vehicles	25. External Cantilevered	Antennae, airfoils, masts, etc.		[2]

[1] Test procedure – see paragraph 4.
[2] See Annexes B, C, D, & E, and the paragraphs related to categories identified in the "Category" column.
[3] Use applicable ESS procedure.
[4] See paragraph 2.3.2 above.
[5] For Navy vessels see Method 528.

Figure 4.4 - Vibration environment categories

The Category 13 has inherent information about the instrument panel of propeller aircrafts as it is the case of the C-130H. This category is focused on material installed in propeller aircrafts. The most desirable test for this category is the procedure I designated as General Vibration. Procedure II is referred to Loose Cargo Transportation, and Procedure III is applied to Large Assembly Transportation. Procedure IV is designated for Assembled Aircraft Store Captive Carriage and Free Flight. Before starting a test, it is recommended to ensure that test details such as procedures, test item configuration, levels, durations, vibration exciter control strategy, failure criteria and instrumentation requirements were reviewed.

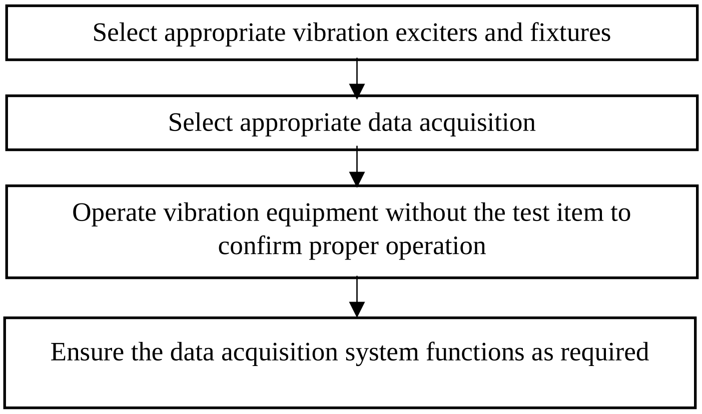
Select appropriate vibration exciters and fixtures
Select appropriate data acquisition
Operate vibration equipment without the test item to confirm proper operation
Ensure the data acquisition system functions as required

Figure 4.5- Preparation for test - preliminary steps

To carry out the appropriate desired test which is the procedure I designated as General Vibration. For this procedure, the test item is secured to a vibration exciter, and vibration is applied to the test item as an input at the interface between fixture and test item. It is necessary to follow several steps to perform the test properly:

- Conduct a fixture modal survey
- Mount the test item to the test fixture properly
- Install control transducers in agreement with the indicated control strategy
- Conduct a test item modal survey
- Apply the required vibration levels to the interface between test item and fixture
- Inspect the test item, fixture, vibration exciter and instrumentation. If failure, wear, looseness, or other anomalies are found, proceed in accordance with the test interruption recovery procedure
- Repeat all previous steps for each required excitation axis
- Remove test item from the fixture and inspect it

4.2.1.1 Propeller vibration exposure

In these cases, the propellers mainly cause vibration. Figure 4.6 shows the PSD input which is designated as a mixed broadband and narrowband signal. This input is appropriate when vibration environment is characterized by quasi-periodic excitation from rotating mechanisms which is the case of the propellers. This type of excitation is called source dwell and is characterized by a broadband random vibration with higher level narrowband random. The narrowband bandwidths are plus and minus five per cent of the center of the excitation frequency. This values was chosen because the enveloped C-130 and P-3 aircraft data in g^2/Hz form exhibited approximately this bandwidth [31].

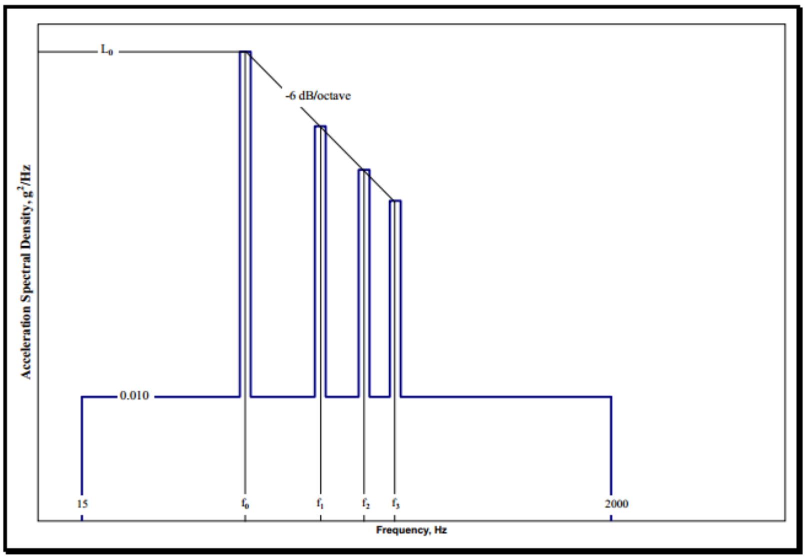

Figure 4.6 - Propeller aircraft vibration exposure (1)[31]

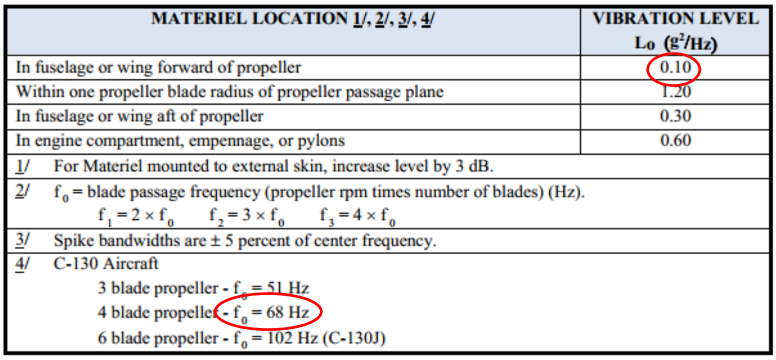

MATERIEL LOCATION 1/, 2/, 3/, 4/	VIBRATION LEVEL Lo (g^2/Hz)
In fuselage or wing forward of propeller	0.10
Within one propeller blade radius of propeller passage plane	1.20
In fuselage or wing aft of propeller	0.30
In engine compartment, empennage, or pylons	0.60

1/ For Materiel mounted to external skin, increase level by 3 dB.

2/ f_0 = blade passage frequency (propeller rpm times number of blades) (Hz).
$f_1 = 2 \times f_0$ $f_2 = 3 \times f_0$ $f_3 = 4 \times f_0$

3/ Spike bandwidths are ± 5 percent of center frequency.

4/ C-130 Aircraft
3 blade propeller - f_0 = 51 Hz
4 blade propeller - f_0 = 68 Hz
6 blade propeller - f_0 = 102 Hz (C-130J)

Figure 4.7 - Propeller aircraft vibration exposure (2)[31]

The values of the center frequencies are represented in (4.1).

$$\begin{cases} Fc_0 = 68\ Hz \\ Fc_1 = 2\times 68 = 136\ Hz \\ Fc_2 = 3\times 68 = 204\ Hz \\ Fc_3 = 4\times 68 = 272\ Hz \end{cases} \tag{4.1}$$

The vibration input shown is a log-log plot of acceleration spectral density expressed in g^2/Hz over frequency expressed in Hz. The slope is expressed in $dB/octave$. An octave is the interval between one frequency and another differing by 2:1. The decibel (dB) is a logarithmic unit used to express the ratio of two values of power or intensity. In this case, +/- 3 dB represents the increase or decrease of the Power Spectral Density value by a factor of 2. On the following formula are shown the calculation of PSD peak values for each center frequency with n ranging from integers 1 and 3. It is showed the calculation for $n = 1$.

Table 4.1 - ASD level of vibration calculation

General	For n = 1
$\#\mathrm{Octaves} = \frac{\log\left(\frac{F_n}{F_0}\right)}{\log(2)}$	$\Rightarrow \frac{\log\left(\frac{136}{68}\right)}{\log(2)} = 1$
$x = \left(\frac{\mathrm{dB}}{\mathrm{Octave}}\right) \times \#\mathrm{Octaves}$	$\Rightarrow -6 \times 1 = -6$
$\mathrm{ASD}_n = \mathrm{ASD}_0 \times (10)^{\frac{x}{10}}$	$\Rightarrow 0.10 \times (10)^{\frac{-6}{10}} = 0.025\ \frac{g^2}{\mathrm{Hz}}$

Therefore, applying these calculations for all center frequencies, the MIL-STD-810 standard indicates a vibration exposure which is shown on Figure 4.8. This PSD level of vibration will be applied as an input in all carried out simulations.

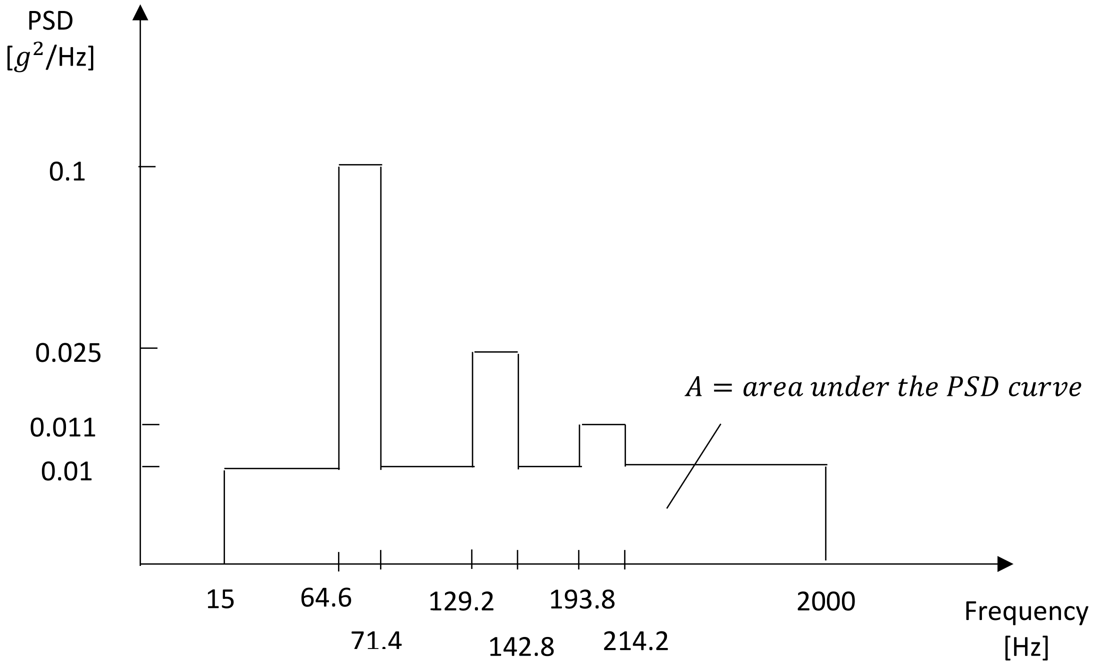

Figure 4.8 - Propeller vibration exposure that will be applied as input in all simulation analysis

4.2.1.2 Tolerances

The measured vibration response level is directly related to the specification level by these tolerances of acceptance. The standard recommends to use the following tolerances:

- g_{RMS} level should not deviate +/- 10% from required level
- PSD level should not deviate $\begin{cases} \text{+/- 3 dB below 500 Hz} \\ \text{+/- 6 dB above 500 Hz} \end{cases}$
- Bandwidth of the filter not exceed $\begin{cases} \text{2.5 Hz at 25 Hz or below} \\ 5\ Hz\ at\ frequencies\ above\ 25\ Hz \end{cases}$

The g_{RMS} input level from specification is obtained by calculating the square root of the area below the PSD-Frequency function. The g_{RMS} value is represented in (4.2).

$$\Rightarrow \sqrt{A} = 4.54\ g_{RMS} \tag{4.2}$$

5 Case Study

5.1 Introduction

The methodology was created from the simulation results of a case study which was a Lockheed Martin Hercules C-130 instruments panel. Three structures were created in order to analyze and understand the influence of the instruments on the structure. All structures provide important information about the behavior of the panel. On Figure 5.1, it is shown the panel that was taken as a reference to all analyses.

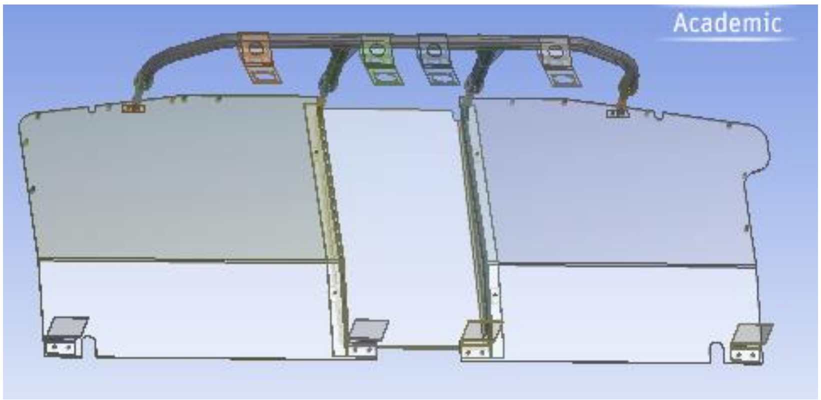

Figure 5.1 - Lockheed Martin Hercules C-130 instruments panel

The required vibration analysis of the test item was not performed in a shaker with a proper fixture in a laboratory. In this preliminary design phase, this type of experimental test is not suitable. The prediction of the physical behavior of the structures was simulated through finite element method (FEM).

5.2 Finite Element Method

The basic idea in the FEM is to solve a complex problem by replacing it by an approximated simpler one [37]. The solution region is considered as buildup of multiple small and interconnected sub regions called finite elements. The smaller are the sub regions the better is the approximation, this improvement is called refinement. The action of dividing a complex domain into smaller simpler domains is called the discretization of the domain. With this approximation it is always associated a numerical mesh discretization error. The more are the sub domains, this associated error will be reduced [38]. The Finite Element Method translates partial differential equation problems into a set of linear algebraic equations as shown in (5.1) for the case of a static linear analysis. K represents the stiffness matrix, u represents the nodal displacement vector and F represents the nodal vector force.

$$[K]\{u\} = \{F\} \tag{5.1}$$

Analytical solutions are not feasible for this kind of problems in engineering sciences, so numerical methods have been evolved to find a solution for the governing equations of the individual problem [39]. The results of the analyses were obtained numerically. It is possible to improve or refine the approximate solution by spending more computational effort since in this way the number of equations is increased.

To carry out the simulation of the case study, two software were used. The CAD models were designed in Solidworks and the finite element analyses (FEA) were conducted in Ansys Workbench. It is essential to convert and save the model as a .step file so that it can be translated into the Ansys Workbench in which it will be performed the FEA.

CAD Modelling
FEA
Results

Figure 5.2 - Simulation Methodology

5.3 Material Properties

The model represents the instruments panel and to predict its behavior it was necessary to perform a simulation with the more suitable material. The bolts were simulated as structural steel and all other components were simulated as an aluminum alloy. On the following Table 5.1 are presented important material properties of the aluminum alloy used in the model which is Aluminum 2024-T3 such as density, modulus of elasticity, Poisson’s ratio, tensile yield strength and ultimate tensile strength. These material properties are relevant and were considered in the finite element analysis [40].

Table 5.1 - Mechanical Properties of Aluminum 2024-T3

	Metric	English
Density	2.78 g/cm^3	0.1 lb/in^3
Modulus of Elasticity	73.1 GPa	10600 ksi
Tensile Yield Strength	345 MPa	50000 psi
Ultimate Tensile Strength	483 Mpa	70000 psi
Poisson’s Ratio	0.33	0.33

5.4 Strategic simplifications

Before conducting the FEA, some simplifications were implemented in order to perform a more fast and efficient analysis. It is essential to de-feature the model by removing chamfers and notches which are considered unnecessary characteristics for conducting the analyses. De-featuring simplifies the model making the analyses quicker. Furthermore, it prevents the possibility of obtaining illusory results near chamfers and notches with forces and stresses that really cannot exist.

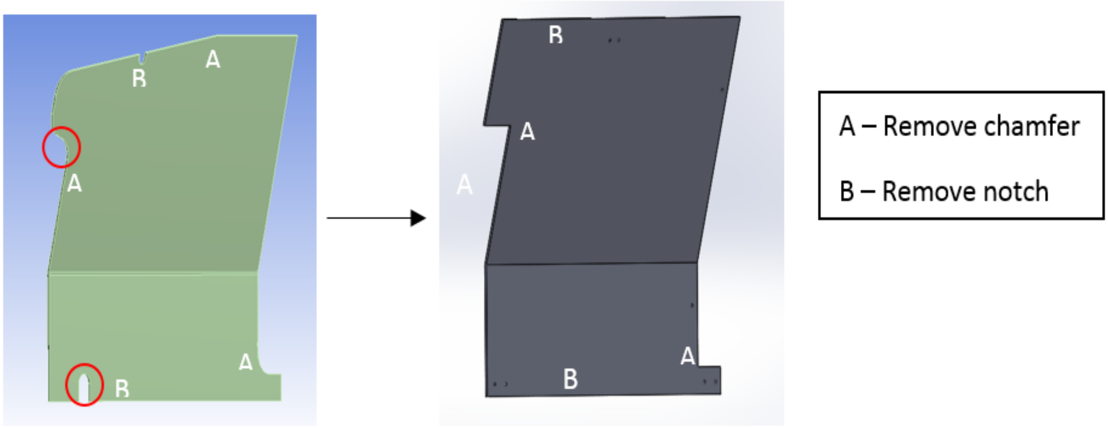

Figure 5.3 – Chamfers and notches simplification

More simplifications were made due to the complex geometry of some components and its interfaces. On Figure 5.4, it is shown in CAD and in Ansys Workbench the following simplification. This interface is simulated as a simply beam with a constant section. This small change on these components does not change the whole behavior of the structure and simplifies the calculation of the results from FEA.

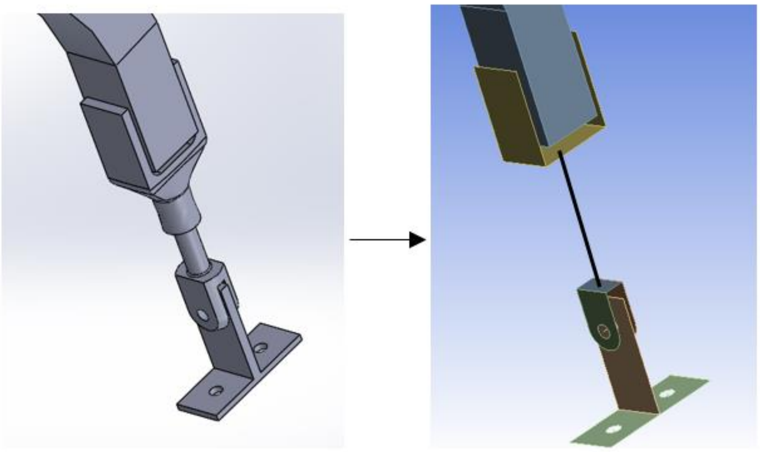

Figure 5.4 - Geometry simplification

Bolts were simply simulated as beams with a constant section. The nodes at the tips are attached with the nodes of other component parts by multiple fixed joints. This fixation guarantees that all bodies are attached to each other. Running modal analyses with a structure that was not absolutely fixed, it was concluded after simulating that all natural frequencies were equal to zero. On the following Figure 5.5 it is represented how bolts were simplified.

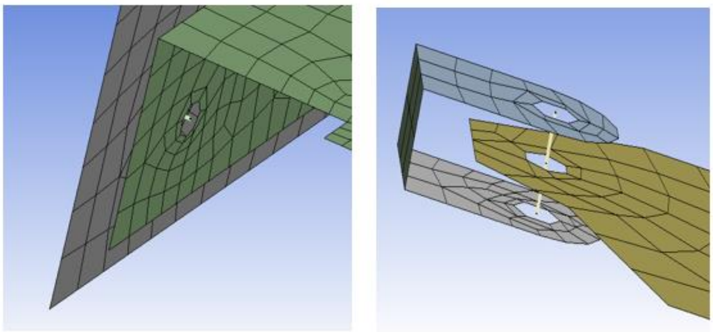

Figure 5.5 - Bolts simplification

5.5 Elements

The Ansys Workbench software has a feature that allows an automatic creation of the mesh. Taking advantage of it, a mesh was automatically created. The created elements were Solid186, Solid187, Beam188, Conta174, Conta175, Targe170 and Shell181. On the following paragraphs, it is exposed a brief theory of these elements. For a more detailed version, it is recommend to see Ansys Theory Manual in [41].

Solid187 is a tetrahedral element with 10 nodes having three degrees of freedom at each node. It is more suitable to use this element instead of using a four-node element.

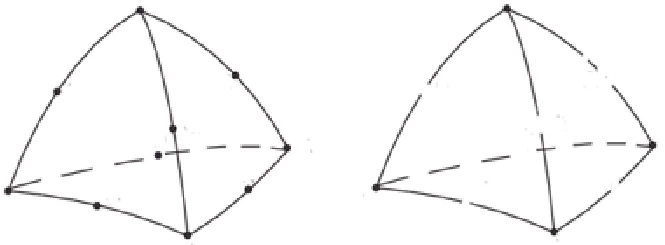

Figure 5.6- Solid187 in comparison to a 4-node tetrahedral element

Solid186 is a solid cubic with 20 nodes having three degrees of freedom per node. It is more suitable to use this element instead of using a four-node element.

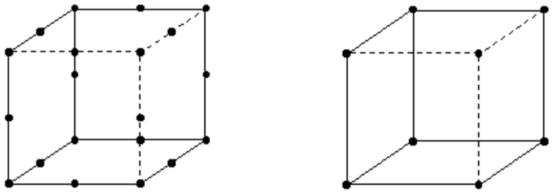

Figure 5.7 - Solid186 in comparison to an 8-node cube element

Conta174 is an element with 8 nodes and it is used to represent contact and sliding between a deformable surface, which is defined by this element and three-dimensional target surfaces Targe170. Associated to Conta174 it always has to be present an element which represents the target surface in order to create the Contact Pair. The element which represents the target surface is Targe170. It is also possible to connect a single point to a target surface through a Targe170-Conta175 contact pair.

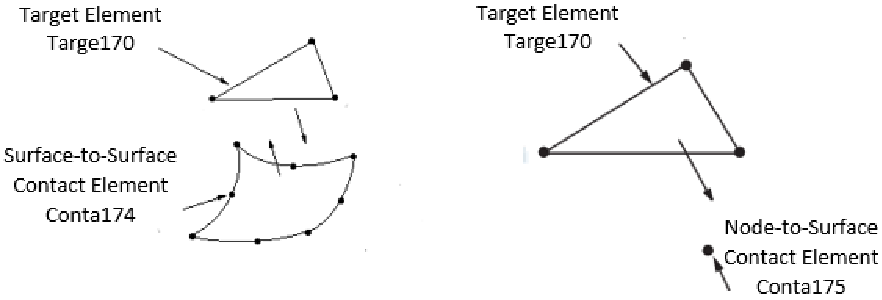
Target Element
Targe170
Surface-to-Surface
Contact Element
Conta174
Target Element
Targe170
Node-to-Surface
Contact Element
Conta175

Figure 5.8 - Target170-Conta174 and Targe170-Conta175 Contact Pairs

Beam188

The Beam188 element is well suited for analyzing slender to moderately thick beam structures. The element is based on Timoshenko beam theory. Beam188 is a linear beam element with two nodes in three-dimensional space with six degrees of freedom at each node.

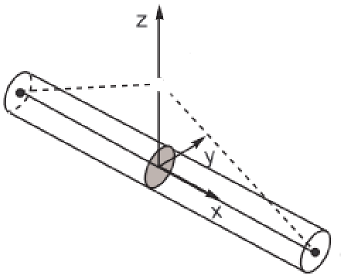

Figure 5.9 - Beam188 Element

Shell 181

The 3D modeling is built from a mid-surface thick-shell to which is added a both sided thickness. Shell181 element is based on Reissner-Mindlin theory. This element is well suited for analyzing thin to moderately-thick shell structures. It is an element with four nodes with six degrees of freedom at each node. The triangular option is not recommended.

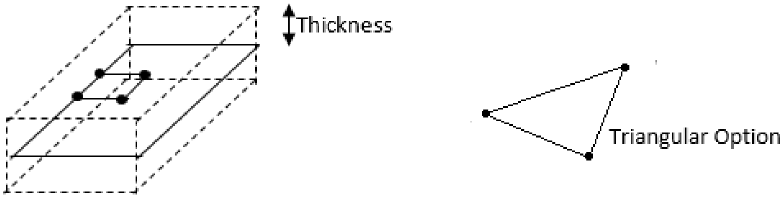

Figure 5.10 - Shell181 Element

5.6 Connections

Connections between components were implemented. The element that allows this feature is called MPC184. This element is classified as multipoint constraint elements that apply constraints between nodes. There are two types of elements: the constrained ones in which are applied fixed connections and the jointed ones in which can be applied revolute connections among others. Constraints can be complicated. For example, a structure may consist of rigid parts and moving parts connected together by rotational or sliding connections. The rigid part of the structure may be modeled with the MPC184 rigid elements, while the moving parts may be connected with any of the MPC184 joint elements. Fixed type MPC184 were applied between several interactions of the modeled structure such as bolts and sheet plates, beams and sheet plates, body and ground. With this method, it is guaranteed that two or more nodes are restrained to each other in all six degree of freedom, suffering therefore the same displacement. In Figure 5.11, some examples of these constraints are represented.

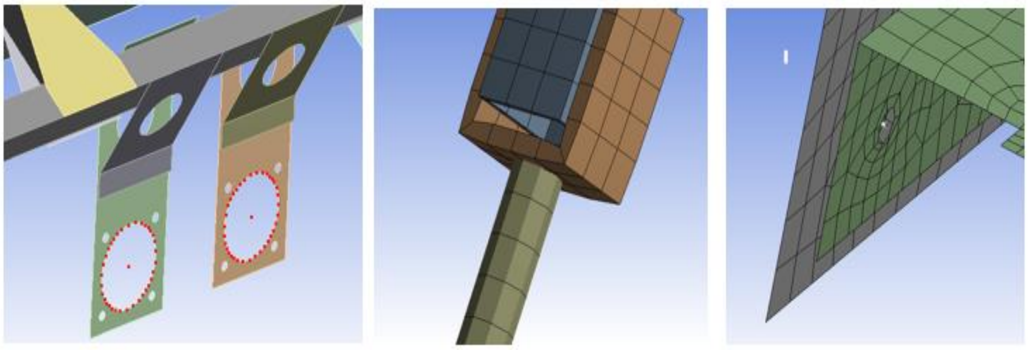

Figure 5.11 - Bolt-sheet plate, beam-sheet plate, body-ground interactions

5.7 Mesh

Despite Ansys Workbench's feature of generating an automatic mesh, it is possible to manipulate the elements. At first the software suggested a mesh composed of 3D solid elements. In order to create a more efficient mesh, elements were manipulated generating the 3D model from 2D shell elements. The modeling was built from a mid-surface thick-shell to which was added a both sided thickness. This formulation was applied in all parts of the structure. It is also possible to manipulate geometry of the elements chosen among triangular or quadratic. In all structure simulations, it was always preferred the quadratic geometry. The triangular elements were only used near bolt holes or corners with curvature.

It is possible to control several characteristics of the mesh such as the level of smoothing, the curvature normal angle, the limit sizing of elements among others. Refinement was applied close to bolt holes' areas and corners with curvature. The mesh can be finer or coarser. In order to understand the influence of the elements formulation on the computational effort, multiple meshes were generated with the following characteristics on Table 5.2:

Table 5.2 - Mesh characteristics on Workbench 17.0

Features	**Selected**
Use Advance Size Function	On: Proximity and Curvature
Use Fixed Size Function for Sheets	No
Relevance Center	Fine
Initial Size Seed	Active Assembly
Smoothing	Medium
Span Angle Center	Fine
Curvature Normal Angle	30º
Number Cells Across Gap	3
Proximity Size Function Sources	Faces and Edges
Min Size	1,93 mm
Proximity Min Size	1,93 mm
Max Face Size	6 mm
Minimum Edge Length	0,006 mm

Two meshes were created based on different formulation principles. On the first one, the model did not suffer any simplifications and it was composed of solid elements. This was the mesh suggested by the Ansys Workbench automatic mesh feature. The second one consists in a simplified model wherein the three-dimensional mesh was created from adding thickness to components mid-surfaces. The generated elements for both meshes are shown on Table 5.3.

Table 5.3- Comparison of generated elements according to solid and shell formulation

	Solid Formulation Mesh	Shell Formulation Mesh
Elements	Solid186 Solid187 Targe170 Conta174 MPC184	Shell181 Beam188 Targe170 Conta174 MPC184

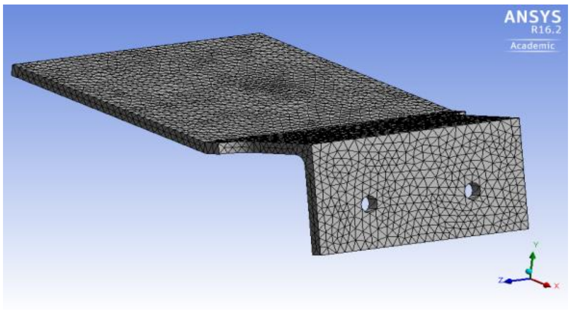

Figure 5.13 - Part meshed with solid elements

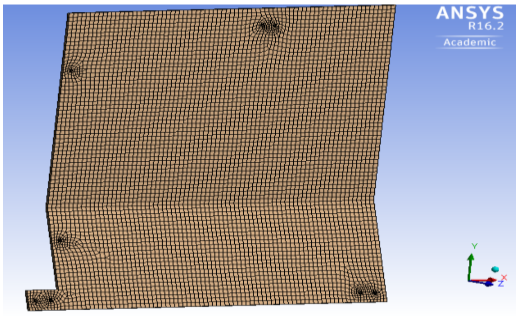

Figure 5.12 - Part meshed with shell elements

On Table 5.4, it is compared the number of elements and nodes generated from a 2D and 3D mesh formulation.

Table 5.4 - Comparison of number of elements between a 3D mesh without simplifications and 2D mesh with simplifications

	3D without simplifications	2D with simplifications	Relation 2D/3D	Reduction [%]
Elements	3418806	29763	0,0087	99,13
Nodes	1945442	31675	0,0163	98,37

Regarding this comparison, it is possible to conclude that the simplified mesh generated from a shell formulation is composed of much less number of elements and nodes. The mesh become much more efficient due to the reduction of computational effort of nearly 99% without affecting the properties of the whole structure.

5.8 Boundary Conditions

The present simulation, which is a random vibration simulation, can be compared to a base-excited forced vibration of harmonic motion presented on Chapter 3. However, in this case, the structure is excited with a random input on the fixed supports similar to a base excited system. The location of the nodes which represent the boundary conditions are shown on Figure 5.14. These nodes are constrained in all six degrees of freedom x, y, z, M_x, M_y and M_z. The excitation of the structure will be on these nodes.

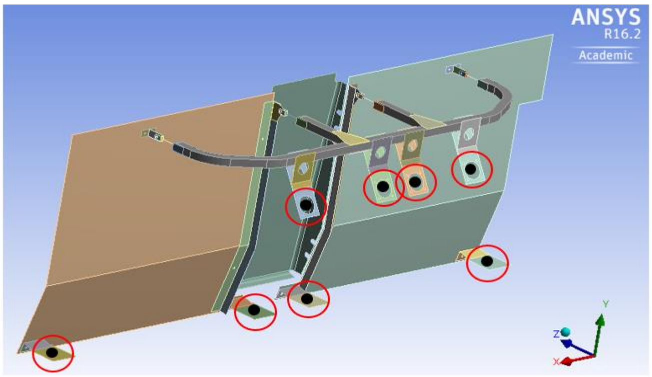

Figure 5.14 - Boundary Conditions

5.9 Natural Frequencies

A study was performed in order to understand the influence of the boundary conditions on the natural frequencies of the structure. It is known that it will exist one natural frequency for each degree of freedom and it is also known that when fixed supports are added these natural frequencies will scatter. The purpose of this study was to analyze the effect of changing the boundary conditions and how the natural frequencies responses would react. The boundary conditions were applied in A, B, C, D, E, F, G and H areas shown on Figure 5.15.

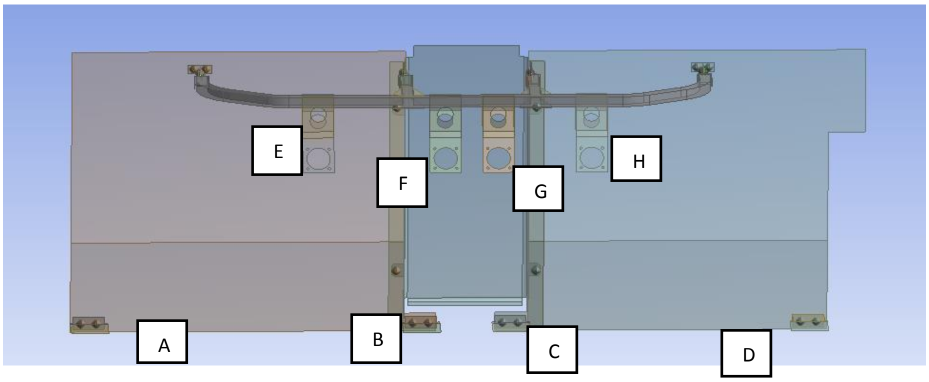

Figure 5.15 - Boundary Conditions Localization

The nodes which were fixed are shown below. The fixation on areas A, B, C, D was applied on the node shown in Figure 5.16 and the fixation on areas E, F, G, and H was applied on the nodes shown in Figure 5.17. Five modal simulations were performed and the natural frequencies were calculated. In the end, another simulation was made maintaining the fixation on areas E, F, G, H and changing the fixation on areas A, B, C, D by adding more fixed nodes as shown in Figure 5.18.

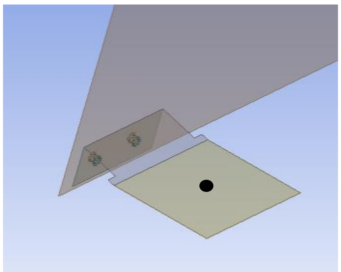

Figure 5.16 - Fixation on areas A, B, C, D

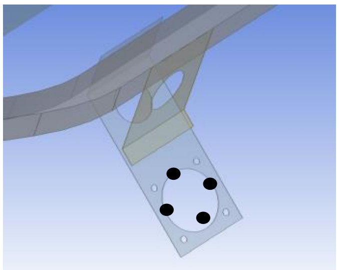

Figure 5.17 - Fixation on areas E, F, G, H

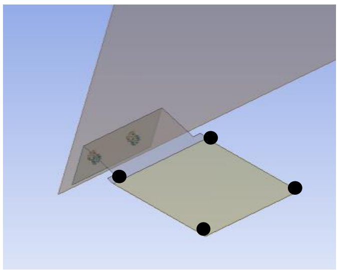

Figure 5.18 - Fixation on areas A, B, C, D for simulation 6

The fixation on these specific nodes was applied by either locking translations in the nodal x, y and z directions or locking translations and rotations in all directions. The description of the fixed degrees of freedom is expressed on Table 5.5:

Table 5.5 - Fixation types applied for all simulations

Simulation	1	2	3	4	5	6
A	Fixed x, y, z	Fixed x, y, z	Fixed x, y, z	Fixed x, y, z	Fixed All	Fixed All
B	Fixed x, y, z	Fixed x, y, z	Fixed x, y, z	Fixed x, y, z	Fixed All	Fixed All
C	Fixed x, y, z	Fixed x, y, z	Fixed x, y, z	Fixed All	Fixed All	Fixed All
D	Fixed x, y, z	Fixed x, y, z	Fixed x, y, z	Fixed All	Fixed All	Fixed All
E	Fixed x, y, z	Fixed x, y, z	Fixed All	Fixed All	Fixed All	Fixed All
F	Fixed x, y, z	Fixed x, y, z	Fixed All	Fixed All	Fixed All	Fixed All
G	Fixed x, y, z	Fixed All	Fixed All	Fixed All	Fixed All	Fixed All
H	Fixed x, y, z	Fixed All	Fixed All	Fixed All	Fixed All	Fixed All

For each simulation it was registered the first, the tenth, the fiftieth and the seventy-fifth natural frequencies. It was also registered the number of natural frequencies within the ranges of 0 and 100 Hz, 100 and 500 Hz, 500 and 900 Hz.

Table 5.6 – Natural Frequencies Results

Simulation		1	2	3	4	5	6
Frequency (Hz)	1st	29.63	31.05	32.54	34.36	34.55	34.78
	10th	97.54	100.06	100.31	102.94	107.01	132.45
	50th	499.03	501.23	519.01	519.02	519.69	536.58
	75th	750.11	758.75	767.39	777.54	778.00	788.72
Quantity of Frequencies	0-100 Hz	10	9	9	9	9	6
	100-500 Hz	40	40	40	40	40	41
	500-900 Hz	44	45	44	41	39	39

Performing these six simulations, it was concluded that natural frequencies of the structure are influenced by the change of the boundary conditions. The natural frequencies have a tendency to increase when the fixation of the structure is becoming more constrained. And consequently, the number of resonant frequencies within the specified ranges decreases. Since it exists a natural frequency for each degree of freedom, the conclusion is that by constraining more the structure, the resonant frequencies grow to values out of the specified ranges above.

5.10 Geometries

Three structures were created in order to analyze and understand the influence of the instruments on the structure. All structures provide important information about the behavior of the panel. On the following paragraphs it will be shown its own characteristics and specifications. The results as well as the concluding remarks of vibration analysis will be presented on Chapter 6.

5.10.1 Structure I

The first structure to be taken into consideration is shown in Figure 5.19. The parts were simulated with Aluminum 2024-T3 properties. All simplification described above were implemented on the model. The three-dimensional mesh was created from adding thickness to all component mid-surfaces. Connections were implemented as explained in the previous topics. The boundary conditions were applied as are shown on previous Figure 5.14.

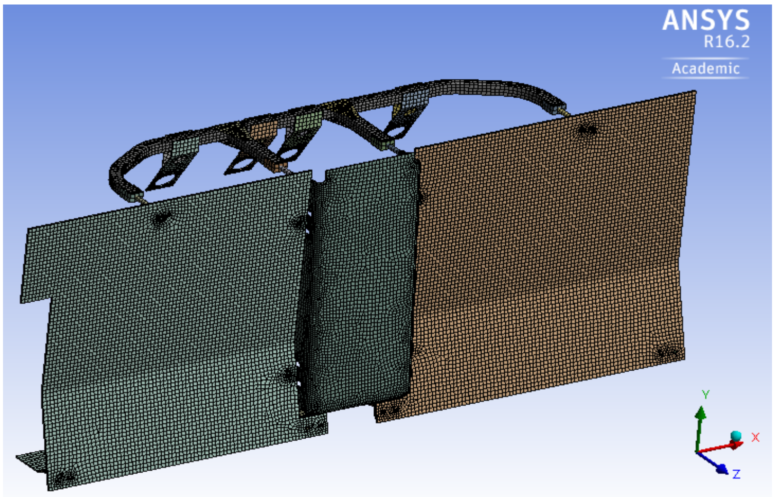

Figure 5.19 - Structure I

Table 5.7 - Structure I element types

Elements	Shell181 Beam188 Targe170 Conta174 MPC184

Table 5.8 - Structure I model properties

Number Nodes	31675
Number Elements	29763
Bodies	58
Mass [Kg]	6.31

5.10.2 Structure II

The second structure to be taken into consideration is shown in Figure 5.20. This model was generated with the same three dimensional mesh formulation, the same material properties, the same conections and the same bondary conditions. The difference of this structure from the previous one lies in the gaps on the panel. This modification results in a decrease of the structure weight.

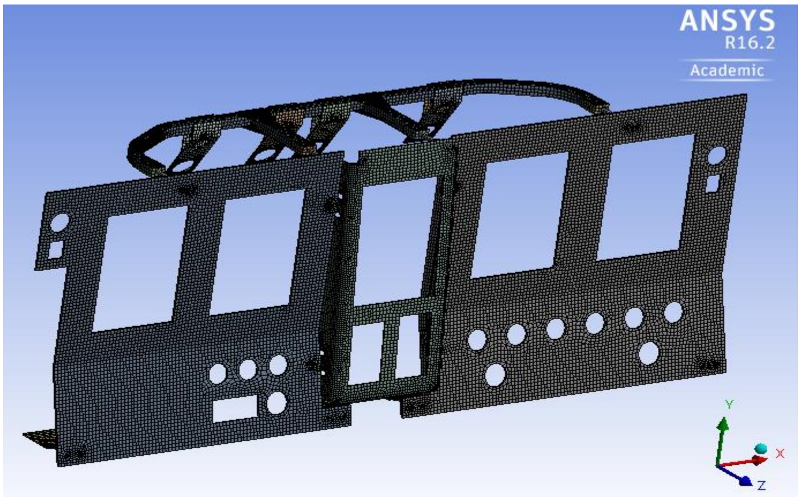

Figure 5.20 - Structure II

Table 5.9 - Structure II element types

Elements	Shell181 Beam188 Targe170 Conta174 MPC184

Table 5.10 - Structure II model properties

Number Nodes	26396
Number Elements	23982
Bodies	58
Mass [Kg]	4.74

5.10.3 Structure III

The third structure to be taken into consideration is shown in Figure 5.21. This model was generated with the same three dimensional mesh formulation, the same material properties, the same conections and the same bondary conditions. The difference of this structure from the previous one lies in the addition of lumped masses in the gaps simulating the instruments. These lumped masses are represented by Mass21 elements. The conection with the structure is accomplished by a Contact Pair constitued by a target element Targe170 and a node-to-surface contact element Conta175.

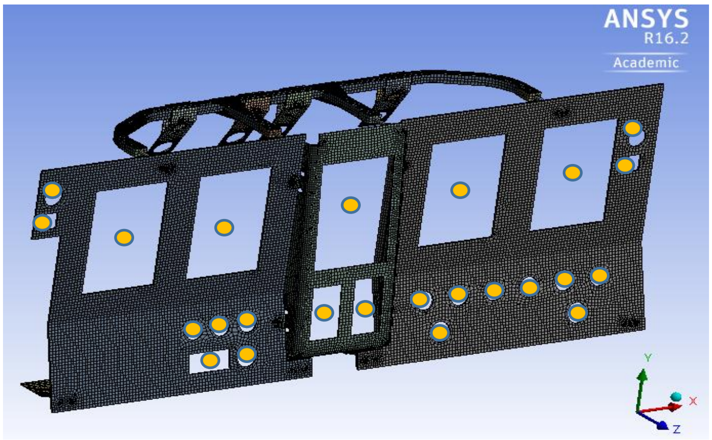

Figure 5.21 - Structure III

Table 5.11 - Structure III element types

Elements	Shell181 Beam188 Targe170 Conta174 MPC184 Mass21 Conta175

Table 5.12 - Structure III model properties

Number Nodes	26420
Number Elements	24080
Bodies	82
Mass [Kg]	59.78

The instruments were simulated by lumped masses represented as small yellow circles. Their weight is described in the Table 5.13. In this table, important information such as the quantity of the instruments and their total weight are provided. The fixation of these lumped masses is accomplished by a connection with the nodes represented in blue. Considering that Structure III weights 59.78 Kg, the instruments represent more than 90% of its total weight.

Table 5.13 - Representation of instruments as lumped point masses

Instruments	Weight [lbs]	Weight [Kg]	Quantity	Total Weight [Kg]
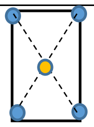	15	6.80	5	34
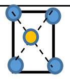	8	3.63	2	7.26
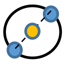	1.5	0.68	14	9.52
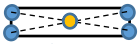	5	2.26	1	2.26
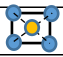	2.20	1	2	2
				Total = 55.04

On the next Chapter, it will be presented the results from the vibration simulation considering the geometry of these three structures. According with the proposed methodology, the random vibration simulation is always carried out after a modal simulation in order to obtain the natural frequencies of the structure at first. For each structure, it will be performed one simulation for each axis. Therefore, nine random vibration simulations will be performed applied for the x, y and z axes considering these three different structures.

6 Results

6.1 Structure I

Before carrying out the random vibration analysis it is necessary to carry out a modal analysis. On Table 6.1, the results are shown for the first twenty natural modes of the structure.

Table 6.1 - Structure I Natural Frequencies

Modes	1	2	3	4	5	6	7	8	9	10
Natural Frequencies (Hz)	34.78	38.98	65.71	76.09	88.02	98.22	110.32	117.92	128.89	132.45
Modes	11	12	13	14	15	16	17	18	19	20
Natural Frequencies (Hz)	137.53	144.22	151.50	159.89	171.67	177.43	180.39	185.37	197.20	200.95

All the following images of the structure follow the color scale of Figure 6.1. The red color represents more severe responses and the dark blue color represents lighter responses of the structure in terms of displacement, velocity and acceleration.

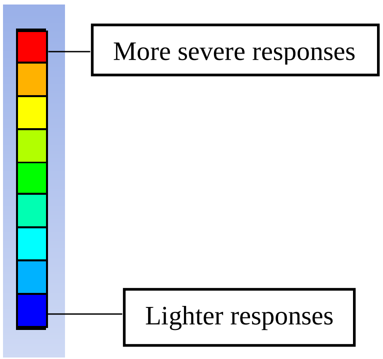

Figure 6.1 - Color scale

All the following images of the structure follow the coordinate system represented on Figure 6.2.

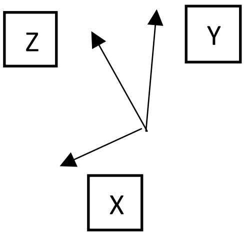

Figure 6.2 - Coordinate system

6.1.1 X-axis input simulation

Random vibration simulations can only be applied in one single direction at each time. On the first simulation, the vibration input was applied in the X-axis.

The distribution of colors of the displacement, velocity and acceleration responses is very similar when the simulation is performed for the same structure with the same input in the same axis. The responses in all three axes are exposed on Table 6.2:

Table 6.2 - Structure I most critical areas after X-Axis Input

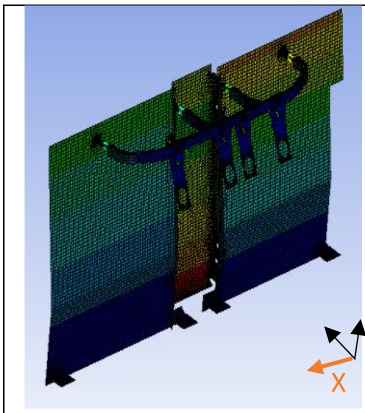	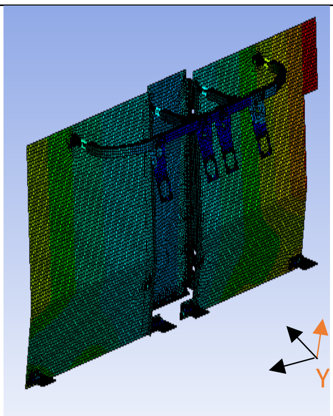	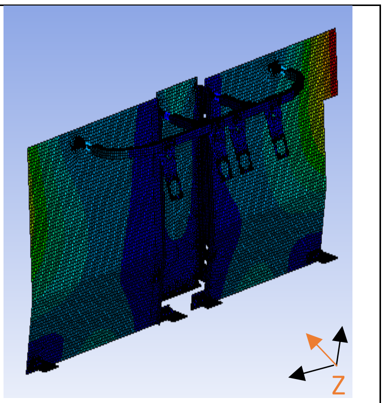
X-Axis Response	Y-Axis Response	Z-Axis Response

The most critical results are shown on Table 6.3:

Table 6.3 - Most critical results after X-Axis Input

	1σ Values			3σ Values		
	X	Y	Z	x	y	z
Displacement (mm)	0.13	0.13	0.91	0.39	0.40	2.72
Velocity (m/s)	0.13	0.10	0.24	0.39	0.29	0.72
Acceleration (g)	12.71	8.62	18.82	38.14	25.86	56.47

The PSD response is obtained from single points of the structure. The identification of these points is shown on Figure 6.3:

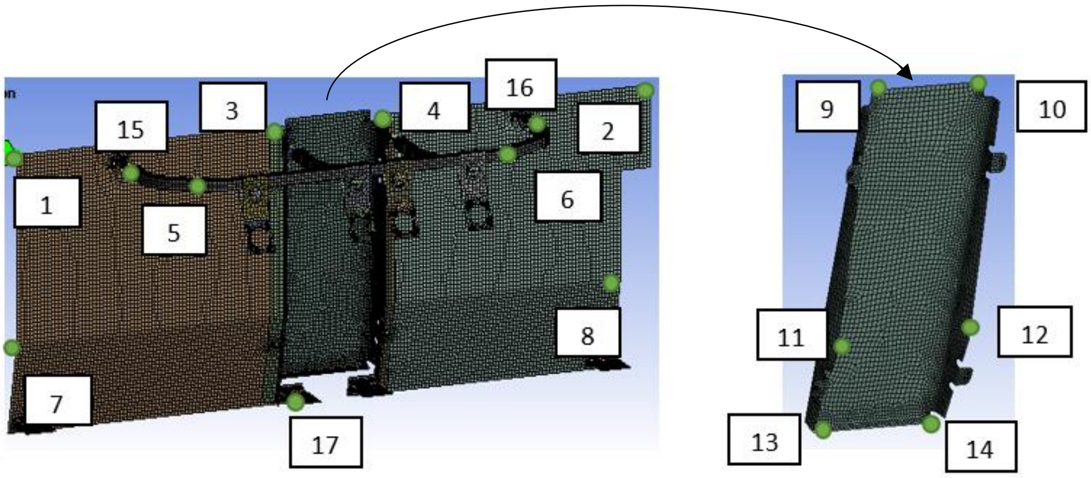

Figure 6.3 - Identification of points that will provide information about PSD response (1)

Tables of results are filled in with the PSD peak and the identification of the most critical frequency. The method to obtain those values is described in Figure 6.4 which represents the PSD response of the point identified as 1. The overall g_{rms} value is obtained by calculating the square root of the area below the PSD curve.

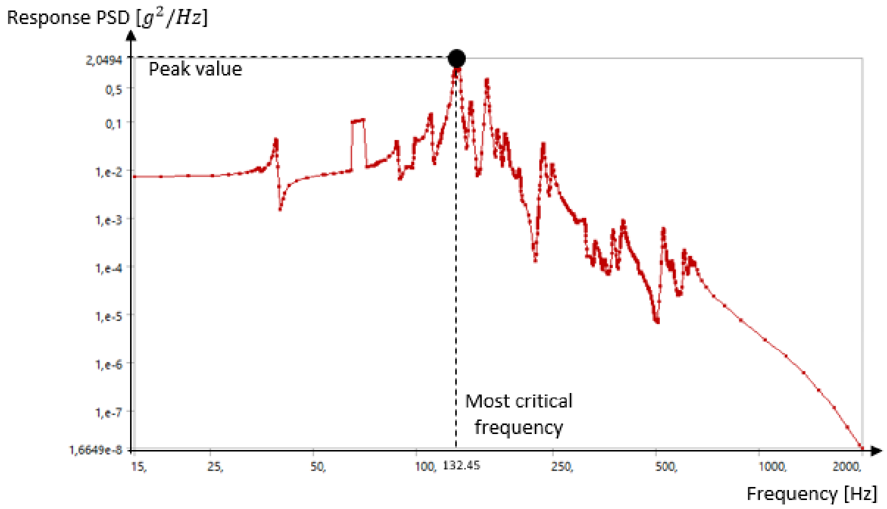

Figure 6.4 - PSD response of point 1 and clarification of the concepts peak value and most critical frequency

The purpose of the last column is to identify if the most critical frequency of the structure is within the range of ±5% of the excitation frequencies generated by the propeller. These ranges are shown on Table 6.4:

Table 6.4 - Range of excitation frequencies generated by the propellers

	1^{st} Excitation	2^{nd} Excitation	3^{rd} Excitation	4^{th} Excitation
Range [Hz]	64.6 to 71.4	129.2 to 142.8	193.8 to 214.2	258.4 to 285.6

The PSD results for the identified points are shown on Table 6.5:

Table 6.5 - PSD response for X-axis excitation

Points	Peak (g^2/Hz)	Most Critical Frequency (Hz)	Natural Frequency	Within the range of excitation generated by the propeller	Overall g_{rms}
1	2.05	132.45	10^{th}	Yes	4.39
2	9.99	137.53	11^{th}	Yes	6.71
3	2.02	132.45	10^{th}	Yes	4.36
4	9.88	137.53	11^{th}	Yes	6.67
5	$2.1\mathrm{x}10^{-2}$	132.45	10^{th}	Yes	0.57
6	$1.2\mathrm{x}10^{-2}$	98.22	6^{th}	No	0.61
7	0.21	132.45	10^{th}	Yes	3.34
8	0.70	132.45	10^{th}	Yes	3.54
9	5.86	132.45	10^{th}	Yes	7.62
10	5.84	132.45	10^{th}	Yes	7.61
11	4.01	128.89	9^{th}	No	9.92
12	1.99	128.89	9^{th}	No	10.14
13	24.11	159.89	14^{th}	No	12.71
14	24.10	159.89	14^{th}	No	12.71
15	0.59	132.45	10^{th}	Yes	3.23
16	2.91	132.45	10^{th}	Yes	4.44
17	0.10	-	-		4.54

6.1.2 Y-axis input simulation

On the second simulation, the vibration input was applied in the Y-axis. Displacement, velocity and acceleration responses in all three axes are exposed on Table 6.6:

Table 6.6 - Structure I most critical areas after Y-Axis Input

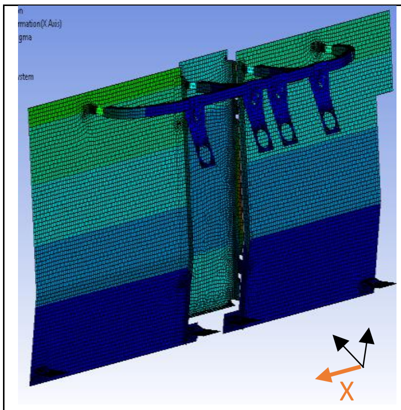	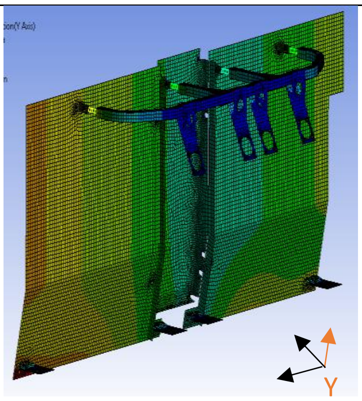	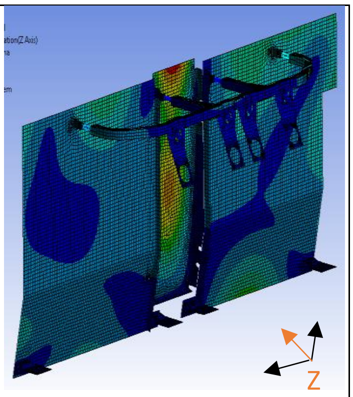
X-Axis Response	Y-Axis Response	Z-Axis Response

The most critical results are shown on Table 6.7:

Table 6.7 - Most critical results after Y-Axis Input

	1σ Values			3σ Values		
	X	Y	Z	x	y	z
Displacement (mm)	0.24	0.22	0.63	0.72	0.66	1.88
Velocity (m/s)	0.20	0.19	0.50	0.61	0.58	1.51
Acceleration (g)	18.12	16.60	43.05	54.36	49.81	129.14

The PSD response is obtained from single points of the structure. The identification of these points is shown on Figure 6.5.

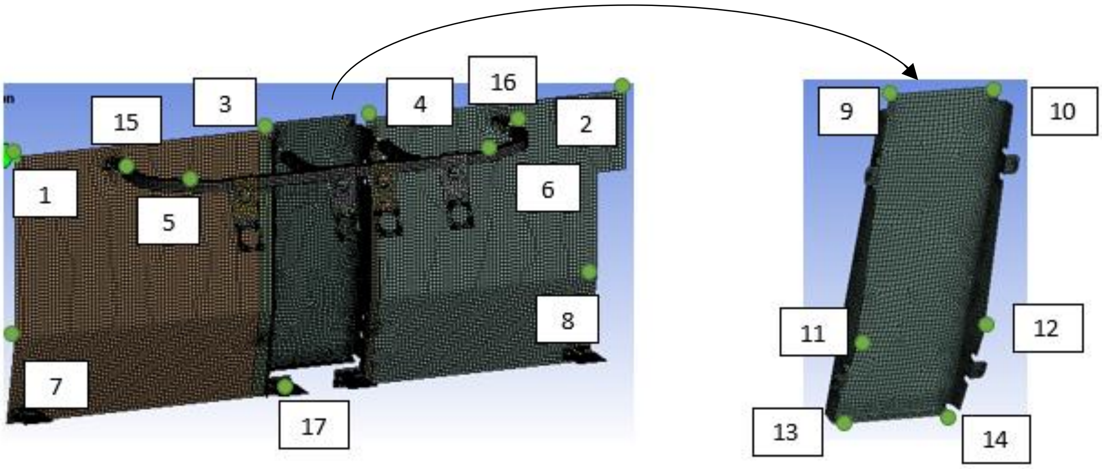

Figure 6.5 - Identification of points that will provide information about PSD response (2)

The PSD results for the identified points are shown on Table 6.8:

Table 6.8 - PSD response for Y-axis excitation

Points	Peak (g^2/Hz)	Most Critical Frequency (Hz)	Natural Frequency	Within the range of excitation generated by the propeller	Overall g_{rms}
1	45.06	137.53	11^{th}	Yes	14.09
2	13.34	132.45	10^{th}	Yes	10.06
3	13.73	137.53	11^{th}	Yes	9.17
4	5.80	137.53	11^{th}	Yes	7.20
5	7.75 x10^{-2}	88.02	5^{th}	No	1.16
6	0.63	132.45	10^{th}	Yes	1.94
7	44.77	137.53	11^{th}	Yes	14.05

Points	Peak (g^2/Hz)	Most Critical Frequency (Hz)	Natural Frequency	Within the range of excitation generated by the propeller	Overall g_{rms}
8	11.84	137.53	11^{th}	Yes	9.38
9	11.53	137.53	11^{th}	Yes	8.43
10	5.24	137.53	11^{th}	Yes	6.78
11	13.63	137.53	11^{th}	Yes	9.04
12	5.52	137.53	11^{th}	Yes	7.02
13	13.57	137.53	11^{th}	Yes	9.19
14	5.02	137.53	11^{th}	Yes	7.01
15	21.69	137.53	11^{th}	Yes	10.57
16	5.27	132.45	10^{th}	Yes	7.31
17	0.10	-	-		4.54

6.1.3 Z-axis input simulation

On the third simulation, the vibration input was applied in the Z-axis. Displacement, velocity and acceleration responses in all three axes are exposed on Table 6.9:

Table 6.9 - Structure I most critical areas after Z-Axis Input

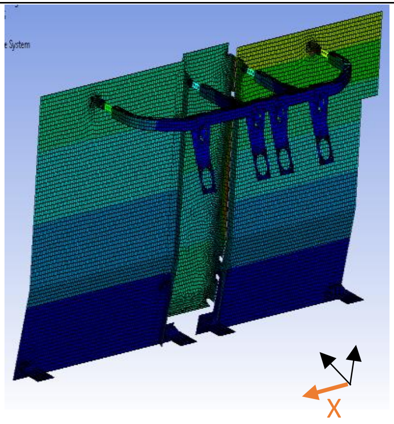	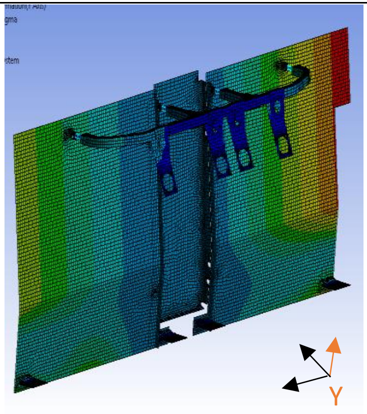	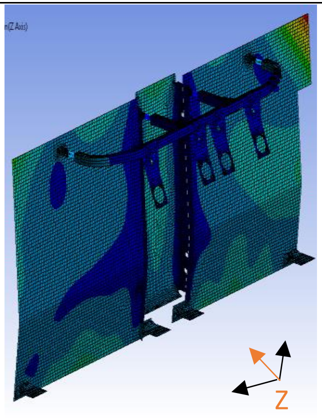
X-Axis Response	Y-Axis Response	Z-Axis Response

The most critical results are shown on Table 6.10:

Table 6.10 - Most critical results after Z-Axis Input

	1σ Values			3σ Values		
	x	y	Z	x	y	z
Displacement (mm)	0.08	0.15	2.04	0.25	0.45	6.12
Velocity (m/s)	0.06	0.07	0.79	0.19	0.21	2.36
Acceleration (g)	6.33	6.54	33.61	18.98	19.62	100.82

The PSD response is obtained from single points of the structure. The identification of these points is shown on Figure 6.6.

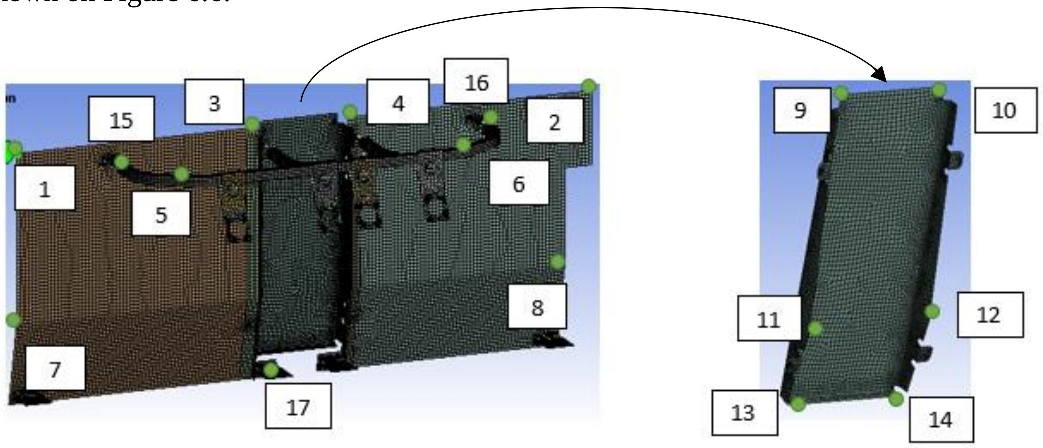

Figure 6.6 - Identification of points that will provide information about PSD response (3)

The PSD results for the identified points are shown on Table 6.11:

Table 6.11 - PSD response for Z-axis excitation

Points	Peak (g^2/Hz)	Most Critical Frequency (Hz)	Natural Frequency	Within the range of excitation generated by the propeller	Overall g_{rms}
1	55.73	76.09	4^{th}	No	16.57
2	612.26	65.71	3^{rd}	Yes	33.61
3	0.14	137.53	11^{th}	Yes	2.33
4	8.54 x10^{-2}	132.45	10^{th}	Yes	1.90
5	0.64	110.32	7^{th}	No	2.75
6	0.24	132.45	10^{th}	Yes	2.28
7	6.64	38.98	2^{nd}	No	5.96
8	68.98	65.71	3^{rd}	Yes	11.59
9	2.55	128.89	9^{th}	No	6.99
10	1.98	128.89	9^{th}	No	6.17
11	0.22	137.53	11^{th}	Yes	2.82
12	0.44	65.71	3^{rd}	Yes	2.51
13	1.10	310.28	29^{th}	No	5.47
14	0.52	65.71	3^{rd}	Yes	4.56
15	1.88	110.32	7^{th}	No	4.28
16	1.25	137.53	11^{th}	Yes	4.29
17	0.10	-	-		4.54

6.1.4 Data Evaluation

The aim of the selection of the point denominated as number 17 was to ensure that the PSD response was equal to PSD input. The input vibration was applied on that point which was fixed, so the vibration response had to be equal to the input. The result obtained prove that this base-excited forced vibration simulation was well performed.

As demonstrated on Chapter 4, the input signal is equal to 4.54 g_{rms}. Considering the acceptable tolerance specified of 10%, the responses ($g_{rms}\ out$) should not be superior to a determined value taken as reference ($g_{rms}\ ref$). This reference will be taken into account for future data evaluations of second and third structures and it is represented in (6.1).

$$g_{rms}\ ref = 1.1 \times 4.54 \cong 5\ g_{rms} \tag{6.1}$$

A data collection is presented on Table 6.12:

Table 6.12 - Structure I data collection

Simulation	Number of Points		%
	Dimension	$g_{rms}\ out >\ g_{rms}\ ref$	
X-Axis Input	17	8	47%
Y-Axis Input	17	14	82%
Z-Axis Input	17	7	41%

All simulations in all three axes have points with a level of vibration ($g_{rms}\ out$) higher than the reference. A justification for this fact is that critical frequencies which correspond to structural natural frequencies are within the range of the frequencies generated by the propeller as shown on the following Table 6.13:

Table 6.13 - Number of points whose critical frequency is within the range of propellers

Simulation	Number of Points		%
	Dimension	Critical frequency within the range of the frequencies generated by the propeller	
X-Axis Input	17	11	65%
Y-Axis Input	17	15	88%
Z-Axis Input	17	9	53%

The higher value of vibration was detected in the Z-axis input simulation on the point determined as number 2. The response of 33.61 g_{rms}, which is much higher than the reference, represents a resonance. The peak value of the PSD response is 612.26 g^2/Hz is much higher than peak value of the input 0.1 g^2/Hz. This result demonstrates the effect of a resonance in the structure. Structure natural frequencies have to be without the range of the frequencies generated by the propellers in order to ensure that structure does not resonate.

6.2 Structure II

Similarly to what was applied for the Structure I, a modal simulation was carried out before the random vibration analysis. On Table 6.14, it is expressed the results for the first twenty natural modes of the structure.

Table 6.14 – Structure II Natural Frequencies

Modes	1	2	3	4	5	6	7	8	9	10
Natural Frequencies (Hz)	32.05	38.47	60.69	65.78	86.68	102.96	103.70	116.21	130.35	143.52
Modes	11	12	13	14	15	16	17	18	19	20
Natural Frequencies (Hz)	144.58	149.64	154.32	156.20	159.24	167.74	174.62	179.88	186.86	193.10

6.2.1 X-axis input simulation

On the first simulation, the vibration input was applied in the X-axis. Displacement, velocity and acceleration responses in all three axes are presented on Table 6.15.

Table 6.15 -Structure II most critical areas after X-Axis Input

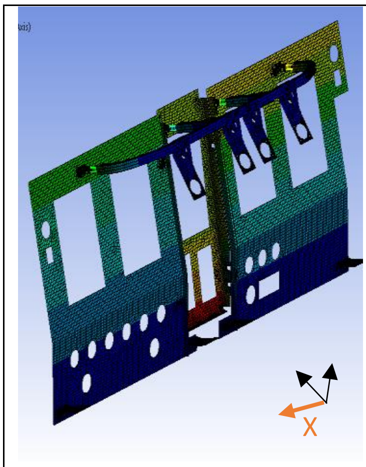	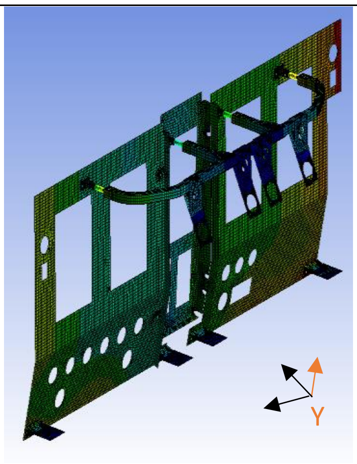	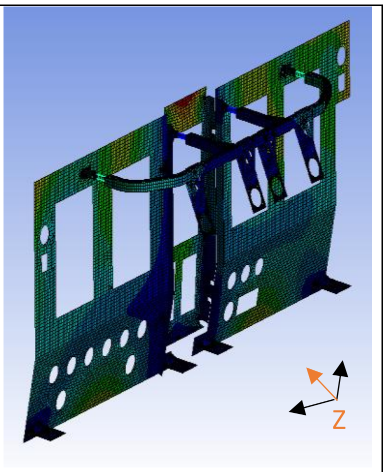
X-Axis Response	Y-Axis Response	Z-Axis Response

The most critical results are shown on Table 6.16:

Table 6.16 - Most critical results after X-Axis Input

	1σ Values			3σ Values		
	x	y	Z	x	y	z
Displacement (mm)	0.09	0.07	0.56	0.27	0.22	1.69
Velocity (m/s)	0.10	0.06	0.21	0.30	0.19	0.64
Acceleration (g)	34.83	16.06	60.75	104.39	48.18	182.25

The PSD response is obtained from single points of the structure. The identification of these points is shown on Figure 6.7.

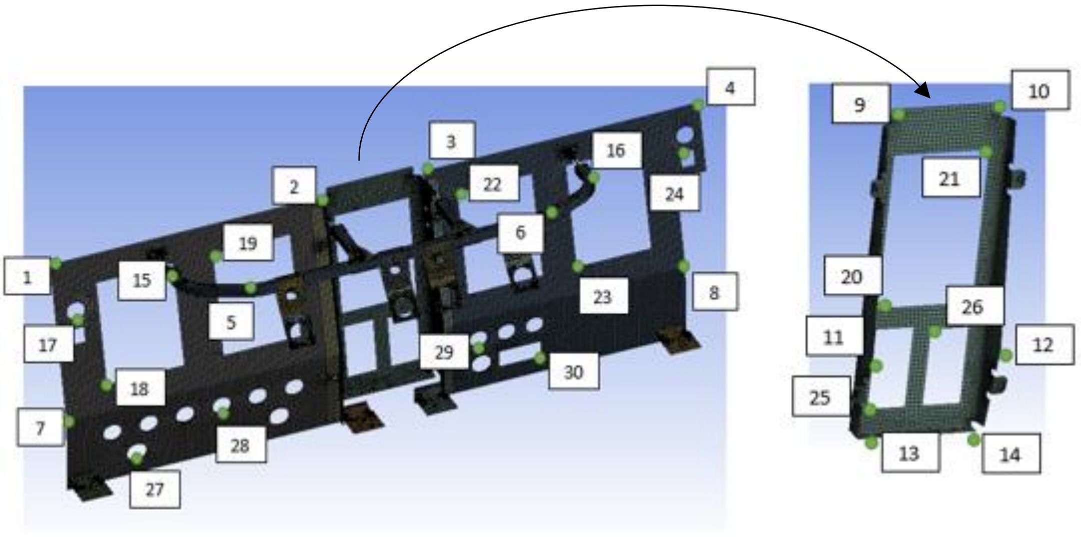

Figure 6.7 - Identification of points that will provide information about PSD response (4)

PSD results for the identified points are shown on Table 6.17:

Table 6.17 - PSD response for X-axis excitation

Points	Peak (g^2/Hz)	Most Critical Frequency (Hz)	Natural Frequency	Within the range of excitation generated by the propeller	Overall g_{rms}
1	1.60	143.52	10^{th}	No	6.72
2	1.58	143.52	10^{th}	No	6.55
3	4.40	143.52	10^{th}	No	6.09
4	4.48	143.52	10^{th}	No	6.24
5	$5.85\text{x}10^{-2}$	968.0	99^{th}	No	2.17
6	$3.67\text{x}10^{-2}$	968.0	99^{th}	No	2.09
7	0.21	143.52	10^{th}	No	3.53
8	0.43	143.52	10^{th}	No	3.62

Points	Peak (g^2/Hz)	Most Critical Frequency (Hz)	Natural Frequency	Within the range of excitation generated by the propeller	Overall g_{rms}
9	3.22	143.52	10^{th}	No	10.11
10	3.21	143.52	10^{th}	No	10.11
11	19.60	754.09	73^{th}	No	34.83
12	23.85	754.09	73^{th}	No	33.54
13	9.71	167.74	16^{th}	No	12.12
14	9.72	167.74	16^{th}	No	12.43
15	3.91	968.31	99^{th}	No	14.65
16	1.37	102.96	6^{th}	No	11.22
17	0.92	143.52	10^{th}	No	4.62
18	0.35	143.52	10^{th}	No	3.30
19	1.26	143.52	10^{th}	No	6.46
20	2.12	143.52	10^{th}	No	8.49
21	2.93	143.52	10^{th}	No	10.28
22	3.42	143.52	10^{th}	No	5.59
23	0.81	143.52	10^{th}	No	3.72
24	2.91	143.52	10^{th}	No	5.07
25	7.42	167.74	16^{th}	No	10.28
26	3.02	167.74	16^{th}	No	8.15
27	0.10	65.78	4^{th}	Yes	4.38
28	0.10	65.78	4^{th}	Yes	3.81
29	0.16	143.52	10^{th}	No	3.79
30	0.10	65.78	4^{th}	Yes	4.25

6.2.2 Y-axis input simulation

On the second simulation, the vibration input was applied in the Y-axis. Displacement, velocity and acceleration responses in all three axes are exposed on Table 6.18:

Table 6.18 – Structure II most critical areas after Y-Axis Input

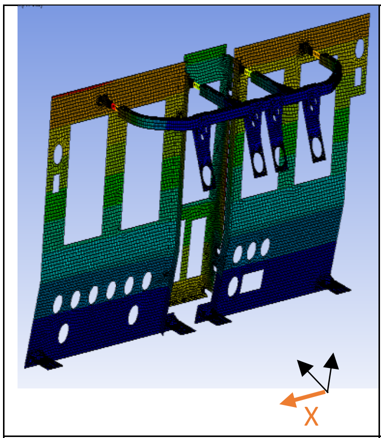	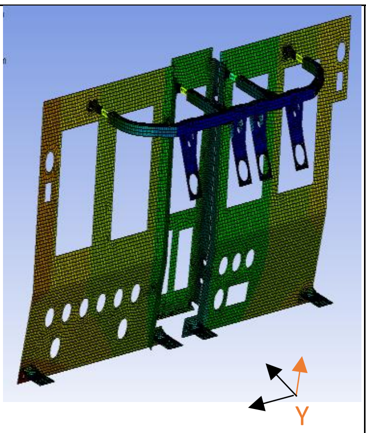	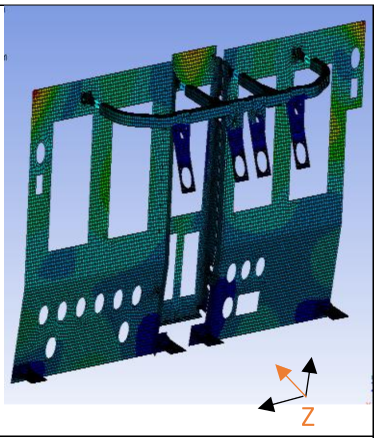
X-Axis Response	Y-Axis Response	Z-Axis Response

The most critical results are shown on Table 6.19:

Table 6.19 - Most critical results after Y-Axis Input

	1σ Values			3σ Values		
	x	y	Z	x	y	Z
Displacement (mm)	0.08	0.17	0.51	0.26	0.51	1.54
Velocity (m/s)	0.08	0.16	0.29	0.24	0.48	0.89
Acceleration (g)	8.16	14.21	27.76	24.47	42.63	83.28

The PSD response is obtained from single points of the structure. The identification of these points is shown on Figure 6.8.

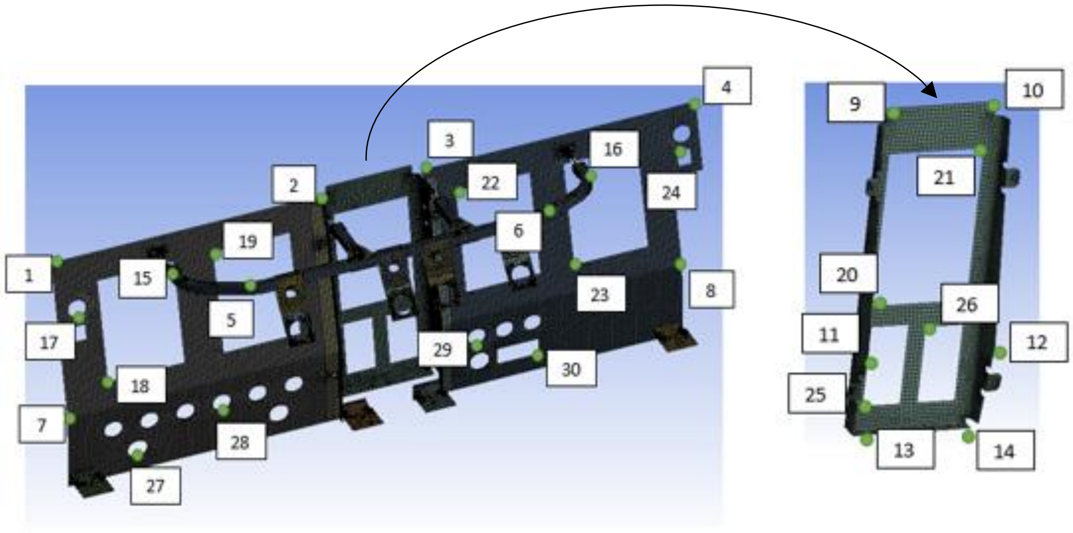

Figure 6.8 - Identification of points that will provide information about PSD response (5)

The PSD results for the identified points are shown on Table 6.20:

Table 6.20 - PSD response for Y-axis excitation

Points	Peak (g^2/Hz)	Most Critical Frequency (Hz)	Natural Frequency	Within the range of excitation generated by the propeller	Overall g_{rms}
1	25.69	144.58	11^{th}	No	11.91
2	5.48	143.52	10^{th}	No	7.83
3	3.94	154.32	13^{th}	No	6.26
4	25.66	144.58	11^{th}	No	11.05
5	5.27×10^{-2}	193.10	20^{th}	No	1.39
6	7.42×10^{-2}	102.96	6^{th}	No	1.19
7	25.59	144.58	11^{th}	No	11.89
8	21.57	144.58	11^{th}	No	10.25
9	5.17	143,52	10^{th}	No	7.69

Points	Peak (g^2/Hz)	Most Critical Frequency (Hz)	Natural Frequency	Within the range of excitation generated by the propeller	Overall g_{rms}
10	4.07	154.32	13^{th}	No	6.34
11	5.53	143,52	10^{th}	No	7.71
12	3.53	154.32	13^{th}	No	6.12
13	7.05	143,52	10^{th}	No	8.44
14	3.51	154.32	13^{th}	No	6.51
15	9.36	144.58	11^{th}	No	8.50
16	8.19	143,52	10^{th}	No	8.14
17	23.41	143,52	10^{th}	No	11.44
18	20.94	143,52	10^{th}	No	10.91
19	10.80	143,52	10^{th}	No	8.88
20	6.24	143,52	10^{th}	No	7.91
21	3.69	154.32	13^{th}	No	6.44
22	3.99	143,52	10^{th}	No	6.52
23	10.86	143,52	10^{th}	No	8.16
24	22.62	143,52	10^{th}	No	10.48
25	6.18	143,52	10^{th}	No	7.87
26	5.03	143,52	10^{th}	No	7.28
27	19.56	143,52	10^{th}	No	10.85
28	12.39	143,52	10^{th}	No	9.27
29	4.97	143,52	10^{th}	No	6.59
30	10.05	143,52	10^{th}	No	7.70

6.2.3 Z-axis input simulation

On the third simulation, the vibration input was applied in the Z-axis. Displacement, velocity and acceleration responses in all three axes are exposed on Table 6.21:

Table 6.21 – Structure II most critical areas after Z-Axis Input

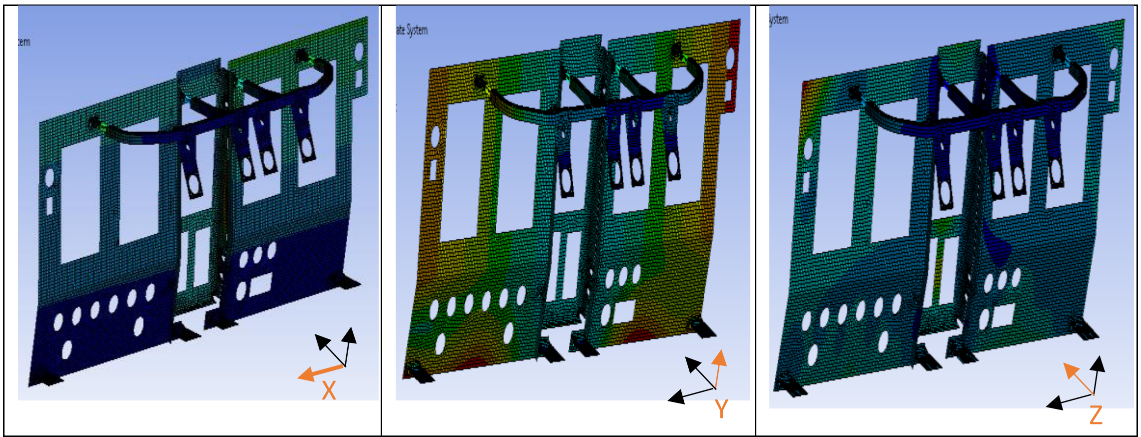

X-Axis Response

Y-Axis Response

Z-Axis Response

The most critical results are shown on Table 6.22:

Table 6.22 - Most critical results after Z-Axis Input

	1σ Values			3σ Values		
	x	y	z	x	y	z
Displacement (mm)	0.08	0.11	1.88	0.24	0.32	5.65
Velocity (m/s)	0.07	0.05	0.73	0.21	0.15	2.20
Acceleration (g)	11.8	4.83	31.17	35.40	14.48	93.50

The PSD response is obtained from single points of the structure. The identification of these points is shown on Figure 6.9.

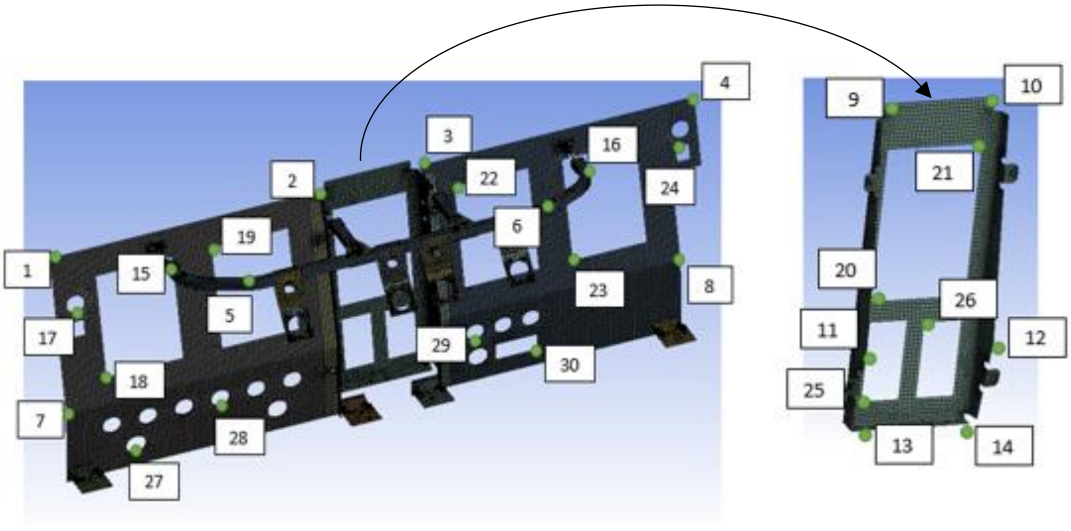

Figure 6.9 - Identification of points that will provide information about PSD response (6)

The PSD results for the identified points are shown on Table 6.23:

Table 6.23 - PSD response for Z-axis excitation

Points	Peak (g^2/Hz)	Most Critical Frequency (Hz)	Natural Frequency	Within the range of excitation generated by the propeller	Overall g_{rms}
1	523.11	65.78	4^{th}	Yes	31.17
2	0.19	143.52	10^{th}	No	2.74
3	0.19	144.58	11^{th}	No	2.81
4	47.61	60.69	3^{rd}	No	15.10
5	0.54	102.96	6^{th}	No	2.76
6	0.48	116.21	8^{th}	No	2.70
7	39.42	65.78	4^{th}	Yes	9.74
8	10.29	60.69	3^{rd}	No	6.84
9	2.27	130.35	9^{th}	Yes	11.64

Points	Peak (g^2/Hz)	Most Critical Frequency (Hz)	Natural Frequency	Within the range of excitation generated by the propeller	Overall g_{rms}
10	2.03	130.35	9^{th}	Yes	10.37
11	0.39	193.10	20^{th}	No	3.24
12	0.66	447.36	45^{th}	No	4.06
13	0.98	447.36	45^{th}	No	7.55
14	2.24	447.36	45^{th}	No	8.14
15	1.92	102.96	6^{th}	No	4.20
16	1.91	116.21	8^{th}	No	4.33
17	43.18	65.78	4^{th}	Yes	10.25
18	35.01	65.78	4^{th}	Yes	9.29
19	22.56	65.78	4^{th}	Yes	10.19
20	3.06	149.64	12^{th}	No	6.15
21	1.31	116.21	8^{th}	No	5.55
22	0.69	116.21	8^{th}	No	4.39
23	6.31	60.69	3^{rd}	No	6.17
24	11.80	32.05	1^{st}	No	5.38
25	0.95	275.09	27^{th}	Yes	6.59
26	27.57	149.64	12^{th}	No	13.42
27	2.35	393.53	41^{th}	No	9.07
28	5.07	65.78	4^{th}	Yes	9.46
29	1.49	116.21	8^{th}	No	6.10
30	23.79	116.21	8^{th}	No	11.25

6.2.4 Data evaluation

The first structure weights 6.31 Kg whereas the second structure weights 4.74 Kg. The purpose of performing this simulation was to analyze the effect of the reduction of weight caused by the gaps. In this simulation, more points were selected in order to obtain more vibration results. The data collection is presented on the following Table 6.24:

Table 6.24 - Structure II data collection

Simulation	Number of Points		%
	Dimension	$g_{rms}\ out >\ g_{rms}\ ref$	
X-Axis Input	30	19	63%
Y-Axis Input	30	28	93%
Z-Axis Input	30	21	70%

In this structure, the ratio of points with a higher level of vibration than the reference has increased when compared with first structure values. However, it is important to notice that the highest and most critical response in terms of displacement is just 1.88 mm. The following Table 6.25 shows the number of points in which its critical frequency is within the range of the frequencies generated by the propellers.

Table 6.25 - Number of points whose critical frequency is within the range of propellers

Simulation	Number of Points		%
	Dimension	Critical frequency within the range of the frequencies generated by the propeller	
X-Axis Input	30	3	10%
Y-Axis Input	30	0	0%
Z-Axis Input	30	7	23%

The number of points in which its critical frequency is within the range of the frequencies generated by the propeller has decreased when compared to the number of points of Structure I. However, the number of points with a level of vibration higher than reference has increased. The geometry and weight of the structure influence the level of vibration even though its critical frequency is not within the range of frequencies generated by the propeller. Considering the same point, in this structure denominated as 4, the response is 15.10 g_{rms} and the peak value of the PSD response is 47.61 g^2/Hz. Despite its critical frequency is without the range of the frequencies generated by the propeller, this response demonstrates also a resonance. In order to guarantee that responses do not exceed the reference value of vibration, it is necessary to balance structure geometry, its weight and stiffness.

6.3 Structure III

On Table 6.26, it is expressed the results for the first twenty natural modes of the structure.

Table 6.26 - Structure III Natural Frequencies

Modes	1	2	3	4	5	6	7	8	9	10
Natural Frequencies (Hz)	12.28	13.13	27.46	28.89	31.82	34.78	36.62	38.55	39.77	42.35
Modes	11	12	13	14	15	16	17	18	19	20
Natural Frequencies (Hz)	45.09	51.62	58.39	60.68	62.07	68.34	88.25	95.53	99.71	106.52

6.3.1 X-axis input simulation

On the first simulation the vibration input was applied in the X-axis. Displacement, velocity and acceleration responses in all three axes are presented on Table 6.27:

Table 6.27 - Structure III most critical areas after X-Axis Input

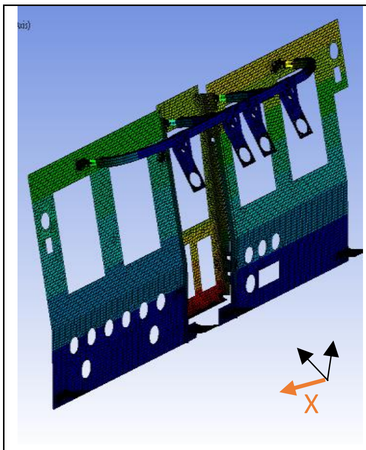	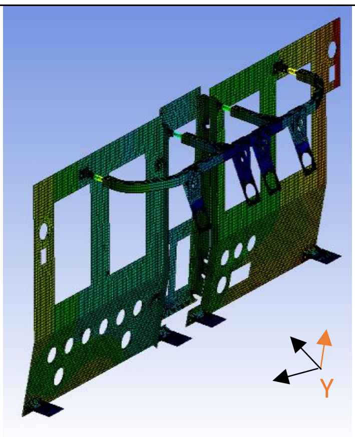	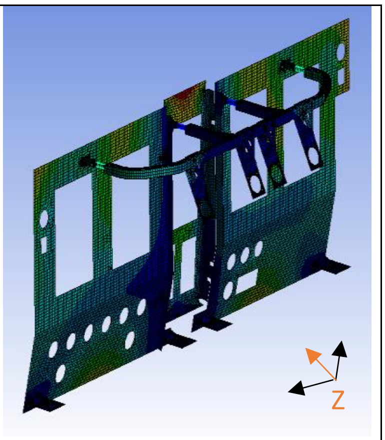
X-Axis Response	Y-Axis Response	Z-Axis Response

The most critical results are shown on Table 6.28:

Table 6.28 - Most critical results after X-Axis Input

	1σ Values			3σ Values		
	x	y	z	x	y	z
Displacement (mm)	1.51	0.35	2.24	4.54	1.07	6.73
Velocity (m/s)	0.33	0.14	0.57	0.99	0.43	1.71
Acceleration (g)	83.18	33.26	167.78	249.56	99.80	503.35

The PSD response is obtained from single points of the structure. The identification of these points is shown on Figure 6.10:

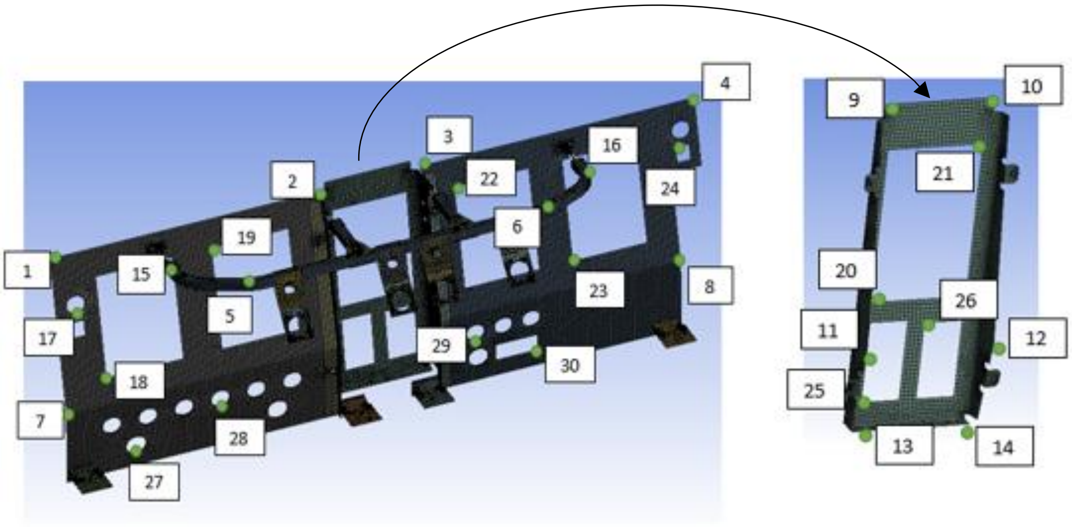

Figure 6.10 - Identification of points that will provide information about PSD response (7)

The PSD results for the identified points are shown on Table 6.29:

Table 6.29 - PSD response for X-axis excitation

Points	Peak (g^2/Hz)	Most Critical Frequency (Hz)	Natural Frequency	Within the range of excitation generated by the propeller	Overall g_{rms}
1	2.49	60.68	14^{th}	No	4.86
2	2.49	60.68	14^{th}	No	4.21
3	1.64	60.68	14^{th}	No	3.74
4	1.67	60.68	14^{th}	No	5.30
5	0.17	421.93	51^{th}	No	3.03
6	$8.38\text{x}10^{-2}$	243.86	33^{th}	No	3.08
7	0.77	243.86	33^{th}	No	4.78
8	0.47	471.17	56^{th}	No	4.58
9	13.75	60.68	14^{th}	No	14.86
10	13.75	60.68	14^{th}	No	14.91
11	12.47	253.33	35^{th}	No	35.88
12	29.21	577.25	66^{th}	No	43.37
13	22.34	28.89	4^{th}	No	13.76
14	21.24	28.89	4^{th}	No	13.67
15	4.41	327.93	42^{th}	No	16.07
16	6.79	499.99	59^{th}	No	19.56
17	1.51	60.68	14^{th}	No	4.76
18	0.80	243.86	33^{th}	No	4.11
19	1.97	60.68	14^{th}	No	3.84
20	13.13	28.89	4^{th}	No	4.10
21	9.02	60.68	14^{th}	No	12.13
22	1.29	60.68	14^{th}	No	3.09
23	0.38	60.68	14^{th}	No	3.99
24	1.13	60.68	14^{th}	No	5.29

Points	Peak (g^2/Hz)	Most Critical Frequency (Hz)	Natural Frequency	Within the range of excitation generated by the propeller	Overall g_{rms}
25	19.50	28.89	4^{th}	No	9.36
26	14.53	28.89	4^{th}	No	4.75
27	0.61	493.93	58^{th}	No	5.54
28	0.66	243.86	33^{th}	No	4.93
29	1.05	471.17	56^{th}	No	5.81
30	1.98	471.17	56^{th}	No	7.68

6.3.2 Y-axis input simulation

On the second simulation the vibration input was applied in the Y-axis. Displacement, velocity and acceleration responses in all three axes are presented on Table 6.30:

Table 6.30 - Structure III most critical areas after Y-Axis Input

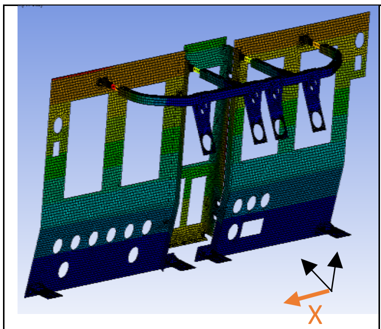	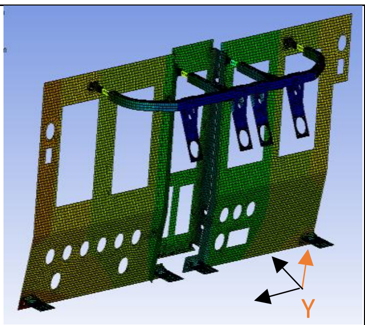	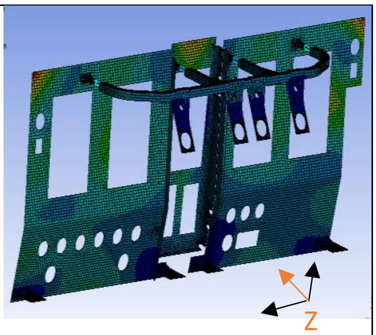
X-Axis Response	Y-Axis Response	Z-Axis Response

The most critical results are shown on Table 6.31:

Table 6.31 - Most critical results after Y-Axis Input

	1σ Values			3σ Values		
	x	y	Z	x	y	Z
Displacement (mm)	0.37	0.82	3.07	1.11	2.46	9.23
Velocity (m/s)	0.08	0.19	0.74	0.25	0.59	2.24
Acceleration (g)	5.88	5.47	18.67	17.65	16.43	56.01

The PSD response is obtained from single points of the structure. The identification of these points is shown on Figure 6.11.

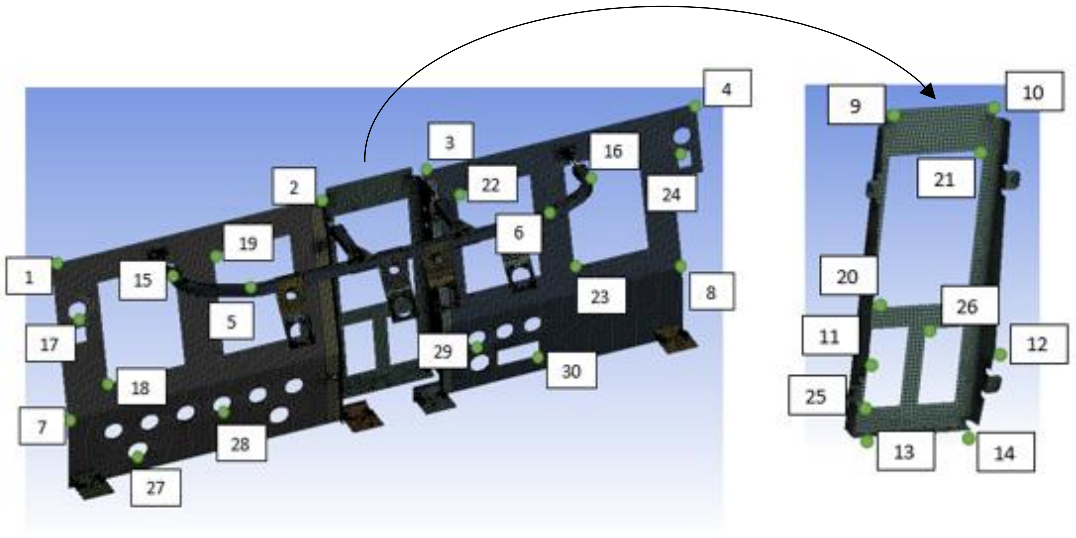

Figure 6.11 - Identification of points that will provide information about PSD response (8)

The PSD results for the identified points are shown on Table 6.32:

Table 6.32 - PSD response for Y-axis excitation

Points	Peak (g^2/Hz)	Most Critical Frequency (Hz)	Natural Frequency	Within the range of excitation generated by the propeller	Overall g_{rms}
1	9.80	39.77	9^{th}	No	3.91
2	10.81	39.77	9^{th}	No	4.08
3	7.51	39.77	9^{th}	No	3.57
4	5.48	39.77	9^{th}	No	3.26
5	0.12	36.62	7^{th}	No	0.85
6	6.83x10^{-2}	34.78	6^{th}	No	0.90
7	9.79	39.77	9^{th}	No	3.91
8	5.62	39.77	9^{th}	No	3.20
9	10.72	39.77	9^{th}	No	4.06
10	7.86	39.77	9^{th}	No	3.61
11	10.96	39.77	9^{th}	No	4.07
12	7.55	39.77	9^{th}	No	3.55
13	10.97	39.77	9^{th}	No	4.23
14	7.44	39.77	9^{th}	No	3.69
15	2.71	39.77	9^{th}	No	3.04
16	3.70	39.77	9^{th}	No	3.11
17	9.86	39.77	9^{th}	No	3.89
18	9.92	39.77	9^{th}	No	3.89
19	10.29	39.77	9^{th}	No	3.92
20	10.86	39.77	9^{th}	No	4.13
21	8.03	39.77	9^{th}	No	3.64
22	7.23	39.77	9^{th}	No	3.46
23	6.36	39.77	9^{th}	No	3.22
24	5.61	39.77	9^{th}	No	3.21

Points	Peak (g^2/Hz)	Most Critical Frequency (Hz)	Natural Frequency	Within the range of excitation generated by the propeller	Overall g_{rms}
25	10.74	39.77	9^{th}	No	4.14
26	9.74	39.77	9^{th}	No	4.03
27	5.46	39.77	9^{th}	No	3.26
28	4.05	39.77	9^{th}	No	3.26
29	5.45	39.77	9^{th}	No	3.33
30	8.80	34.78	6^{th}	No	3.62

6.3.3 Z-axis input simulation

On the third simulation the vibration input was applied in the Z-axis. Displacement, velocity and acceleration responses in all three axes are presented on Table 6.33:

Table 6.33 - Structure III most critical areas after Z-Axis Input

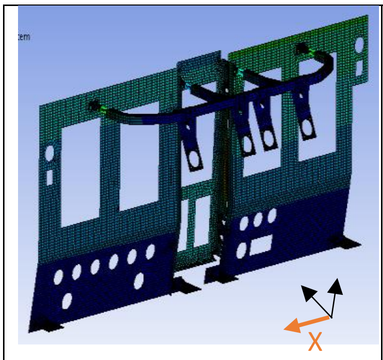	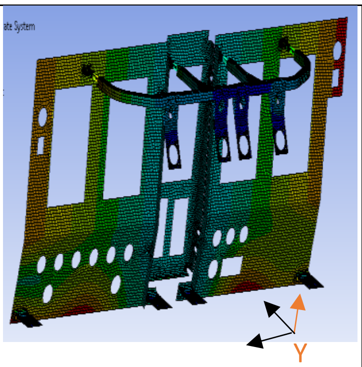	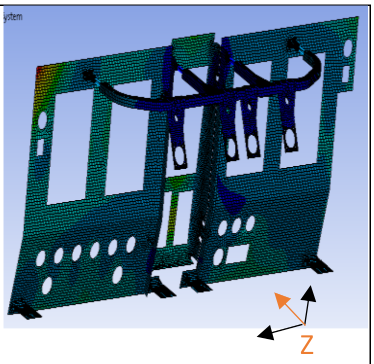
X-Axis Response	Y-Axis Response	Z-Axis Response

The most critical results are shown on Table 6.34:

Table 6.34 - Most critical results after Z-Axis Input

	1σ Values			3σ Values		
	x	y	Z	x	y	Z
Displacement (mm)	0.72	0.34	2.00	2.17	1.01	6.00
Velocity (m/s)	0.13	0.07	0.34	0.39	0.22	1.03
Acceleration (g)	10.77	4.25	8.39	32.31	12.77	25.17

The PSD response is obtained from single points of the structure. The identification of these points is shown on Figure 6.12.

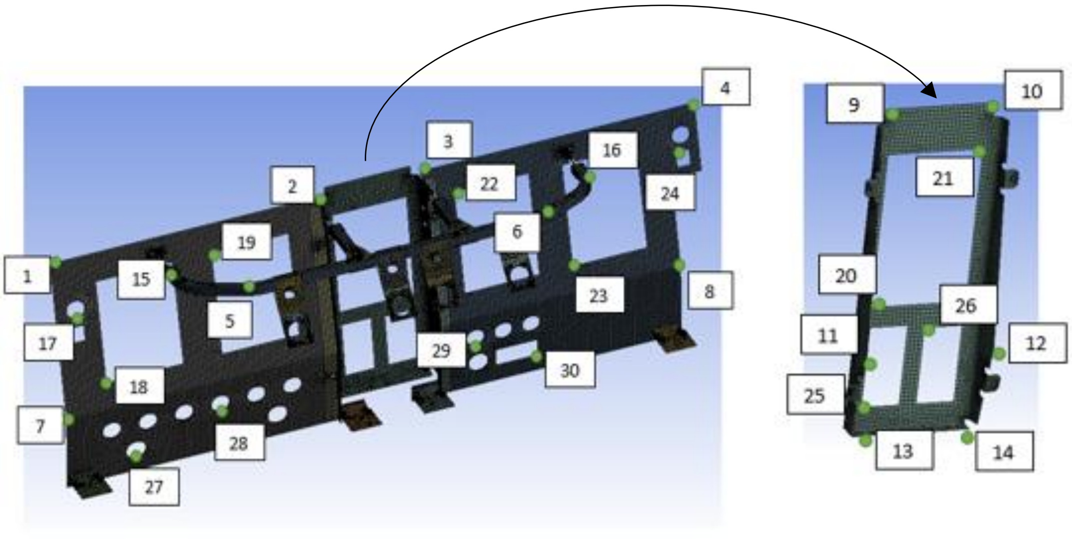

Figure 6.12 - Identification of points that will provide information about PSD response (9)

The PSD results for the identified points are shown on Table 6.35:

Table 6.35 - PSD response for Z-axis excitation

Points	Peak (g^2/Hz)	Most Critical Frequency (Hz)	Natural Frequency	Within the range of excitation generated by the propeller	Overall g_{rms}
1	1.59	38.55	8^{th}	No	5.80
2	9.25x10^{-2}	217.27	28^{th}	No	1.92
3	0.10	27.46	3^{rd}	No	1.58
4	27.63	27.46	3^{rd}	No	8.39
5	0.20	217.27	28^{th}	No	2.34
6	0.45	27.46	3^{rd}	No	2.49
7	0.65	38.55	8^{th}	No	2.95
8	1.44	27.46	3^{rd}	No	3.97
9	0.90	27.46	3^{rd}	No	5.72
10	1.12	27.46	3^{rd}	No	6.05
11	0.18	27.46	3^{rd}	No	2.16
12	0.64	27.46	3^{rd}	No	2.35
13	0.49	27.46	3^{rd}	No	4.44
14	0.89	27.46	3^{rd}	No	4.16
15	0.47	34.78	6^{th}	No	3.01
16	1.45	27.46	3^{rd}	No	3.74
17	3.02	38.55	8^{th}	No	2.70
18	0.32	27.46	3^{rd}	No	2.09
19	0.99	38.55	8^{th}	No	2.95
20	2.02	27.46	3^{rd}	No	2.75
21	1.07	27.46	3^{rd}	No	2.61
22	1.38	27.46	3^{rd}	No	2.66
23	4.15	27.46	3^{rd}	No	3.24
24	10.73	27.46	3^{rd}	No	3.45

Points	Peak (g^2/Hz)	Most Critical Frequency (Hz)	Natural Frequency	Within the range of excitation generated by the propeller	Overall g_{rms}
25	1.26	27.46	3^{rd}	No	2.89
26	2.75	27.46	3^{rd}	No	1.96
27	1.97	38.55	8^{th}	No	3.40
28	4.59	38.55	8^{th}	No	3.65
29	2.43	34.78	6^{th}	No	2.61
30	16.01	34.78	6^{th}	No	4.93

6.3.4 Data evaluation

The weight of Structure III is 59.78 Kg which is much higher than the previous ones due to the addiction of the instruments. This difference of weight has a considerable influence on the results. This simulation is the one which approaches more the instruments panel. The data collection is presented on the following Table 6.36:

Table 6.36 - Structure III data collection

Simulation	Number of Points		%
	Dimension	$g_{rms}\ out > g_{rms}\ ref$	
X-Axis Input	30	15	50%
Y-Axis Input	30	0	0%
Z-Axis Input	30	4	13%

Considering the addiction of the instruments weight, the number of points whose vibration level exceeds the value taken as reference has decreased. The simulation which has more points above the $g_{rms}\ ref$ was the simulation with the X-axis input. Those points belong mostly to the center panel engine indicator. The following Table 6.37 shows the number of points in which its critical frequency is within the range of the frequencies generated by the propeller.

Table 6.37 - Number of points whose critical frequency is within the range of propellers

Simulation	Number of Points		%
	Dimension	Critical frequency within the range of the frequencies generated by the propeller	
X-Axis Input	30	0	0%
Y-Axis Input	30	0	0%
Z-Axis Input	30	0	0%

There are no points whose critical frequency is within the range of the frequencies generated by the propeller. There were several responses values above 10 g_{rms} mostly on points which belong to the center panel engine indicator. The points which are above of the reference value of vibration are located in the superior corners of the panel. In order to ensure that there will not be points with higher level of vibration, it is necessary to proceed to modifications on structure.

6.4 Concluding Remarks

The methodology of random vibration analysis was applied to all three structures. Critical areas were identified and PSD analysis were performed to multiple points. Peak values, critical frequencies, modes of vibration, overall g_{rms} values were registered for each simulation and for each point. It was reported the number of points whose g_{rms} of the response was higher than a reference value. It was noted if the critical frequencies were within the range of the frequencies generated by the propeller. On the following Table 6.38 and Table 6.39, it is presented the overall data collection:

Table 6.38 - Overall data collection

Simulation	Number of Points		%
	Dimension	$g_{rms}\ out > g_{rms}\ ref$	
Total Structure I	51	29	57%
Total Structure II	90	68	76%
Total Structure III	90	19	21%

Table 6.39 - Number of points whose critical frequency is within the range of propellers

Simulation	Number of Points		%
	Dimension	Critical frequency within the range of the frequencies generated by the propeller	
Total 1st Structure	51	35	39%
Total 2nd Structure	90	10	11%
Total 3rd Structure	90	0	0%

The maximum σ-values of acceleration are marked with a yellow background (e.g., 12.71). It is possible to notice that these marked values are very similar to the g_{rms} values of PSD response, as expected.

Resonance phenomena occur not only when structure natural frequencies are within the range of frequencies generated by the propeller. This occurrence is also due to structure geometry. In these situations, it is recommended to proceed to modifications on structure.

For the Structure I and Structure II, the most critical points are identified with a red circle on Figure 6.13. The levels of vibration could be attenuated on these points if the simulation were performed with a glare-shield. A glare-shield is illustrated on Figure 6.14. This part will provide stiffness to the corners of the structure.

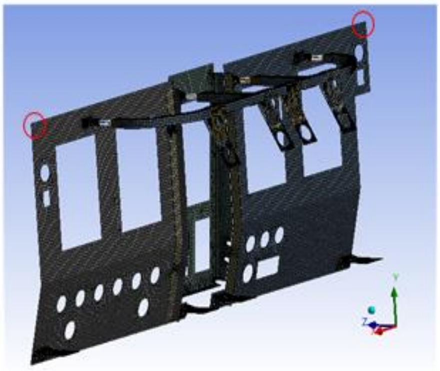

Figure 6.13 - Identification of most critical areas

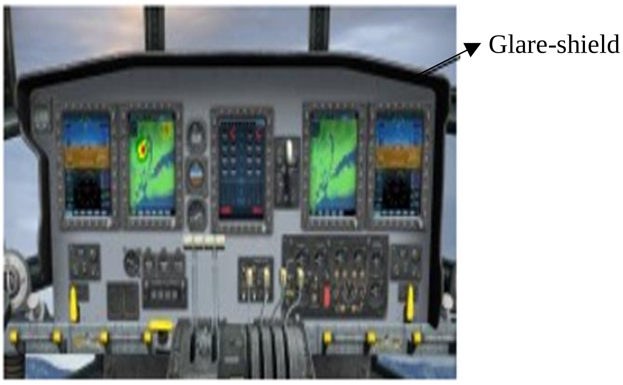

Figure 6.14 - Glare-shield

When the weight of the instruments was added, the vibration level of the corner points was attenuated. However, the levels of vibration on the center panel engine indicator increased. This part is represented in Figure 6.15, the yellow circles symbolize the fixation and the red circles symbolize the critical areas. In order to attenuate these high values, the weight of the instruments on this part has to be reduced or the fixation of the part has to be reinforced providing more stiffness.

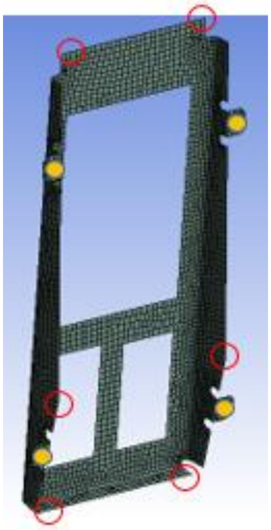

Figure 6.15 - Center panel engine indicator

Another method to attenuate undesirable vibration is by installing damping isolators. In the following chapter, it will be presented the methodology in order to select the most suitable damping isolator.

7 Vibration Isolation

Simulations were carried out without damping isolators. It is important to select a mount to avoid undesirable vibration. The damping isolators will be located at boundary conditions specified in Figure 7.1. Thus, eight mounts will be implemented in the structure providing damping.

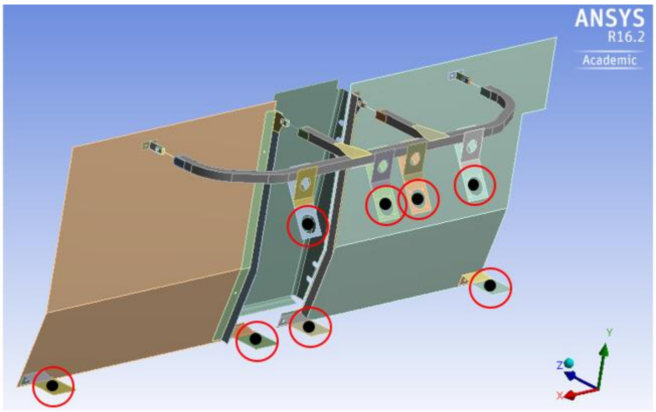

Figure 7.1 - Localization of damping isolators

The selected damping isolator is a low-frequency, highly damped mount for a high level of vibration isolation and belongs to L-Mount Series. Its application is suitable for avionic equipment in propeller driven aircraft and meets vibration and shock requirements of MIL-STD-172C and meets safety requirements of MIL-E-5400. The selected model is the L44 [42]. The following Table 7.1 shows its specifications.

Table 7.1 - L-Mount Specifications

Natural Frequency	7-10 Hz
Transmissibility at Resonance	2.5
Resilient Element	Friction Damped Spring
Standard Materials	Aluminum
Operating Temperature Range	-55°C to +120°C
Weight	0.098 lbs

Combination of springs with air damping

A method of adding damping to a spring is by using an air chamber with an orifice for measuring the air flow. An example of this type of isolator is illustrated in Figure 7.2. In this construction, the load-carrying spring is located within the confines of an elastomeric damping balloon. The air chamber is formed by closing the balloon with a capsule which contains an orifice. Under dynamic excitations the air in the balloon passes through a predetermined sized orifice by which damping is controlled. [43]

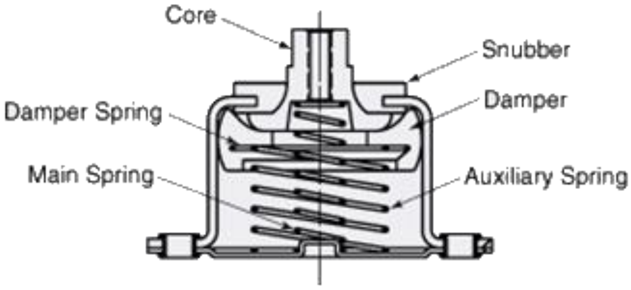

Figure 7.2 - Isolator using friction damped spring

The methodology of mount selection is provided by the OEM and it is presented on the following steps:

Step 1

- Determine the frequency of the disturbing vibration (F_d)
- If the speed is specified in RPM or CPM, it must be converted to cycles per second (Hz) by dividing by 60.
- There could be more than one disturbing frequency. However, if the lowest frequency is isolated, then all the other higher frequencies will also be isolated. In the specific case of the propeller C-130H, the disturbing vibration is described in (7.1).

$$F_d = 68\,Hz \tag{7.1}$$

Step 2

- Determine the minimum isolator natural frequency that will provide isolation ($F_{n,min}$). For this example, $F_{n,min}$ is represented in (7.2).

$$\begin{gathered} F_{n,min} = \frac{F_d}{\sqrt{2}} \\ \Longrightarrow F_{n,min} \cong 48\,Hz \end{gathered} \tag{7.2}$$

If this $F_{n,min}$ is exceeded, this isolation system will not perform properly, and it is quite possible that vibrations will be amplified. Isolators that have a F_n lower than $F_{n,min}$ will provide isolation.

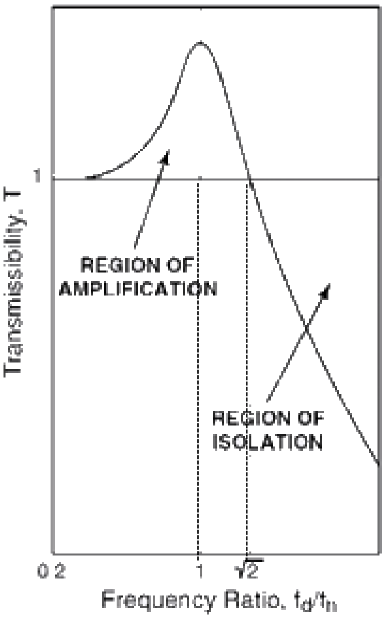

Figure 7.3 - Amplification and isolation regions

Step 3

The chosen isolator L44 Mount has a natural frequency, F_n of 10 Hz. Considering $F_d = 68\ Hz$, it is possible to calculate the transmissibility through equation (7.3).

$$T = \left| \frac{1}{1 - \left(\frac{F_d}{F_n}\right)^2} \right| = 0.022 < 1 \tag{7.3}$$

The level of isolation, V, is calculated trough equation (7.4).

$$T = 1 - V \tag{7.4}$$

Therefore $T = 0.022$ is equal to 97.8 % level of isolation.

In order to verify if the selection of this specific mount is suitable, it is also necessary to ensure that the displacement of the spring at resonance does not exceed the mount deflection capability. The OEM suggests to calculate performance limits based on the relationship of equations (7.5) and (7.6). F_n represents mount's natural frequency expressed in Hz. S_f is the PSD input in the region of isolator resonance expressed in g^2/Hz. T_r represents the resonant transmissibility. Y represents the response displacement expressed in inches.

$${G_{rms}}^2 = \frac{\pi}{2} \cdot F_n \cdot T_r \cdot S_f \tag{7.5}$$

$$Y = \frac{9.8 \cdot G_{rms}}{(F_n)^2} \tag{7.6}$$

Considering the values of (7.7):

$$\begin{cases} F_n = 10\ Hz \\ S_f = 0.01\ \ g^2/Hz \\ T_r = 2.5 \end{cases} \tag{7.7}$$

$$\Longrightarrow\ Y = 0.06\ inches \tag{7.8}$$

Y represents a 1σ-value in random vibration theory. It means that the percentage of probability of occurrence superior deflections is more than 30%. It is important to calculate the 3σ-value to guarantee that there will not be superior deflections with a probability of 99.7%, this value is represented in (7.9).

$$\Longrightarrow\ 3Y = 0.18\ inches \tag{7.959}$$

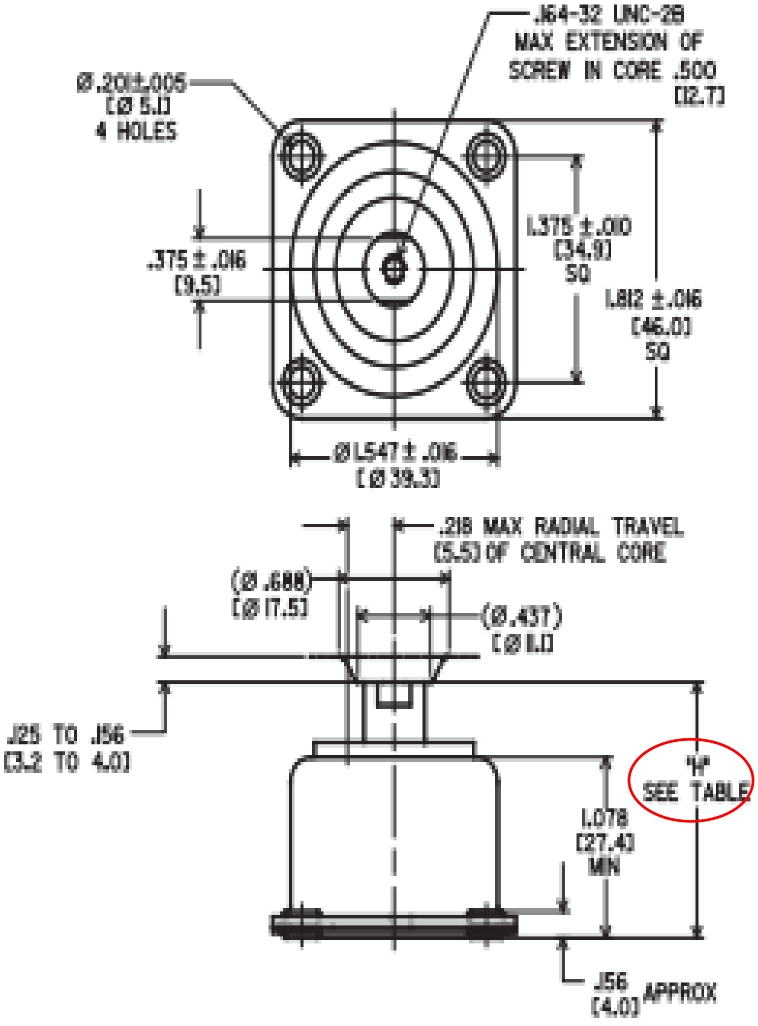
.164-32 UNC-2B
MAX EXTENSION OF
SCREW IN CORE .500
[12.7]
Ø.201±.005
[Ø 5.1]
4 HOLES
1.375 ±.010
[34.9]
SQ
.375 ± .016
[9.5]
1.812 ±.016
[46.0]
SQ
Ø1.547 ± .016
[Ø 39.3]
.218 MAX RADIAL TRAVEL
[5.5] OF CENTRAL CORE
(Ø .688)
[Ø 17.5]
(Ø.437)
[Ø 11.1]
.125 TO .156
[3.2 TO 4.0]
"H"
SEE TABLE
1.078
[27.4]
MIN
.156
[4.0] APPROX

Figure 7.4 - L44 Dimensional Drawing

Table 7.2 - L44 Height of aluminum core

L44 Mount	L-44-AA
Height of aluminum core (inches) – “H”	
Compressed (min)	0.975
Extended (max.)	1.632

As seen from the L44 mount specifications, the height of aluminum core is 0.975 inches when compressed and 1.632 inches when extended. Therefore, the mount deflection capability is 0.657 inches. Thus L44 S-Mount is suitable for this isolation case. [44]

If the calculations were made with the level of vibration input in the region of isolator resonance of $S_f = 0.10\ g^2/Hz$ in a conservative way, the response displacement will be $3Y = 0.58\ inches$ which is also within the range of the mount deflection capability.

8 Methodology

The methodology procedures are presented in the form of flowcharts along the phases of CAD, FEM, dynamic analysis, results and validation results. The diagrams are in Appendix B and are considered as one of the main contribution from this dissertation. The associated symbolism is described in Table 8.1 below:

Table 8.1 - Meaning of flowchart symbols

Symbol	Meaning
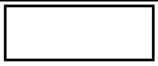	Process
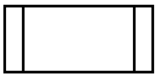	Sub-process
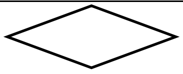	Decision
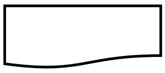	Document
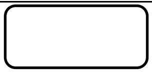	Start/End

The outputs are considered to be a result from the inputs, this transformation is obtained due to a process. The flowchart below is a general example in which it is possible to note that outputs are considered to be a function of the inputs $[Out1, Out2] = f(Inp1, Inp2, Inp3)$.

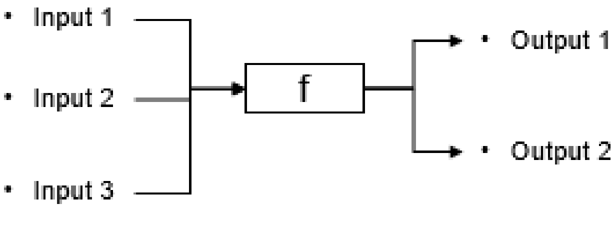

Figure 8.1 - Transformation of inputs and outputs

Along the flowchart methodology, there are three sub-processes that are not detailed. The following flowcharts has the purpose of clarifying the sub-processes of FEM modelling, random vibration test and shock mounts installation.

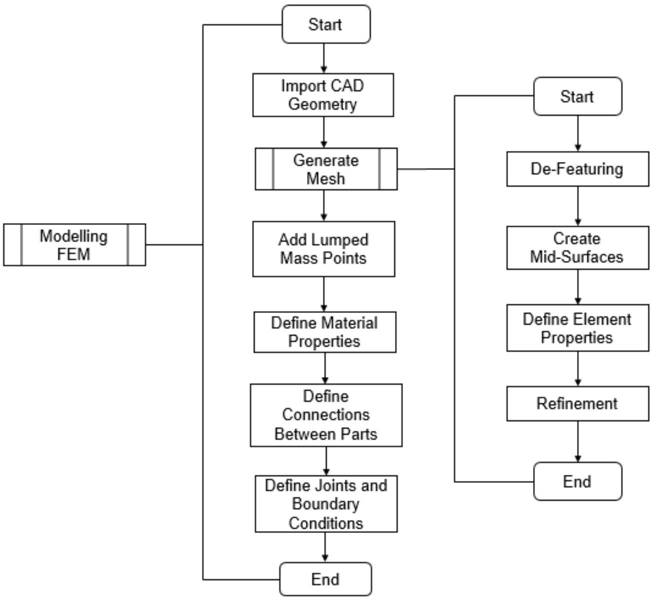
Modelling FEM
Start
Import CAD Geometry
Generate Mesh
Add Lumped Mass Points
Define Material Properties
Define Connections Between Parts
Define Joints and Boundary Conditions
End
Start
De-Featuring
Create Mid-Surfaces
Define Element Properties
Refinement
End

Figure 8.2 – FEM Modelling sub-process

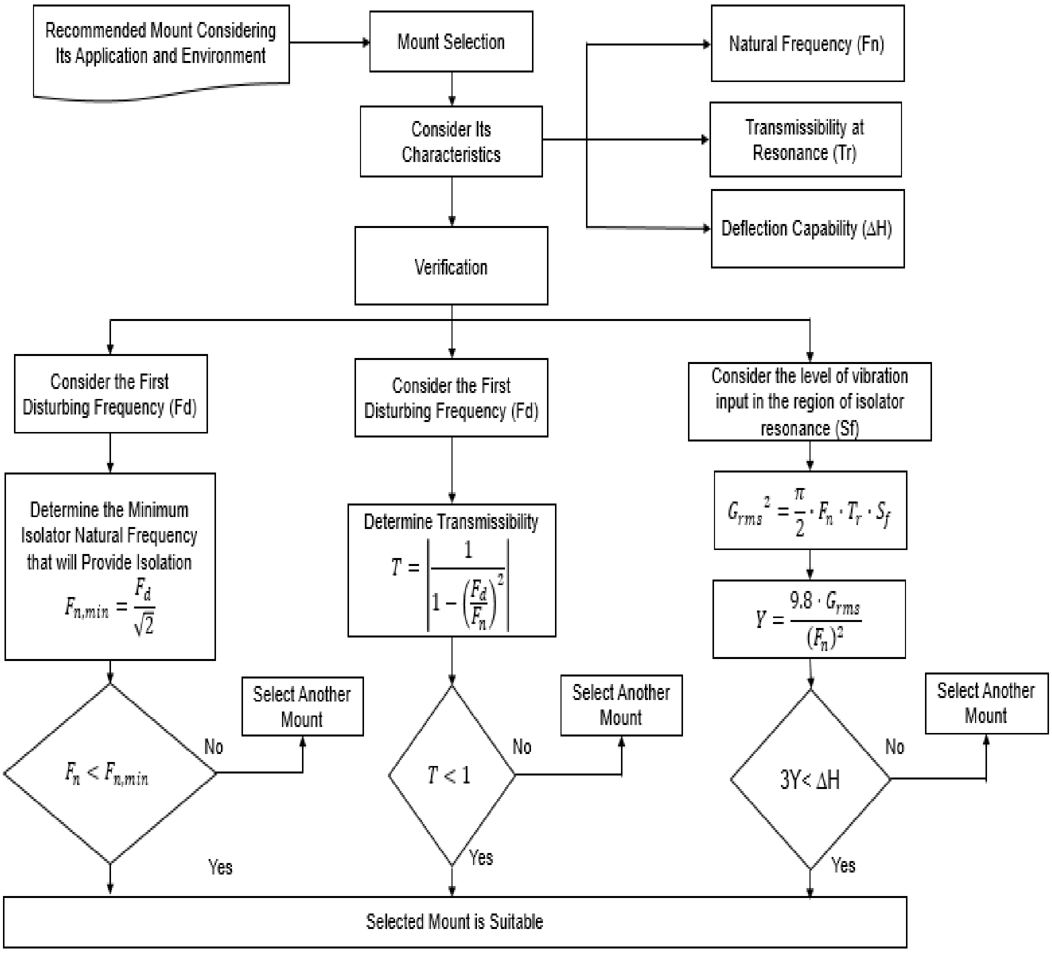
Recommended Mount Considering Its Application and Environment
Mount Selection
Consider Its Characteristics
Natural Frequency (Fn)
Transmissibility at Resonance (Tr)
Deflection Capability (ΔH)
Verification
Consider the First Disturbing Frequency (Fd)
Consider the First Disturbing Frequency (Fd)
Consider the level of vibration input in the region of isolator resonance (Sf)
Determine the Minimum Isolator Natural Frequency that will Provide Isolation
$F_{n,min} = \frac{F_d}{\sqrt{2}}$
Determine Transmissibility
$T = \left| \frac{1}{1 - \left(\frac{F_d}{F_n}\right)^2} \right|$
$G_{rms}{}^2 = \frac{\pi}{2} \cdot F_n \cdot T_r \cdot S_f$
$Y = \frac{9.8 \cdot G_{rms}}{(F_n)^2}$
$F_n < F_{n,min}$
$T < 1$
3Y< ΔH
No
No
No
Select Another Mount
Select Another Mount
Select Another Mount
Yes
Yes
Yes
Selected Mount is Suitable

Figure 8.3 - Shock mounts installation sub-process

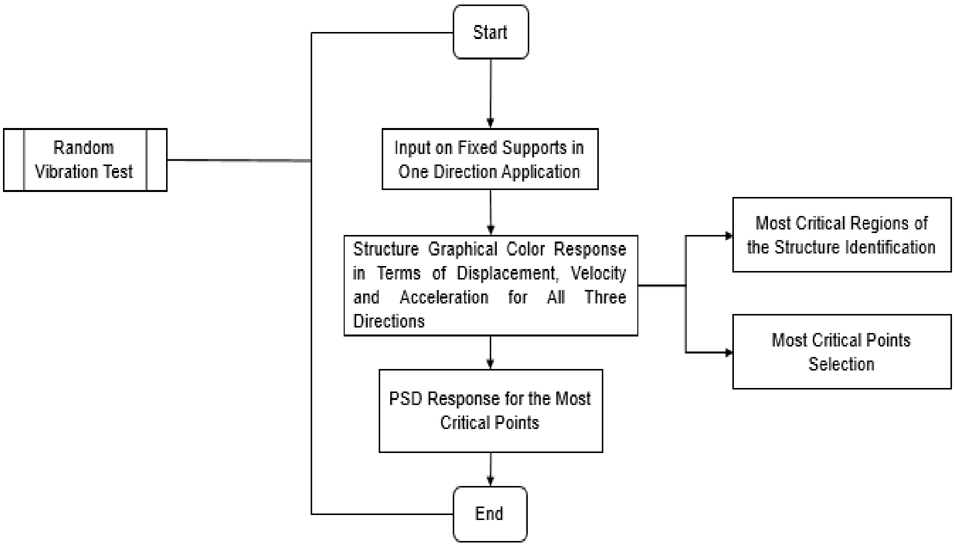
Start
Random Vibration Test
Input on Fixed Supports in One Direction Application
Structure Graphical Color Response in Terms of Displacement, Velocity and Acceleration for All Three Directions
Most Critical Regions of the Structure Identification
Most Critical Points Selection
PSD Response for the Most Critical Points
End

Figure 8.4 - Random vibration sub-process

In the phase of validation results, a decision has to be made according to a factor of safety. A Margin of Safety (MS) was used as a measure of verification to describe the ratio of the strength of the structure to the requirements. Its definition is described in (8.1).

$$MS = \frac{allowable}{applicable} - 1 \tag{8.1}$$

According with STD-MIL-810 tolerances, the level of the response ($g_{rms,in}$) should not be higher than 10% of the level of the input ($g_{rms,in}$) represented in (8.2).

$$\frac{g_{rms,out} - g_{rms,in}}{g_{rms,in}} \leq 0.1 \tag{8.2}$$

Applying to the case study, the margin of safety is described in (8.3).

$$MS = \frac{1.1 \times g_{rms,in}}{g_{rms,out}} - 1 \tag{8.3}$$

When $MS \geq 0$, the tolerance is not exceeded and that leads to a process of an elaboration of assessment report. The output will be the validation of the vibration results.

9 Conclusions

9.1 Concluding remarks

This dissertation has its origin on the necessity of assisting a design certified company credited as DOA in a preliminary phase of project modification. The scope of thesis work definition arose from a company current problem/need. This work was performed in order to be a guidance for future possible projects of modification. The main objective was the implementation of recommended procedure guidelines for a vibration analysis on aircraft components.

A robust explanation of vibration analysis fundamentals was presented. The importance of measuring possible loads which are suitable to be classified as random was clarified. Random vibration can be described in a statistical sense. Its instantaneous magnitude at any time is not possible to predict, but it is feasible to define the probability of its magnitude exceeding a certain value. The concept of PSD was presented which is a sophisticated and extremely useful form of measuring random vibration. A dynamic analysis methodology was presented.

Since the certification in aeronautic industry is a meticulous process, and in order to approve a procedure of aircraft components modification, it is fundamental that simulations of these components are in compliance with international standards. It is essential for a part being considered acceptable. MIL-STD-810G standard was reviewed and chapters of interest were indicated.

Regarding the case study presented herein, the most important technical features of CAD and FEM modelling were detailed. Material properties, strategic simplifications, elements characteristics were exposed in order to obtain a simplified FE model. It was possible to conclude that the simplified mesh generated from a shell formulation was composed of much less number of elements and nodes. The mesh became much more efficient due to the reduction of computational effort without affecting the properties of the whole structure. A study on the natural frequencies was conducted, it was concluded that natural frequencies of the structure are influenced by the change of the boundary conditions. The natural frequencies had a tendency to increase when the fixation of the structure was becoming more constrained. And consequently, the number of resonant frequencies within the specified ranges decreased. Since it exists a natural frequency for each degree of freedom, the conclusion was that by constraining more the structure, the resonant frequencies grew to values out of the specified ranges.

The methodology of random vibration analysis was applied to three structures. Critical areas were identified and PSD analysis were performed to multiple points. Peak values, critical frequencies, modes of vibration, overall g_{rms} values were registered for each simulation and for each point. It was reported the number of points whose g_{rms} of the response was higher than a reference value. It was noted if the critical frequencies were within the range of the frequencies generated by the propellers. It was also concluded that resonance phenomena occur not only when structure natural frequencies are within the range of frequencies generated by the propellers and this occurrence was due to structure geometry. In those situations, it was recommended to proceed to modifications on structure. Critical areas were identified and it was suggested possible modifications on the structure. A methodology was also presented in order to select the most suitable damping isolators.

Appendix B shows the global methodology for the whole process of structural modification which is intended to be a valuable procedure tool that can deliver an effective, prompt and valuable response for a project of this nature, fulfilling in this way the dissertation proposed objectives.

9.2 Future considerations

As future improvements to this dissertation, it will be interesting to implement the recommended modifications in the structure according with the suggested methodology until the vibration results are in compliance with the STD-MIL-810G. Once the simulation results are within the required tolerances, it would also be interesting to carry out an experimental test with a shaker, a proper fixture and accelerometers in a laboratory in order to complement the work.

Taking advantage from Ansys Workbench which was the software in which all simulations were performed, it would be interesting to explore the feature of Design of Experiments. Using this feature, it is possible to optimize the instrument masses and its position in the panel in order to minimize vibrations.

After carrying out a vibration analysis, a study on a fatigue analysis should be implemented. A random fatigue analysis is a further study to a random vibration analysis as follows. The moments of a one-sided (positive frequency) power spectral density are defined as presented in (9.1) wherein M_j represents the jth moment of the one-sided spectral density, f represents the frequency [Hz] and W_S represents the one-sided power spectral density [amplitude^2/Hz] [45].

$$M_j = \int_0^\infty f^j \, W_S(f) df \tag{9.1}$$

The first moment of the PSD response can be calculated and be considered as an ‘Apparent Frequency’. This is an average frequency that the RMS response can be considered to balance under the PSD curve. RMS stress and apparent frequency can be used in fatigue damage calculations by considering the random excitation input as an equivalent sinusoidal history. Its constant period will be the inverse of the apparent frequency. Figure 9.1 is an example of the sinusoidal signal that will be taking into account.

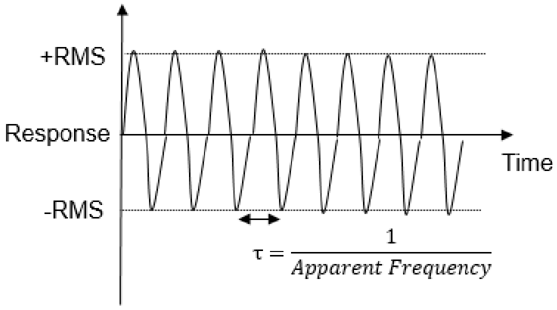

Figure 9.1 - Equivalent sinusoidal history

10 Bibliography

[1] A. Stolzer, *Safety Management Systems in Aviation*, 2nd ed. Ashgate Publishing, 2015

[2] D. M. Anderson, *Design for Manufacturability - How to Use Concurrent Engineering to Rapidly Develop Low-Cost, High-Quality - Products for Lean Production*, 1st ed. CRC Press, 2014

[3] A. Mourão, "O que é um produto" *Departamento Engenharia Mecânica e Industrial Faculdade Ciências e Tecnologia - Universidade Nova de Lisboa*

[4] F. De Florio, *Airworthiness: An Introduction to Aircraft Certification: A Guide to Understanding JAA, EASA, and FAA Standards*, 1st ed. 2006

[5] "ICAO." [Online]. Available: http://www.icao.int/about-icao/Pages/default.aspx.

[6] "EASA." [Online]. Available: https://easa.europa.eu/the-agency

[7] "ANAC." [Online]. Available: http://www.anac.pt/vPT/Generico/ANAC/QuemSomos/Paginas/QuemSomos.aspx

[8] R. Atkinson, "Project management : cost , time and quality , two best guesses and a phenomenon , its time to accept other success criteria" *International Journal of Project Management Elsevier Science*, vol. 17, no. 6, pp. 337–342, 1999

[9] "ISO 9000 - Quality Management." [Online]. Available: http://www.iso.org/iso/home/standards/management-standards/iso_9000.htm

[10] C. Rodgers, "Focus on Confidence in Results" *BenchMark*, 2016

[11] A. Ramsey, "Raising your Game with Good Simulation Governance" *BenchMark*, 2016

[12] J. Smith, "Quality Management in Engineering Simulation" *BenchMark*, 2016

[13] C. de S. W., *Vibration: Fundamentals and Practice*, 2nd ed. Taylos&Francis, 2006

[14] Massachusetts Institute of Technology, [Online]. Available: http://ocw.mit.edu/courses/mechanical-engineering/2-003-modeling-dynamics-and-control-i-spring-2005/labs/lab_3/

[15] A. P. V. Urgueira, "Vibrações Mecânicas e Ruído" *Departamento Engenharia Mecânica e Industrial Faculdade Ciências e Tecnologia - Universidade Nova de Lisboa*, 2015

[16] N. N. Nunes and J. M. Silva, "Introdução às Vibrações Mecânicas"

[17] P. H. Wirsching, T. L. Paez, and K. Ortiz, *Random Vibrations - Theory and Practice*, 1st ed. John Wiley & Sons, Inc.

[18] T. Irvine, “An Introduction to Random Vibration” *Vibration Data Publications*, pp. 1–13, 2000

[19] F. Kihm, A. Halfpenny, and N. S. Ferguson, “Fatigue life from sine-on-random excitations” *Procedia Engeneering*, vol. 101, pp. 235–242, 2015

[20] T. Irvine, “Sine Sweep Frequency and Octave Calculations” *Vibration Data Publications*, pp. 1–5

[21] D. Steinberg, *Vibration Analysis for Electronic Equipment*, 3rd ed. John Wiley & Sons, Inc., 2000

[22] S. S. Rao, *Mechanical Vibrations*, 4th ed. Prentice Hall

[23] J. Van Baren, “What is Random Vibration Testing?” *Sound&Vibration*, pp. 9–12, 2012

[24] T. Irvine, “An Abbreviated Time Domain Analysis Method for a PSD Base Input” *Vibration Data Publications*, pp. 1–8, 2013

[25] A. Halfpenny, “Describing Random Vibrating Loads Using the PSD”, *BenchMark*, pp. 30–38, 2014

[26] A. Halfpenny, “Dynamic Analysis of Both On and Oftshore Wind Turbines in the Frequency Domain” *University College London*, 1998

[27] R. B. Randall, *Application of B & K Equipment to Frequency Analysis*, 2nd ed. Bruel & Kjaer, 1977

[28] T. Irvine, “An Introduction to Spectral Functions” no. 2, pp. 9–10, 2000

[29] W. Tustin, “What is the meaning of PSD in g^2/Hz units?” *VMEbus Systems Magazine*, 2005

[30] S. L. Miller and D. Childers, *Probability and Random Processes With Applications to Signal Processing and Communications*, 2nd ed. Elsevier Inc., 2012

[31] Department of Defense, “MIL-STD-810G DoD Test Method Standard Environmental Engineering Considerations and Laboratory Tests”, 2008

[32] M. Muider and R. Hosman, “Perception of flight information from efis displays” *Pergamon, Elsevier Sci. Ltd*, no. 3, pp. 383–390, 1997

[33] S. Smith, “Dynamic characteristics and human perception of vibration aboard a military propeller aircraft” *Journal Industrial Ergonomics Elsevier*, vol. 38, pp. 868–879, 2008

[34] P. Andersson and T. Alm, “Perception aspects on perspective aircraft displays” *Displays, Elsevier*, vol. 24, pp. 1–13, 2003

[35] P. Andersson and C. Von Hofsten, “Readability of vertically vibrating aircraft displays” *Displays, Elsevier*, vol. 20, pp. 23–30, 1999

[36] RTCA, “RTCA DO-160F - Environmental Conditions and Test Procedures for Airborne Equipment”, 2007

[37] S. S. Rao, *The Finite Element Method in Engineering*, 4th ed. Butterworth-Heinemann ltd, Elsevier, 2005

[38] P. G. Coelho and J. B. Cardoso, “Métodos Computacionais Em Engenharia Mecânica” *Departamento Engenharia Mecânica e Industrial Faculadade Ciências e Tecnologia - Universidade Nova de Lisboa*, p. 171, 2012

[39] T. Nelson and E. Wang, “Reliable FE-Modeling with ANSYS” *Cadfem Gmbh*, 2004

[40] “MathWeb.” [Online]. Available: http://asm.matweb.com/search/SpecificMaterial.asp?bassnum=MA2024T3

[41] “ANSYS Mechanical APDL Theory Reference 15.0” 2013

[42] “Hutchinson Aerospace & Industry” [Online]. Available: http://www.hutchinsonai.com/products/product.cfm?cid=3&fid=15

[43] “Barry Controls” [Online]. Available: http://www.novibration.com/lmounts.htm

[44] BarryControls, “OEM Technical Information”

[45] C. E. Larsen and T. Irvine, “A review of spectral methods for variable amplitude fatigue prediction and new results” *Procedia Engineering*, vol. 101, pp. 243–250, 2015

[46] K. Mobley, *Vibration Fundamentals*, 1st ed. Butterworth-Heinemann ltd, Elsevier, 1999

[47] D. E. Newland, *An Introduction to Random Vibrations, Spectral & Wavelet Analysis*, 3rd ed. Dover Publications Inc.

[48] J. Fourier, *The Analytical Theory of Heat(Unabridged)*, Cosimo Classics

[49] A. Halfpenny, “What is the Frequency Domain and how do we use a PSD”, *nCode International Ltd.*

[50] N. N. Nunes, “Contribuição para a Concepção de Sistemas Inteligentes de Dignóstico em Controlo de Condição por Análise de Vibrações de Motores de Aeronaves” *Istituto Superior Técnico*, 2005

[51] B. J. W. Cooley and J. W. Tukey, “An Algorithm for the Machine Calculation Complex Fourier Series” pp. 297–301, 1964

[52] R. B. Randall, *Frequency Analysis*, 3rd ed. 1987

11 Appendix A

11.1 The Fourier Transform

Vibration can be acquired and analysed in two datas types: time domain and frequency domain. These are associated with each other. In fact, frequency domain is simply another way of representing a time history. Furthermore, the frequency domain is used in order to get a different perspective on a time signal. Both domains provide usefull information so it is often to transform signals. This transformation between time and frequency domain is accomplished using the Fourier Transform.

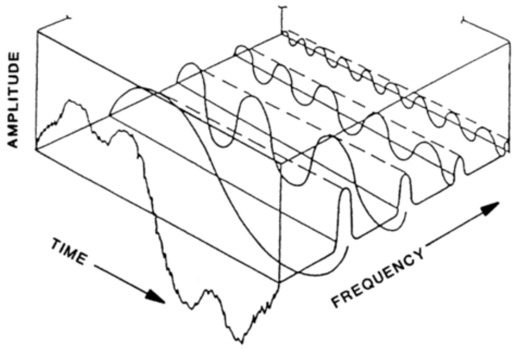

Figure 11.1-Relationship between time domain and frequency domain[46]

Fourier's Hypothesis

A signal which repeats itself in time is considered a periodic signal. A periodical function is shown in the (11.1) wherein T represents the period:

$$f(t) = f(t+T) \tag{11.1}$$

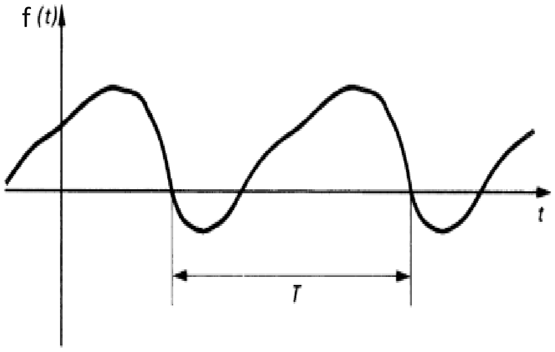

Figure 11.2- Arbitrary periodic function of time[47]

Mathematical theory shows that any periodic function of time can be represented by a series of sine functions of various amplitude, frequency and phase [48]. If $f(t)$ is a periodic function of time, it is possible to express $f(t)$ as an infinite trigonometric series. This is the principle on which the Fourier series is based on. Equation (11.2) represent the Fourier series expansion.

$$f(t) = a_0 + \sum_{k=1}^{\infty} \left(a_k \cdot \cos\left(\frac{2\pi \cdot k}{T} \cdot t\right) + b_k \cdot \sin\left(\frac{2\pi \cdot k}{T} \cdot t\right)\right) \tag{11.2}$$

$$a_0 = \frac{1}{T} \int_{-T/2}^{T/2} f(t)\, dt \tag{11.3}$$

$$a_k = \frac{2}{T} \int_{-T/2}^{T/2} f(t) \cdot \cos\left(\frac{2\pi \cdot k}{T} \cdot t\right) dt \tag{11.4}$$

$$b_k = \frac{2}{T} \int_{-T/2}^{T/2} f(t) \cdot \sin\left(\frac{2\pi \cdot k}{T} \cdot t\right) dt \tag{11.5}$$

$$k = 1,2,3 \ldots$$

$$k \in \mathbb{Z}$$

$$T = period$$

The Fourier coefficients a_0, a_k, b_k provide information on the frequency content of time history. a_0 represents the mean value of the time history while a_k and b_k effectively filter the time history to provide the amplitude of the trigonometric waves from which the history is comprised.

However, manipulate algebraically these coefficients is an arduous task because of the different sine and cosine terms associated with them. In order to simplify this problem, it is used a complex coefficient C_k which replaces all other three represented in (11.6).

$$C_k = \frac{1}{2}(a_k - ib_k) \tag{11.6}$$

The sine and cosine terms can be expressed in the exponential form in (11.7).

$$e^{\pm i\theta} = \cos\theta \pm i \sin\theta \tag{11.7}$$

Consequently, the complex Fourier series expansion representation of a time history can be represented as shown in (11.8).

$$f(t) = \sum_{k=0}^{\infty} C_k \cdot e^{i\left(\frac{2\pi k}{T} \cdot t\right)} \tag{11.8}$$

The complex coefficient C_k represented in (11.9) has a real and an imaginary component. The plot of these components represents in effect the frequency domain.

$$C_k = \frac{2}{T}\int_{-T/2}^{T/2} f(t)\cdot e^{-i\left(\frac{2\pi k}{T}\cdot t\right)}dt \tag{11.9}$$

C_k provides information on frequency content of the time history. The k^{th} coefficient relates to a sinusoidal wave of frequency k/T Hz. The modulus of the complex number $|C_k|$ determines the amplitude of the wave and the initial phase of the wave by its argument. From the frequency plots below there are information about the real and imaginary components related to the second harmonic (k=2). Therefore, it is possible to calculate the frequency, amplitude and phase of this specific wave.

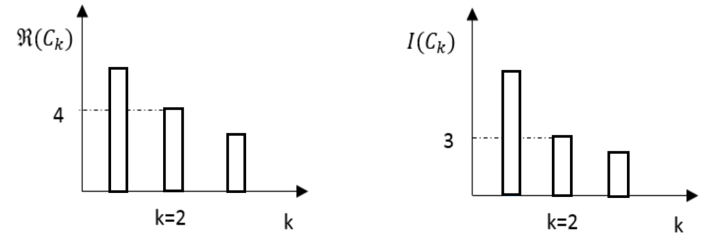

Figure 11.3 - Real and imaginary Fourier coefficients

However, each Fourier coefficient can only be obtained for discrete frequencies at k/T Hz. This is a problem because when the same time history is sampled with different sample periods, the information about sinusoidal waves is given for a set of different frequencies.

This dependence on the sample period, T, has to be eliminated in order to normalize the coefficients. The normalized coefficients take the form of a density function and by taking the area under the density curve for the range of Δf it is possible to obtain the real and imaginary Fourier coefficient.

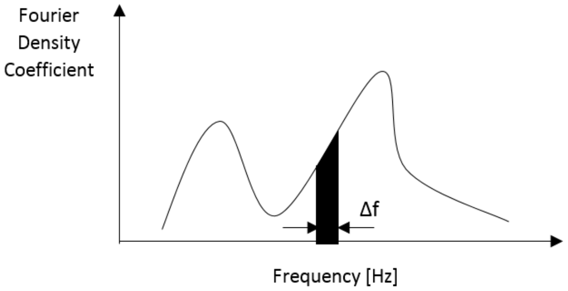

Figure 11.4 - The Fourier density spectrum

When Δf tends to zero it is possible to express the summation of discrete values in Equation (11.10) as an integral with limits between $-\infty$ and $+\infty$ in a continuous process. The following equations are the classical and the definition of Fourier Transform and Inverse Fourier Transform.

Fourier Transform from time to frequency domain is represented in (11.10).

$$F(f) = \int_{-\infty}^{\infty} f(t) \cdot e^{-i2\pi \cdot f \cdot t} dt \tag{11.10}$$

Fourier Transform from frequency to time domain is represented in (11.11).

$$f(t) = \int_{-\infty}^{\infty} F(f) \cdot e^{i2\pi \cdot f \cdot t} df \tag{11.11}$$

The complex coefficients C_k which are discrete values for each value of k have been changed for $y(t)$ which is continuous with all frequencies [49].

This transformation between time and frequency domains is the theoretical approach.

11.1.1 Discrete Fourier Transform

The theoretical approach is not suitable to apply in real situations since actually there is neither infinitive time nor infinitive frequency.

In practice, time histories are recorded in a digitally way by a computer in a discrete format. The Discrete Fourier Transform is similar to the formal Fourier Transform but operates on digitally recorded data. The conversion of the signal from analogical into digital is shown in Figure 11.5. In this group of discrete values each element y_i is related to the value of the signal at time t_i.

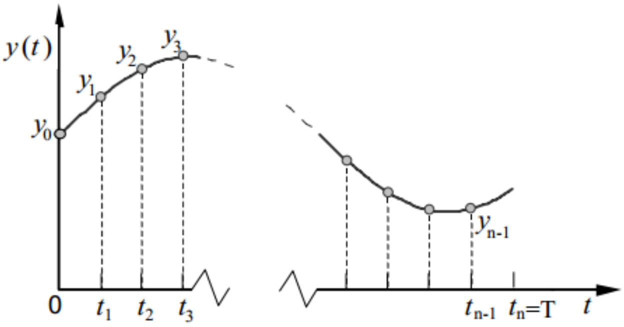

Figure 11.5 - Analog to Digital Conversion [50]

The sample time history from 0 to T is divided by equal n intervals called sample periods. Considering n as integers varying between $n = 0, 1, 2, \ldots, N-1$ it is possible to calculate sample periods as $\Delta t = T/n$

The Discrete Fourier Transform (DFT) is expressed in (11.12).

$$y(f_k) = \sum_{n=0}^{N-1} y(t_n) \cdot e^{-2\pi ikn/N} \tag{11.12}$$

$$k \in \mathbb{Z}$$

The Inverse Discrete Fourier Transform is expressed (11.13).

$$y(t_n) = \frac{1}{N} \sum_{n=0}^{N-1} y(f_n) \cdot e^{2\pi ikn/N} \tag{11.13}$$

$$k \in \mathbb{Z}$$

DFT algorithm approximates the signal in a very reasonable way and it is simple to implement. However, the time spent on calculation of the Fourier coefficients can be very high since the algorithm needs to perform N^2 calculations. Even with small sample time history the algorithm spends too much time in processing time signal, it also requires a lot of computational resources.

11.1.2 Fast Fourier Transform

The Fast Fourier Transform is an algorithm which performs the Discrete Fourier Transform in a quicker way. The algorithm was introduced by James W. Cooley and John W. Tukey in 1965 [51]. In the meantime, modifications have been made to reduce even more the time spent on calculation operations.

The big advantage of FFT is that it only needs to perform $N \cdot \log_2(N)$ calculations. Thus, computational effort is reduced. On the following Table 11.1, it is shown the comparison between the computational effort of FFT and DFT.

Table 11.1 - FFT and DFT Computational Effort

Number of points N	DFT N^2 Operations	FFT $N \cdot \log_2(N)$ Operations	Racio between FFT over DFT
8	64	24	37,50%
16	256	64	25,00%
32	1024	160	15,63%
64	4096	384	9,38%
128	16384	896	5,47%
256	65536	2048	3,13%
512	262144	4608	1,76%
1024	1048576	10240	0,98%
4096	16777216	49152	0,29%

The disadvantage of performing FFT is that time signals must contain exactly 2^n data points so that the algorithm can be applied. In real time signal processing, most time signals do not contain exact multiples of 2 points. To overcome this problem, time signals are divided into sets of points called buffers. Each buffer has 2^n data points so that is possible to apply FFT.

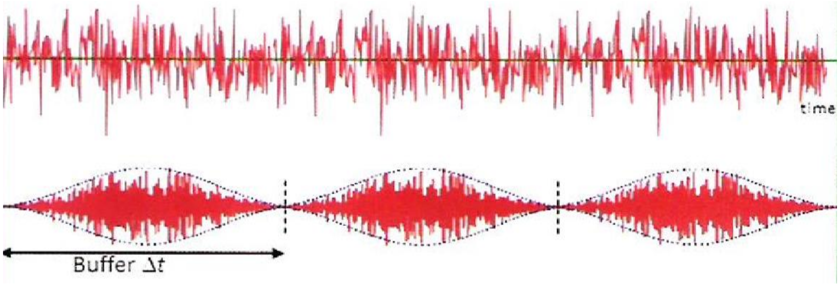

Figure 11.6 - Buffer example

Buffers can also bring undesirable problems in time signal processing. Fourier's supposition is based on the fact that summation of sinusoidal harmonics can represent any periodic time signal. Because of that the buffer should repeat itself exactly. Most times the last point of the buffer is different from the first one originating discontinuity between repeated buffers. This error is called leakage.

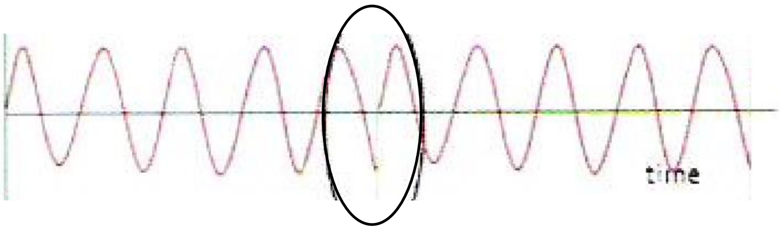

Figure 11.7 - Discontinuity between repeating buffers results in spectral leakage

To avoid leakage each buffer is multiplied by a smooth windowing function. This functions force the first point of the buffer and the last one to zero, preventing undesirable jumps between these points.

The most common used is the Hanning Window. There are various window functions such as Hamming, Triangular, Flat-top, Welch, Gaussian. Even though they differ in shape, they all start and end at zero, they tend to unit at the center and they are symmetric.

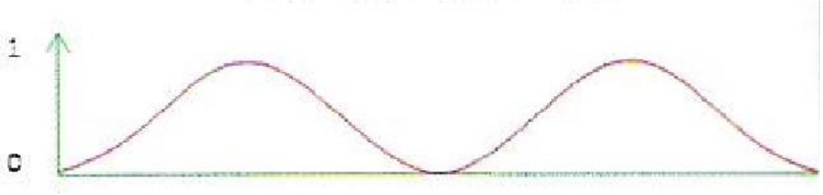

Figure 11.8 - Hanning window function

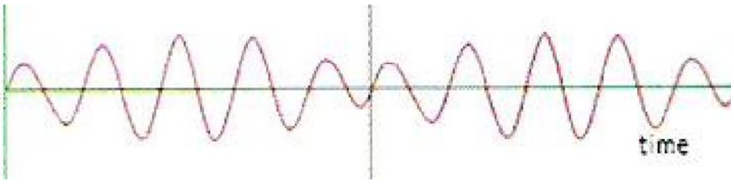

Figure 11.9 - Reduction of spectral leakage by multiplying the signal with a window function

When carrying out the Fourier analysis for a set of discrete data in time domain it is necessary to take into consideration that the analysis results in frequency domain are also discrete.

The resolution β is defined as the frequency increment between lines in the spectrum, this is related to the number of samples in the original time series (N). In (11.14) f_N represents the Nyquist frequency and f_s represents the sampling frequency.

$$\beta = \frac{1}{2} \cdot \frac{f_s}{N} = \frac{f_N}{N} \tag{11.14}$$

The bandwidth B is determined by the resolution and by any time weighting function (time window) applied to the data. For linearity weighted data the effective bandwidth is equal to the resolution in (11.15)

$$B = \beta \tag{11.15}$$

Once the windowing functions attenuate large portions of the signal it is important to overcome this problem in order to does not miss features near the edges of the buffers. This happens because these regions are multiplied by a very small value in the windowing function. To avoid this problem, it is necessary to overlap the buffers. On Figure 11.10, it is represented an example of a 50% buffer overlap.

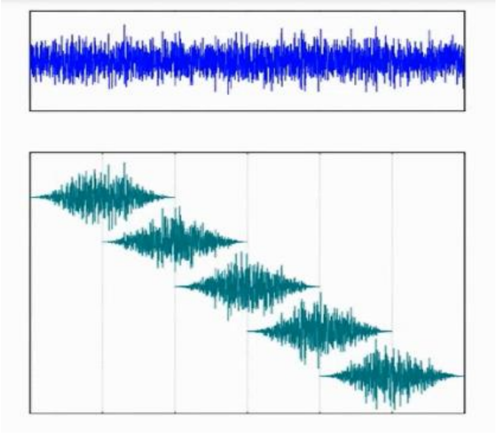

Figure 11.10 - 50% Overlapping

It is also possible to see that the first and the last buffers are not complete. In this situations, it is common to apply a zero-padding process which consists in padding the start or the end buffer with zeroes. This can compromise the quality of that particular buffer but is unlikely to affect the overall statistic average.

Another error that can occur is when signal become indistinguishable when sampled. That error is called aliasing. To avoid it the sampling range of the frequencies should comply with the Nyquist conditions. The Nyquist frequency is the maximum frequency that can be seen and is equal to one-half of the sampling rate. Shannon’ s sampling theorem states that a sampled time signal must not contain components at frequencies above the Nyquist frequency[52]

The example shown in Figure 11.11 summarizes the Fourier Transform and its inverse. In this example, the Fourier Transform decomposes the simple square wave time signal into its constituent sinusoidal harmonics. If all these are added up, the original square wave is obtained by using the Inverse Fourier Transform.

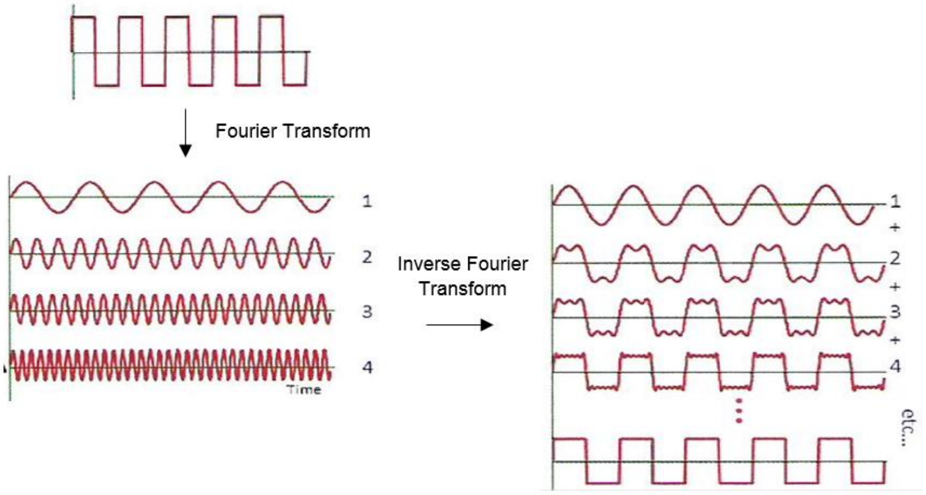

Figure 11.11 - Fourier Transform and its inverse

12 Appendix B

THEORETICAL BACKGROUND

$$[M]\{\ddot{x}\}+[K]\{x\}=0$$

$$(-\omega^2[M]+[K])\bar{x}=0$$

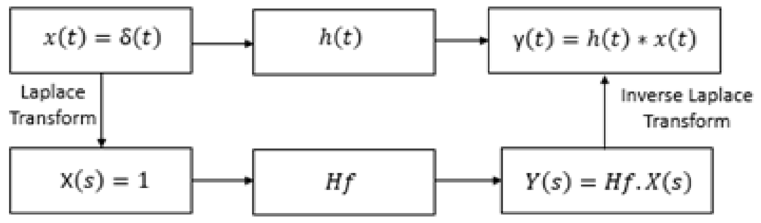
$x(t)=\delta(t)$
$h(t)$
$y(t)=h(t)*x(t)$
Laplace Transform
Inverse Laplace Transform
$X(s)=1$
Hf
$Y(s)=Hf.X(s)$

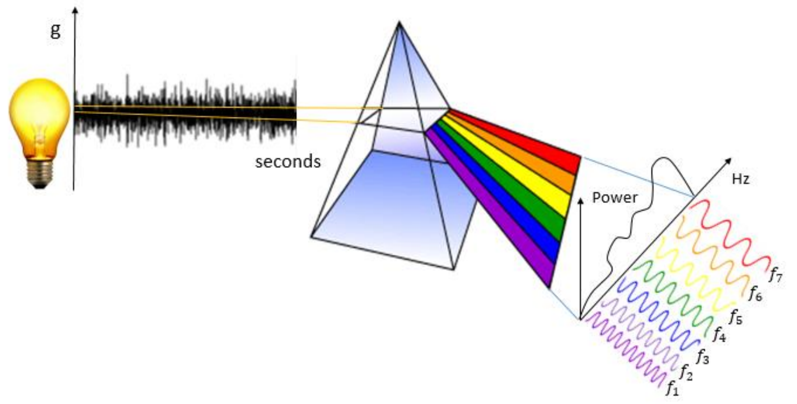
g
seconds
Power
Hz
f_7
f_6
f_5
f_4
f_3
f_2
f_1

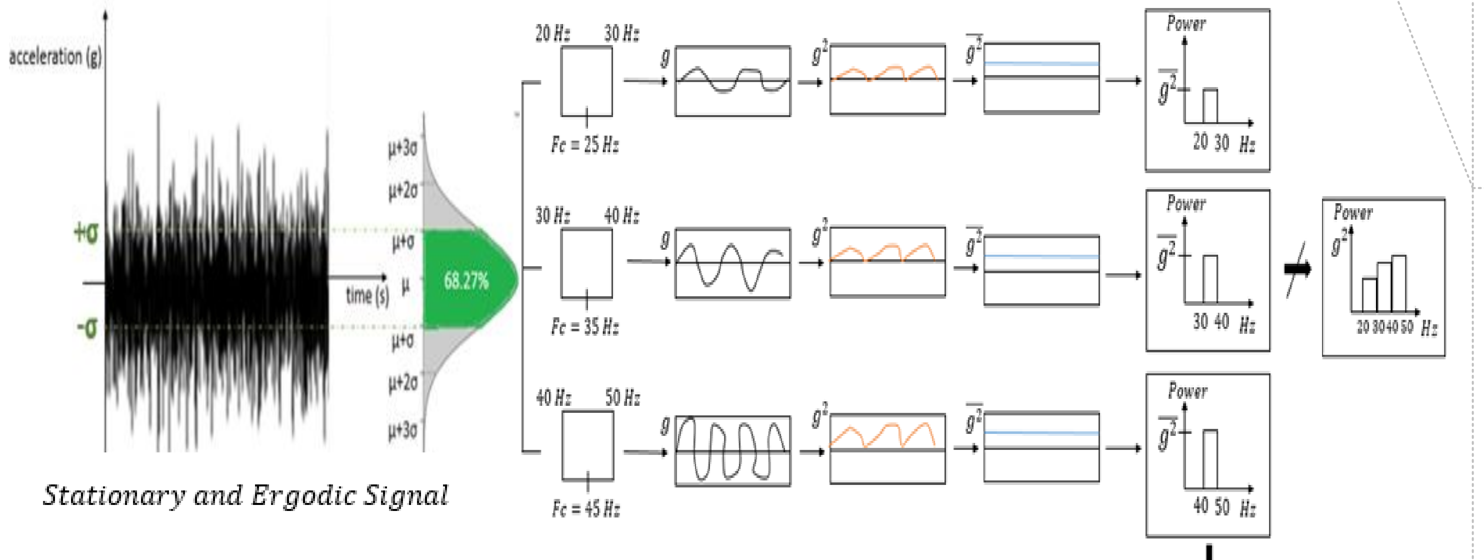
acceleration (g)
+σ
-σ
time (s)
μ+3σ
μ+2σ
μ+σ
μ
μ+σ
μ+2σ
μ+3σ
68.27%
20 Hz
30 Hz
Fc = 25 Hz
30 Hz
40 Hz
Fc = 35 Hz
40 Hz
50 Hz
Fc = 45 Hz
g
g^2
$\overline{g^2}$
Power
20 30 Hz
30 40 Hz
40 50 Hz
20 30 40 50 Hz

Stationary and Ergodic Signal

$$N(\mu=0,\sigma^2)$$

$$PSD_{out}=|Hf|^2.PSD_{in}\qquad \sqrt{A}=g_{rms}=\sigma\qquad A=\int_{f1}^{f2}PSD_{out}(f)\,df$$

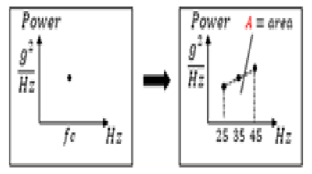

$$MS=\frac{allowable}{applicable}-1\leq 0$$

$$MS=\frac{1.1\times g_{rms,in}}{g_{rms,out}}-1\leq 0$$

$$\frac{g_{rms,out}-g_{rms,in}}{g_{rms,in}}\leq 0.1$$

INPUTS

PROCESSES

OUTPUTS

PHASE

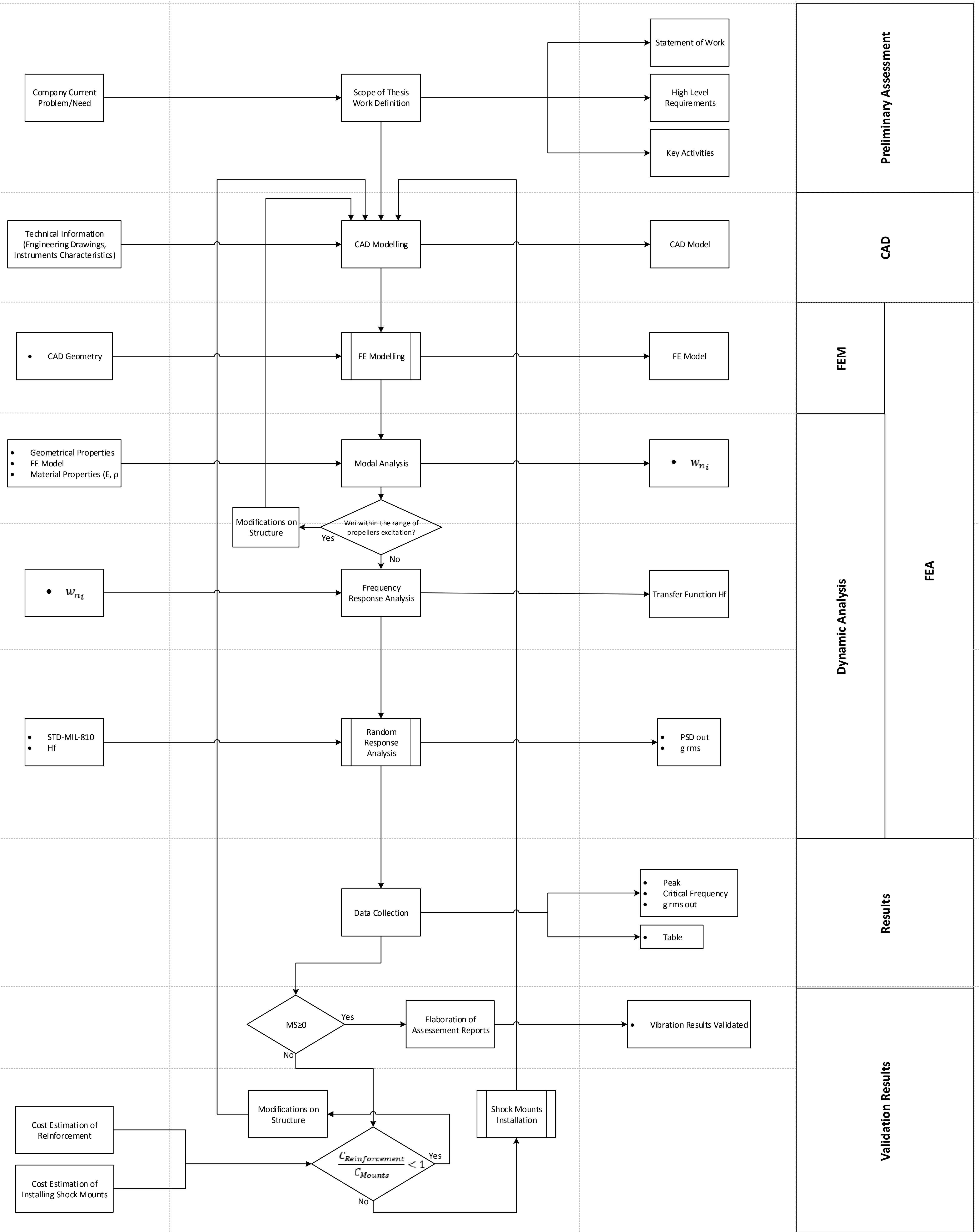
Company Current Problem/Need
Scope of Thesis Work Definition
Statement of Work
High Level Requirements
Key Activities
Technical Information (Engineering Drawings, Instruments Characteristics)
CAD Modelling
CAD Model
CAD Geometry
FE Modelling
FE Model
Geometrical Properties
FE Model
Material Properties (E, ρ
Modal Analysis
w_{n_i}
Modifications on Structure
Wni within the range of propellers excitation?
Yes
No
w_{n_i}
Frequency Response Analysis
Transfer Function Hf
STD-MIL-810
Hf
Random Response Analysis
PSD out
g rms
Data Collection
Peak
Critical Frequency
g rms out
Table
MS≥0
Yes
No
Elaboration of Assessement Reports
Vibration Results Validated
Modifications on Structure
Shock Mounts Installation
Cost Estimation of Reinforcement
Cost Estimation of Installing Shock Mounts
$\frac{C_{Reinforcement}}{C_{Mounts}}<1$
Yes
No
Preliminary Assessment
CAD
FEM
FEA
Dynamic Analysis
Results
Validation Results

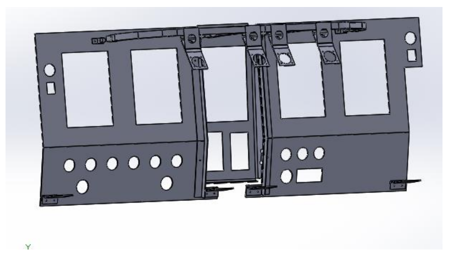

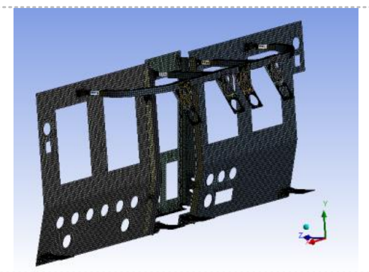

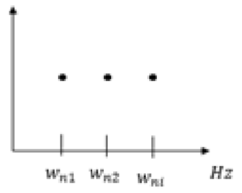

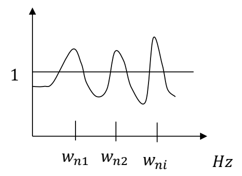

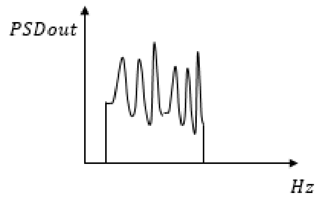

Points	Peak (g^2/Hz)	Most Critical Frequency (Hz)	Natural Frequency	Within the range of excitation generated by the propeller	Overall g_{rms}
1	2.05	132.45	10^{th}	Yes	4.39
2	9.99	137.53	11^{th}	Yes	6.71
3	2.02	132.45	10^{th}	Yes	4.36
4	9.88	137.53	11^{th}	Yes	6.67